New approaches in systems diagnosis:

combining metabolomics and ultra-weak photon emission.

Financial support for the printing of this thesis was provided by:
Leiden Academic Centre for Drug Research (LACDR)

ISBN: 978-94-92679-22-2

Thesis layout by Rosilene Cristina Rossetto Burgos

Cover design: Fred Frij

Printed by: Print Service Ede

New approaches in systems diagnosis:

combining metabolomics and ultra-weak photon emission.

Proefschrift

ter verkrijging van

de graad van Doctor aan de Universiteit Leiden,

op gezag van Rector Magnificus prof.mr.C.J.J.M. Stolker,

volgens besluit van het college voor Promoties

te verdedigen op donderdag 14 december 2017

klokke 11:15 uur.

door

Rosilene Cristina Rossetto Burgos

Geboren te Mineiros do Tietê, SP – Brasil

in 1983

PROMOTOR

Prof.dr. Jan van der Greef

CO-PROMOTORS

Dr. Rawi Ramautar

Dr. Eduard van Wijk

PROMOTIECOMMISSIE

Prof.dr. Hubertus Irth (Chair)
Leiden University

Prof.dr. Joke Bouwstra (Secretary)
Leiden University

Dr. Cristiano M. Gallep
Universidade Estadual de Campinas (UNICAMP)

Prof.dr. Gert-Jan B. van Ommen
Leiden University Medical Center (LUMC)

Prof.dr. Wim Jiskoot
Leiden University

The research presented in this thesis was financially supported by the National Council for Scientific and Technological Development - CNPq, Brazil, “Science without Borders Program” (230827/2012-8).

“Scientia potentia est”

“Knowledge is power”

Leviathan, Thomas Hobbes

Contents

Chapter 1

General introduction and aim of the thesis

GENERAL INTRODUCTION

Biological systems, including the human body, are inherently complex[1]. In order to understand its functions, the body can be viewed as a sophisticated system that utilizes multiple interacting and self-regulating subsystems. These subsystems use distinct forms of interactions (e.g., physical, biochemical, cellular, physiological, and social interactions) that involve numerous rhythms, oscillations, and pseudo-chaotic patterns at the level of biochemical reactions[2] and/or physical quantities. In this context, "health" can be defined as a state of well-balanced, unperturbed interconnected systems, whereas "disease" can be defined as an impairment of this normal functioning either due to an interaction with external factors or due to an intrinsic malfunction.

For centuries, the complexity of biological systems has caused scientists to explore the human body as a collection of largely isolated individual components; as a consequence of this approach, drug development has focused largely on a single target (i.e., the "one disease - one target - one drug" approach). This reductionist approach, in which a complex system is divided into smaller parts or units, generally excludes the role of interactions between several components within the system[3]. Although this approach has yielded important results, its limits have been reached, given the simplifications that it uses.

Following the great success of molecular biology in the 1980s and the subsequent development of high-throughput technologies for DNA sequencing, culminating in completion of the Human Genome Project in 2003, scientists were then confronted with a challenging question: How do genes interact, and how is this connectivity related to system-wide behavior. For example, complex diseases such as atherosclerosis, cancer, and asthma are clear examples of interconnected genes and the need for these interactions to be understood in the proper context. Each individual carries unique genomic information and has a unique interaction with his/her environment. This interaction determines gene activity in a unique contextual manner. For example, cellular metabolism — which is controlled by genetic information contained in the cell's nucleus — drives many complex molecular interactions. These activities are continuously changing over time and differ for each individual due to unique interactions with environmental factors and conditions.

From the perspective of diagnostics, this reductionist approach focuses strictly on evaluating individual biomarkers at a limited number of time points. For example, when attempting to diagnose type 2 diabetes, a practitioner measures changes in blood glucose levels under fasting conditions and in response to nutrition. However, glucose levels can vary widely throughout the day based on many factors, only one of which is food intake. Moreover, type2

diabetes is often associated with many other factors, including stress, lifestyle, etc. Given the vast differences between individuals, several subtypes of type 2 diabetes have been observed[4-6]. In addition, type 2 diabetes is strongly associated with other diseases and conditions, including cardiovascular disease and obesity[7]. These examples underscore the need to develop specific intervention strategies tailored to specific phenotypes[8]. This new contemporary view has emerged as a novel strategy for medical diagnostics.

The goal of personalized medicine (or precision medicine) is to improve diagnostics at earlier stages of the disease[9]. These features are essential for realizing a better global healthcare system based on phenotypic and dynamic information regarding the biological system. Personalized health care uses a systems biology approach[10-12], which provides predictive tools for assessing and interpreting health risks. This approach also facilitates the design of personalized healthcare plans for patients in order to reduce risks, improve treatment efficacy, and help prevent disease. Therefore, "health" can be best viewed from a holistic perspective and — in the early stages of disease — health can be supported by the use of a personalized approach in order to maintain or restore homeostasis.

Systems biology as an approach to understanding health and disease

Systems biology is the use of computational and mathematical modeling in order to obtain a holistic understanding of complex biological systems[10]. This approach, which appeared near the end of the 20th century, focuses on understanding the entire system's complexity and on understanding the dynamic characteristics observed using chemistry, physics, biology, and medicine. Reductionist approaches have provided a vast amount of data in the biosciences, and systems biology attempts to understand relationships in the data by attempting to understand the interconnectivity within biological systems. In addition, novel informatics tools have greatly improved data processing, yielding rapid progress and developments[13].

An integrated approach facilitates the analysis of the dynamics and complexity of biological systems using computational modeling to integrate distinct types of biology-based interdisciplinary data. Using mechanistic models, systems networks are created and used to analyze the relationships and systems-based interactions by taking into consideration as many parameters as possible. For example, a cellular network can be modeled in a computational model by considering all of the metabolic networks with their related biochemical pathways and all available kinetic parameters[14]. Analyzing dynamic changes and patterns in whole-system networks can reveal the system's limitations and/or abilities (i.e., resilience testing). This strategy provides the opportunity to discover new biomarkers, and it can provide an improved understanding of biological mechanisms and the prediction of biological variations[15].

Metabolomics as a tool for systems biology

In order to measure the global biochemical readout of a biological system, the so-called "omics" fields have been used extensively in systems biology. Omics technologies provide the precise and simultaneous analysis of thousands of genes (genomics), proteins (proteomics), or metabolites (metabolomics)[16]. Metabolomics has emerged as a powerful technology for understanding the complexity of biological systems, as metabolites are the final products of regulatory cellular processes. Unlike proteomics and genomics, metabolomics closely reflects the phenotype of distinct biological systems[17,18]. In addition, metabolic profiles can reveal genomic changes due to external factors (e.g., environmental and physiological conditions, diet, lifestyle, drug use, etc.), thereby providing a valuable biochemical readout ranging from the normal physiological state to various pathophysiological conditions[17,18]. In recent years, metabolomics has been applied to several pathophysiological studies in order to obtain detailed phenotypic information, thereby providing sub-classifications of diseases as well as facilitating the discovery of new biomarkers while improving our understanding of the underlying mechanisms in a variety of diseases[19-22]. Therefore, determining an individual's phenotypic status can provide better, more individualized data regarding his/her health status, providing applications for metabolomics in drug discovery and precision medicine[23-25].

In metabolomics, high-throughput separation techniques such as chromatography (e.g., gas chromatography, liquid chromatography, and capillary electrophoresis) coupled with mass spectrometry (MS) and nuclear magnetic resonance (NMR) are used to detect and profile metabolites in a wide variety of biological samples, including body fluids (e.g., urine and blood), tissue samples, and cell extracts[26]. Currently, mass spectrometry is the preferred technique for detecting metabolites, as it can readily detect biochemical substances in the picomolar range[27].

In metabolomics studies, various strategies can be used to identify metabolites. The targeted metabolomics strategy focuses on a select group of metabolites in specific biochemical pathways[28], whereas the untargeted approach measures a more global metabolic fingerprint (by measuring as many metabolites as possible) using established databases containing a wide diversity of chemical structures combined with mass spectrometry features[18,29]. Both strategies contribute in their own way to determining changes in metabolic pathways and in related networks for each subject in a study.

Despite their advantages, however, current metabolomics technologies do not allow for efficient time-resolved metabolic profiling on a time scale that is on par with the processes being studied; therefore, integrated concentrations are often measured. Overcoming this

obstacle is important in order to better understand the dynamics of metabolic pathways and the connections between these pathways. In this respect, combining metabolomics with other technologies might be highly important and relevant.

Ultra-weak photon emission

Ultra-weak photon emission (UPE) is the emission of low levels of endogenous light by living systems[30-33]. All biological systems spontaneously emit small yet measurable numbers of photons (on the order of 0.1–10,000 photons·s^{-1}·cm^{-2}) in the visible range of the electromagnetic spectrum, including parts of the near-ultraviolet and near-infrared regions, thus covering the spectrum from approximately 350 nm to 1270 nm[30-33]. Several terms have been used to describe this phenomenon, including low-level chemiluminescence, biophoton emissions, auto-luminescence, and spontaneous ultra-weak light emission[31,32]. UPE can be classified into two main types: spontaneous UPE and induced UPE. Spontaneous UPE is generated from physiological oxidative metabolism with no external stimulation, whereas induced UPE is initiated by external factors[31]. UPE is generated as the result of oxidative metabolic reactions at the cellular level[31]. The products of oxidative metabolism, which include reactive oxygen species (ROS) and reactive nitrogen species (RNS), react with biomolecules, inducing various levels of electron excitation. When the electrons return to the ground state (e.g., the singlet, triplet, or carbonyl excited level), photons of corresponding wavelengths are emitted[31,34].

Thanks to the direct correlation between ROS production and UPE, UPE represents a promising new diagnostic tool for measuring the dynamics of biological systems related to oxidative metabolism processes. UPE is non-invasive, relatively cost-effective, and provides label-free measurements. However, the signal produced by UPE is a single time series comprised of highly complex multi-parameter/multi-dimension information.

Because UPE can provide complex molecular information regarding biochemical processes, it can be combined with other approaches (e.g., metabolomics and other omics-based technologies) in order to obtain detailed biochemical information while also improving our understanding of the mechanisms that underlie UPE. From a systems biology view, UPE might also yield additional integrative data, including dynamic information regarding biological systems. Combining robust mathematical tools with precise knowledge regarding the biochemical origin of UPE is necessary for the advanced analysis of multi-variate data, providing an improved biological interpretation of the relevance of UPE. Once this is achieved, metabolomics and UPE can be effectively combined for use in diagnostics. This combined approach will likely provide a higher level of integrative data regarding the dynamics of biological systems and — ultimately — a novel diagnostic view of biology.

The HL-60 cell line as a study model

The HL-60 cell line was established in 1977 from peripheral blood leukocytes obtained from a female patient with acute promyelocytic leukemia[35,36]. Since then, this cell line has been used extensively as a model for studying human myeloid cell differentiation[37], neutrophil function, migration, chemotaxis, and inflammatory cell responses[38,39]. HL-60 cells can be differentiated into granulocytes using specific compounds such as all-*trans*-retinoic acid (ATRA)[40] and dimethyl sulfoxide (DMSO)[41], providing an *in vitro* model for studying the immune response.

An important component in the immune system, respiratory burst is the first mechanism of defense activated by specialized cells such as neutrophils in response to invading pathogens. Respiratory burst uses the rapid consumption of molecular oxygen in order to produce elevated concentrations of ROS, which are used to kill the invading pathogens[42-44]. Under physiological conditions, ROS are produced primarily in the mitochondria as a product of the normal respiration process; however, during respiratory burst, NADPH oxidase serves as the main source of ROS production for cellular defense[45,46]. The primary function of NADPH oxidase is to catalyze the production of $O_2^{\cdot-}$. NADPH serves as an electron donor by reducing molecular oxygen, whereas other NADPH subunits translocate from the cytosol to the plasma membrane, forming a functional multi-component electron transfer system[43,47]. Differentiated HL-60 cells express genes that encode NADPH oxidase subunits analogous to those expressed in human neutrophils[48]; therefore, these cells were used in this project as a robust ROS generator that can also be monitored using ultra-weak photon emission (UPE).

Scope and outline of this thesis

Using metabolomics, we used HL-60 cells as a model system for studying the relationship between UPE and the corresponding biochemical readout. Because UPE is believed to reflect higher organizational levels, we combined it with metabolomics, providing the bridge with biochemistry studied at lower organizational levels. In this study, we explored the potential of using UPE in combination with metabolomics in order to achieve systems-based UPE-metabolomics diagnostics.

First, we evaluated whether the UPE signal can be correlated with changes in biochemistry by examining statistical correlations between UPE and metabolomics data. Next, we assessed the potential of using UPE as a tool for measuring oxidative stress metabolism. Finally, we used UPE to monitor drug-induced responses in order to obtain a systems-wide pharmacology view.

In **Chapter 2**, we introduce our perspectives regarding the use of a combined platform consisting of metabolomics and UPE as a new approach for assessing both health and disease.

Chapters 3, **4**, **5** and **6** describe the experiments performed using HL-60 cells. In **Chapter 3**, we introduce HL-60 cells as an *in vitro* model. Moreover, we developed a dynamic experimental design in order to analyze the correlation between metabolomics and UPE in differentiated HL-60 cells. We also developed an optimized targeted metabolomics platform using capillary electrophoresis-mass spectrometry (CE-MS) in order to profile amino acids and nucleosides. Finally, we studied the statistical correlations between the metabolomics data and dynamic UPE data.

In **Chapter 4**, we describe the potential of using UPE as a readout tool for monitoring oxidative stress metabolism. Using a dedicated platform for assessing metabolic inflammation and oxidative stress — including classes of compounds such as prostaglandins, isoprostanes, nitro-fatty acids, and lyso-sphingolipids — we examined the statistical correlations between photon emissions and dynamic changes in the levels of various metabolites. We used diphenyleneiodonium chloride (DPI), a general inhibitor of NADPH oxidase, in order to study the effects of inhibiting NADPH oxidase on specific biochemical pathways.

In **Chapter 5**, we evaluate the correlation between the dynamic UPE profile and the endogenous intracellular antioxidant glutathione in HL-60 cells. We developed and optimized a method for the derivatization and analysis of glutathione using CE-MS in HL-60 cells. We included both forms of glutathione — i.e., derivatized glutathione (GS-NEM) and oxidized glutathione (GSSG) — in our analysis. In addition, our newly developed method was compared with conventional spectrophotometric methods of measuring glutathione in HL-60 cells during respiratory burst. We therefore evaluated the correlation between UPE intensity and glutathione levels. The intracellular redox state (i.e., the GS-NEM/GSSG ratio) was also considered when respiratory burst was induced.

In **Chapter 6**, we describe the feasibility of using UPE as a diagnostic tool from the perspective of pharmacology. Several inhibitors of NADPH oxidase were tested, and their effects on the UPE profile were evaluated and are discussed. We also evaluated a specific inhibitor of NADPH oxidase and an inhibitor of myeloperoxidase with high potential for use in pharmacotherapy.

Finally, in **Chapter 7** we summarize the findings in this thesis and draw general conclusions. We also discuss interesting topics that have emerged in this research field, including both challenges and advantages, and we provide suggestions for future studies.

REFERENCES

1 Weng, G., Bhalla, U. S. & Iyengar, R. Complexity in biological signaling systems. *Science* **284**, 92-96 (1999).
2 Ravasz, E., Somera, A. L., Mongru, D. A., Oltvai, Z. N. & Barabasi, A. L. Hierarchical organization of modularity in metabolic networks. *Science* **297**, 1551-1555, (2002).
3 Kaiser, M. I. The limits of reductionism in the life sciences. *Hist Philos Life Sci* **33**, 453-476 (2011).
4 Sun, M. *et al.* Measuring ultra-weak photon emission as a non-invasive diagnostic tool for detecting early-stage type 2 diabetes: A step toward personalized medicine. *J Photochem Photobiol B* **166**, 86-93, (2017).
5 Hu, C. *et al.* Linking biological activity with herbal constituents by systems biology-based approaches: effects of Panax ginseng in type 2 diabetic Goto-Kakizaki rats. *Mol BioSyst* **7**, 3094-3103, (2011).
6 Wei, H. *et al.* Urine metabolomics combined with the personalized diagnosis guided by Chinese medicine reveals subtypes of pre-diabetes. *Mol BioSyst* **8**, 1482-1491, (2012).
7 Kahn, S. E., Hull, R. L. & Utzschneider, K. M. Mechanisms linking obesity to insulin resistance and type 2 diabetes. *Nature* **444**, 840-846, (2006).
8 Malandrino, N. & Smith, R. J. Personalized medicine in diabetes. *Clin Chem* **57**, 231-240, (2011).
9 Schork, N. J. Personalized medicine: time for one-person trials. *Nature* **520**, 609-611 (2015).
10 Kitano, H. Systems biology: a brief overview. *Science* **295**, 1662-1664, (2002).
11 Loscalzo, J. Systems biology and personalized medicine: a network approach to human disease. *Proc Am Thorac Soc* **8**, 196-198, (2011).
12 Weston, A. D. & Hood, L. Systems biology, proteomics, and the future of health care: toward predictive, preventative, and personalized medicine. *J Proteome Res* **3**, 179-196 (2004).
13 Shulaev, V. Metabolomics technology and bioinformatics. *Brief Bioinform* **7**, 128-139, (2006).
14 Kell, D. B. Systems biology, metabolic modelling and metabolomics in drug discovery and development. *Drug Discov Today* **11**, 1085-1092, (2006).
15 Hood, L., Heath, J. R., Phelps, M. E. & Lin, B. Systems biology and new technologies enable predictive and preventative medicine. *Science* **306**, 640-643, (2004).
16 Joyce, A. R. & Palsson, B. O. The model organism as a system: integrating 'omics' data sets. *Nat Rev Mol Cell Bio* **7**, 198-210, (2006).
17 Mathew, A. K. & Padmanaban, V. Metabolomics: the apogee of the omics trilogy. *Int J Pharm Pharm Sci* **5**, 45-48 (2013).
18 Patti, G. J., Yanes, O. & Siuzdak, G. Innovation: Metabolomics: the apogee of the omics trilogy. *Nat Rev Mol Cell Biol* **13**, 263-269, (2012).
19 Ommen, B., Greef, J., Ordovas, J. M. & Daniel, H. Phenotypic flexibility as key factor in the human nutrition and health relationship. *Genes Nutr* **9**, 423 (2014).
20 Bain, J. R. *et al.* Metabolomics applied to diabetes research: moving from information to knowledge. *Diabetes* **58**, 2429-2443, (2009).
21 Gowda, G. A. *et al.* Metabolomics-based methods for early disease diagnostics. *Expert Rev Mol Diagn* **8**, 617-633, (2008).

22 Rankin, N. J., Preiss, D., Welsh, P. & Sattar, N. Applying metabolomics to cardiometabolic intervention studies and trials: past experiences and a roadmap for the future. *Int J Epidemiol* **45**, 1351-1371, (2016).
23 Wishart, D. S. Emerging applications of metabolomics in drug discovery and precision medicine. *Nat Rev Drug Discov* **15**, 473-484, (2016).
24 Beger, R. D. *et al.* Metabolomics enables precision medicine: "A White Paper, Community Perspective". *Metabolomics* **12**, 149, (2016).
25 Kaddurah-Daouk, R., Kristal, B. S. & Weinshilboum, R. M. Metabolomics: a global biochemical approach to drug response and disease. *Annu Rev Pharmacol Toxicol* **48**, 653-683, (2008).
26 Pan, Z. & Raftery, D. Comparing and combining NMR spectroscopy and mass spectrometry in metabolomics. *Anal Bioanal Chem* **387**, 525-527, (2007).
27 Dettmer, K., Aronov, P. A. & Hammock, B. D. Mass spectrometry-based metabolomics. *Mass Spectrom Rev* **26**, 51-78, (2007).
28 Lu, W., Bennett, B. D. & Rabinowitz, J. D. Analytical strategies for LC-MS-based targeted metabolomics. *J Chromatogr B Analyt Technol Biomed Life Sci* **871**, 236-242, (2008).
29 Tautenhahn, R. *et al.* An accelerated workflow for untargeted metabolomics using the METLIN database. *Nat Biotechnol* **30**, 826-828, (2012).
30 Slawinska, D. & Slawinski, J. Biological chemiluminescence. *Photochem. and Photobiol.* **37**, 709-715 (1983).
31 Cifra, M. & Pospisil, P. Ultra-weak photon emission from biological samples: definition, mechanisms, properties, detection and applications. *J Photochem Photobiol B* **139**, 2-10, (2014).
32 Devaraj, B., Usa, M. & Inaba, H. Biophotons: Ultraweak light emission from living systems. *Curr Opin Solid St M* **2**, 188-193, (1997).
33 Inaba, H. Super-high sensitivity systems for detection and spectral analysis of ultraweak photon emission from biological cells and tissues. *Experientia* **44**, 550-559, (1988).
34 Pospisil, P., Prasad, A. & Rac, M. Role of reactive oxygen species in ultra-weak photon emission in biological systems. *J Photochem Photobiol B* **139**, 11-23, (2014).
35 Collins, S. J. The HL-60 promyelocytic leukemia cell line: proliferation, differentiation, and cellular oncogene expression. *Blood* **70**, 1233-1244 (1987).
36 Collins, S. J., Gallo, R. C. & Gallagher, R. E. Continuous growth and differentiation of human myeloid leukaemic cells in suspension culture. *Nature* **270**, 347-349 (1977).
37 Birnie, G. D. The HL60 cell line: a model system for studying human myeloid cell differentiation. *Br J Cancer Suppl* **9**, 41-45 (1988).
38 Mollinedo, F., Santos-Beneit, A. M. & Gajate, C. in *Animal Cell Culture Techniques* (ed Martin Clynes) 264-297 (Springer Berlin Heidelberg, 1998).
39 Hauert, A. B., Martinelli, S., Marone, C. & Niggli, V. Differentiated HL-60 cells are a valid model system for the analysis of human neutrophil migration and chemotaxis. *Int J Biochem Cell Biol* **34**, 838-854, (2002).
40 Breitman, T. R., Selonick, S. E. & Collins, S. J. Induction of differentiation of the human promyelocytic leukemia cell line (HL-60) by retinoic acid. *Proc Natl Acad Sci U S A* **77**, 2936-2940 (1980).
41 Sham, R. L., Phatak, P. D., Belanger, K. A. & Packman, C. H. Functional properties of HL60 cells matured with all-trans-retinoic acid and DMSO: differences in response to interleukin-8 and fMLP. *Leuk Res* **19**, 1-6 (1995).
42 Babior, B. M. in *Molecular Aspects of Inflammation*, 41-47 (Springer, 1991).
43 Dahlgren, C. & Karlsson, A. Respiratory burst in human neutrophils. *J Immunol Methods* **232**, 3-14 (1999).
44 Glass, G. A. *et al.* The Respiratory Burst Oxidase of Human-Neutrophils - Further-Studies of the Purified Enzyme. *J Biol Chem* **261**, 3247-3251 (1986).

45 Bylund, J., Brown, K. L., Movitz, C., Dahlgren, C. & Karlsson, A. Intracellular generation of superoxide by the phagocyte NADPH oxidase: how, where, and what for? *Free Radic Biol Med* **49**, 1834-1845 (2010).
46 Panday, A., Sahoo, M. K., Osorio, D. & Batra, S. NADPH oxidases: an overview from structure to innate immunity-associated pathologies. *Cell Mol Immunol* **12**, 5-23, (2015).
47 Babior, B. M. NADPH oxidase: an update. *Blood* **93**, 1464-1476 (1999).
48 Bedard, K. & Krause, K. H. The NOX family of ROS-generating NADPH oxidases: physiology and pathophysiology. *Physiol Rev* **87**, 245-313, (2007).

Chapter 2

Crossing the boundaries of our current healthcare system by integrating ultra-weak photon emissions with metabolomics

Based on

Rosilene Cristina Rossetto Burgos, Eduard P. A. Van Wijk, Roeland van Wijk, Min He, Jan van der Greef

Crossing the boundaries of our current healthcare system by integrating ultra-weak photon emissions with metabolomics

Frontiers in Physiology **7**:611, (2016)

doi:10.3389/fphys.2016.00611

ABSTRACT

The current healthcare system is hampered by a reductionist approach in which diagnostics and interventions focus on a specific target, resulting in medicines that center on generic, static phenomena while excluding inherent dynamic nature of biological processes, let alone psychosocial parameters. In this essay, we present some limitations of the current healthcare system and introduce the novel and potential approach of combining ultra-weak photon emission (UPE) with metabolomics technology in order to provide a dynamic readout of higher organizational systems. We argue that the combination of metabolomics and UPE can bring a new, broader, view of health state and can potentially help to shift healthcare towards more personalized approach that improves patient well-being.

INTRODUCTION

There is currently a global need for a change in the healthcare system, including healthcare policies. Specifically, we have clearly reached the boundaries of our current system, and rising costs make healthcare increasingly less affordable.

The past success of the healthcare system is based on a paradigm that — ironically — is now a limitation. The discovery of penicillin in 1928 by Alexander Fleming started an era of antibiotic development and laid the foundation for a "war against" system of healthcare. Over the past century, this concept became increasingly popular and has been particularly successful for treating acute illnesses. This paradigm is exemplified by terms commonly used in modern medicine with prefixes and suffixes such as "anti-" (e.g., antibiotic), "-inhibitor" (e.g., angiotensin-converting-enzyme inhibitor - ACE), and "-blocker" (e.g., beta-blocker). This approach led to the development of a disease management system rather than a bona fide healthcare system. Most importantly, this system largely overlooks chronic illness and preventive strategies[1,2].

Rather than extrapolating current disease management knowledge into disease prevention and the promotion of health — a strategy that is likely to fail — we suggest that a radically different, transformative approach is needed. This novel approach is based on a systems — or ecological — view on health and well-being[3,4]. With this approach, the focus shifts naturally from a more reductionist, single-symptom approach to a dynamic perspective based on systems regulation. In addition, each individual patient is considered in context, providing a more biopsychosocial view rather than a strict biomedical perspective. Such a shift from the traditional "one-size-fits-all" approach — which typically leads to a "one-size-fits-none" outcome — to personalized medicine/healthcare is a central theme in the new paradigm referred to as "P4 Health": Preventive, Predictive, Personalized, Participatory healthcare[5].

In a health ecosystem, human-human interactions are the most important basis, with compassion and respect for each other's world view serving as the central theme[6]. Moreover, politicians and policy-makers must change their focus from a short-term "quick-fix" approach, which is typically driven by short-term electoral cycles, to achieving long-term, sustainable improvements in our healthcare system at the societal level. The drastic, wide-reaching effects of our changing lifestyle on health and well-being — which has created the so-called "diseases of comfort" — must be considered from a much wider perspective, requiring an approach that crosses cultures as well as disciplines. This approach will improve integrative medicine and facilitate health-focused prevention, thereby reaffirming the importance of the relationship between the physician and patient by focusing on the whole person; moreover,

this approach will be evidence-based and will integrate all appropriate therapeutic and lifestyle strategies, healthcare system, and disciplines in order to achieve optimal health and healing[7].

From the perspective of diagnostics, current approaches focus only on a single time point or a limited number of time points; however, human physiology is based on a wide spectrum of endogenous biological rhythms and oscillations[8]. Such rhythms serve as a fingerprint representing higher-order dynamic systems and various time scales ranging from long periods such as diurnal/nocturnal, monthly, seasonal, and annual rhythms to short periods on the order of minutes, seconds, or fractions of seconds. In this context, human physiology tends to maintain a homeostatic state due to a complex network of regulatory feedback circuits driven by various rhythms. Therefore, homeostasis and allostasis go hand-in-hand with dynamic systems concepts[9,10], and changes in oscillation patterns and/or rhythms can indicate a perturbation in the system. Indeed, evidence suggests that examining one's biological clock might help with determining a clinical diagnosis[11]. However, current clinical biochemistry tools are limited with respect to bridging different rhythmic time scales. Therefore, methods for measuring ultra-weak photon emissions (UPE) have been developed and appear to be suitable for measuring systems dynamics. In addition, UPE can be measured in real time and is non-invasive, label-free, and cost-effective.

A growing body of evidence suggests that UPE reflects the coherence of self-organizing systems and might therefore be used to measure health at a higher organizational level[12-14], providing a novel tool for reading the state of dynamic biological systems. UPE is intrinsic to every living system that undergoes respiration and utilizes oxygen; therefore, the dynamics of UPE reflect the biological processes that underlie this emission[15-17]. We therefore suggest that UPE may be combined with metabolomics technologies in order to develop an integrated diagnostic tool for detecting the transition from health to disease by combining the sensitivity of biochemical pattern recognition with the high temporal resolution of UPE measurement.

Metabolomics has been described as the comprehensive analysis of all metabolites in a biological sample (e.g., cells, tissues, and/or bodily fluids)[18,19]. Together with other omics technologies (i.e., genomics, transcriptomics, and proteomics), metabolomics provides a holistic picture of the metabolic phenotype[20]. The major advantage of using metabolomics over other omics technologies is the ability to investigate dynamic regulatory mechanisms at the molecular level, providing insight into how distinct biochemical pathways are interconnected[18]. Thus, a more personalized approach to health assessment can be achieved.

In addition, new ideas regarding systems-based thinking have appeared, accelerating our understanding of concepts regarding the complexities of life[21]. Nevertheless, our healthcare system's current focus on disease management using a reductionist approach does not consider influences of the biopsychosocial environment. Moreover, novel fundamental advances in our understanding of the dynamics of life have led to the development of a new biological picture. In this view, the organizational metabolic network is represented as a hierarchical model (i.e., as a pyramid; see **Fig. 1**). Another newly recognized feature is the dynamic, oscillatory aspect of metabolic flows, in which metabolic regulatory information is controlled by repetitive, pulsing dynamic systems[22].

In this essay, we address the potential new diagnostic tools as a stepping stone toward realizing novel intervention-based strategies in a health ecosystem based on promoting the healthy state (i.e., salutogenesis). The salutogenesis concept has been used in many health practices. The concept can be seen as complementary to the biomedical model as it focuses on the complex self-healing processes rather than concentrating on a singular pathogenic factor[23,24].

MOVING TOWARD A NEW VISION

Our current medical system is based on pathogenesis, defining disease, and developing standardized treatments. However, the cornerstones of the healthcare system of the future will be the definition of health, the ability to monitor changes in health status, and the ability to provide evidence-based interventions that improve health at both the population (i.e., generic) level and at the individual patient level[25]. In recent years, a large number of publications have focused on establishing a new definition of health, thereby departing from the current static WHO definition toward a dynamic definition of health[26-29].

As illustrated in **Fig. 1**, health can be depicted as the dynamic behavior between a physiological range, indicated by homeostasis and allostasis in normal daily life with physical, psychological, and social challenges and rhythms. The allostasis concept describes the system's response to an environmental challenge by anticipating, preparing for, and controlling the challenge[9]. When the challenge is over and the environment is restored to previous conditions, the system returns to its normal state. However, if the system cannot return to its healthy state, the system can enter a disease state, which can even become irreversible in an advanced stage[10,19]. In addition, the "life pyramid" depicted in **Fig. 1** is integrated, underscoring the need to reach higher overarching network dynamics in order to develop optimal strategies for promoting health. Because health is dependent upon the environment (as discussed above), this higher level organization must be studied from a

broad perspective that includes the dynamic interactions between the human body and its psychosocial environment.

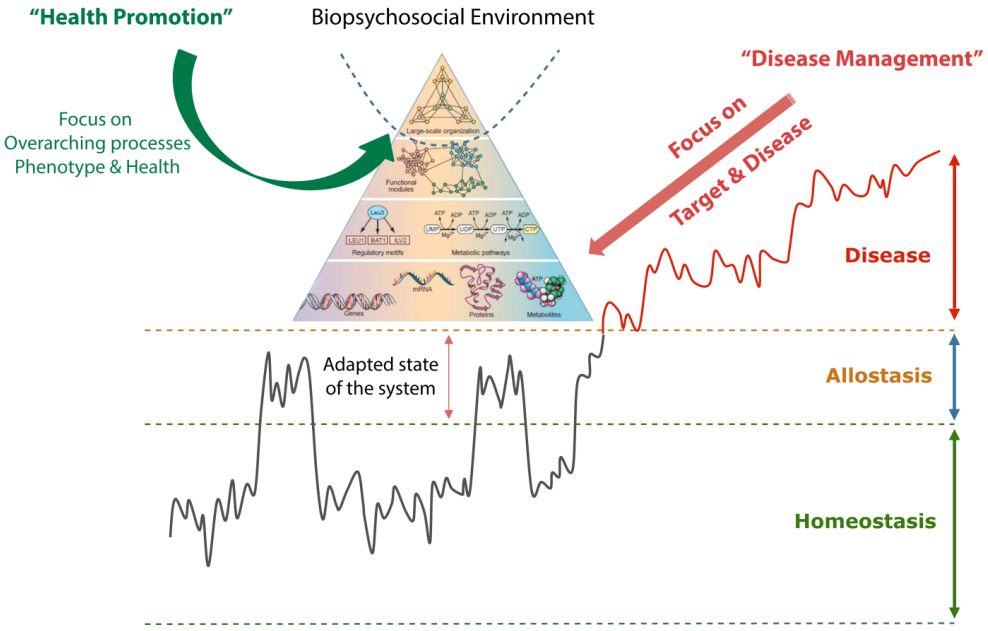

Figure 1. Schematic depiction of the development from Health into a disease state. It shows how challenges to homeostasis can be regulated by allostasis by adapting the set points of the regulatory system. If the resilience is lost over time, the system can develop into a disease state. The last part is often handled by disease management focusing on single symptoms. The "life pyramid" view represents the notion of how biological systems are interconnected at different organizational levels and how the biopsychosocial environment acts dynamically within the system and therefore reflects the information at the lower levels. This integrated picture is more applicable to the pre-disease and healthy state and represents the newly emerging picture of how the future healthcare system should focus on promoting health rather than treating disease. Adapted from (Oltvai and Barabasi, 2002; Ramautar et al., 2013; van der Greef et al., 2013).

The key feature of this view is that the system can restore itself via self-regulatory mechanisms, thereby maintaining health, whereas disease develops when the system loses this ability. In other words, in a disease situation, the system loses its ability to recover fully. In this situation, a strategy for promoting health is needed that differs fundamentally from the current strategy designed to simply manage disease. For this reason, preventive strategies that use pathology-based methodologies are not applicable, and we should not focus on a change in the concentration of a given molecule (for example, glucose). Thus, with type 2 diabetes, for example, we must focus on dynamic regulatory mechanisms in the system's response to a challenge (e.g., an oral glucose tolerance test). Such strategies have been developed recently using metabolomics-based strategies[30,31]; however, the need still exists

for a dynamic tool that can integrate, interpret, and correlate detailed information regarding regulatory mechanisms with a higher level of systems-based thinking.

Systems-based thinking has developed through systems biology in life sciences and is used to study organizations in a wider context. An important feature of systems-based thinking is its focus on relationships rather than individual variables[32]. In such a view, the relationships between biological, psychological, social, and environmental factors — and changes in these relationships over time — are central features. By considering the complexity of these interactions, we can develop a personalized approach that is applicable in the context of the individual. This approach is centered on achieving an optimal relationship between the patient and the healthcare provider.

Metabolomics technologies are used to measure metabolite profiles in bodily fluids, thus reflecting the complex interaction between the environment and the body[10]. To date, most system-wide measurements have been interpreted at the "medium-to-low" level of the triangle (see **Fig. 1**) using metabolomics. Indeed, dynamic measurements of metabolites can give insight into the development of diseases and the early stages of metabolic dysfunction[33]. Extremely early changes at higher levels are believed to be responsible for a shift toward disease, and detecting these changes is essential in order to develop prevention-based strategies to promote health. Indeed, measuring a system's coherence may serve as a tool for measuring the system's resilience and the individual's homeostatic and allostatic capacity.

Recent evidence suggests that recording metabolic shifts by measuring UPE-related metabolic processes in the human body can reflect the dynamics of metabolic organization[12,13]. Photobiological response (the result of chemical and/or physical changes induced by light in biological systems) and low-level biological luminescence (the production and emission of photons) are considered to be complementary manifestations of the photons' role in metabolism. Thus, the recorded photon emissions reflect the net activity of a subset of these reactions, thereby reflecting the body's current metabolic state. UPE may therefore serve as a suitable complementary tool for analyzing a biological dynamic system in combination with metabolomics technology.

UPE is present in all living organisms[17] and is low-intensity (non-thermal) light emitted from living systems without the use of an external intervention[15,34,35]. Biological systems spontaneously emit a measurable number of photons within a specific range of the electromagnetic spectrum (UV and UV/VIS) as a result of normal biochemical reactions. In living systems, these photons are usually in the 300-750 nm range[13], depending on the

system. In human tissues, the wavelength ranges from 420 to 570 nm[36]. The rate of photon emissions is generally on the order of 10^1-10^3 photons·s^{-1}·cm^{-2},[15], and these photons originate from oxidative metabolic reactions and are therefore closely related to the rate of electronic transport in mitochondria and the generation of reactive oxygen species (ROS), reactive nitrogen species (RNS), and/or lipid peroxidation[15,16,37]. When perturbed, these reactions can give rise to excessive amounts of ROS, causing damage to lipids, nucleic acids, and proteins. These damaged biomolecules can cause a loss of cellular functions, including cell signaling, immune responses, and pathways that regulate pro-inflammatory and/or anti-inflammatory processes[16,38], ultimately leading to cell death.

The feasibility of recording UPE as a tool for measuring dynamic changes in human health and various physiological conditions has been reported[12,13,17] and was reviewed recently[39]. For example, a wide diversity of conditions are associated with changes in the UPE profile, including aging[40], diurnal biological rhythms[41-45], and conscious activities[46-48]. In addition, some groups have suggested that UPE properties can be used as a diagnostic tool in measuring health and disease[49-53].

The technology needed to continuously monitor spontaneous UPE in the visible range in human subjects includes a sensitive photomultiplier tube (PMT) in a sealed dark environment. Such equipment has been developed and validated and is now considered a rapid, relatively inexpensive, non-invasive technology for reliably measuring UPE[12].

COMBINING UPE WITH METABOLOMICS TECHNOLOGY

The ability to combine and correlate UPE data with metabolomics data is an essential step toward personalized monitoring of physiological changes associated with health and disease. In life sciences, most specialized techniques generate profiles that provide a representative (i.e., generic) picture of a biological system. Both metabolomics and UPE provide an efficient readout providing valuable information regarding the dynamics of the biological systems. The challenge is to combine these two methodologies in order to link the detailed biochemistry with higher organizational information. **Fig. 2** illustrates the four steps that are needed: sampling, analysis, sub-grouping, and correlation. Analyzing UPE data can require robust mathematical procedures in order to study the spatial and/or temporal features of the signal, as well as to determine the photon count distributions for more sophisticated analyses[13,54-57]. Finally, the two sets of data are used to build network correlations between UPE and metabolic profiles, which can then be used for individual/personalized diagnostics.

As illustrated in **Fig. 2**, this integration approach can be exemplified in an explorative study using UPE and metabolomics data measured in pre-diabetic subjects. In this example,

metabolomics data was acquired using plasma samples. Samples were analyzed using established chromatographic methodologies using GC-MS and LC-MS[58-60], followed by data processing[61]. UPE data were acquired from the same subjects measuring the hands of each subject. Subsequently, derived parameters were calculated applying photon counting statistics[13,57,62]. Correlation analysis between metabolomics and UPE data was performed using Spearman's rank correlation observing the correlation networks built in CytoScape with the MetScape plugin[63,64]. The resulting network shows correlations between the metabolomics data and the UPE data (**Fig. 2**). Specifically, sugar metabolites and amine metabolites (which are related to energy metabolism) were positively and negatively correlated, respectively, with the UPE data (**Fig. 2**). Lipids are known to relate to cellular signaling and energy processes and this class of compounds were also correlated with UPE parameters. The outcome might indicate an essential role in both pre-diabetes as well as the production of UPE, which is associated with energy production[65-67].

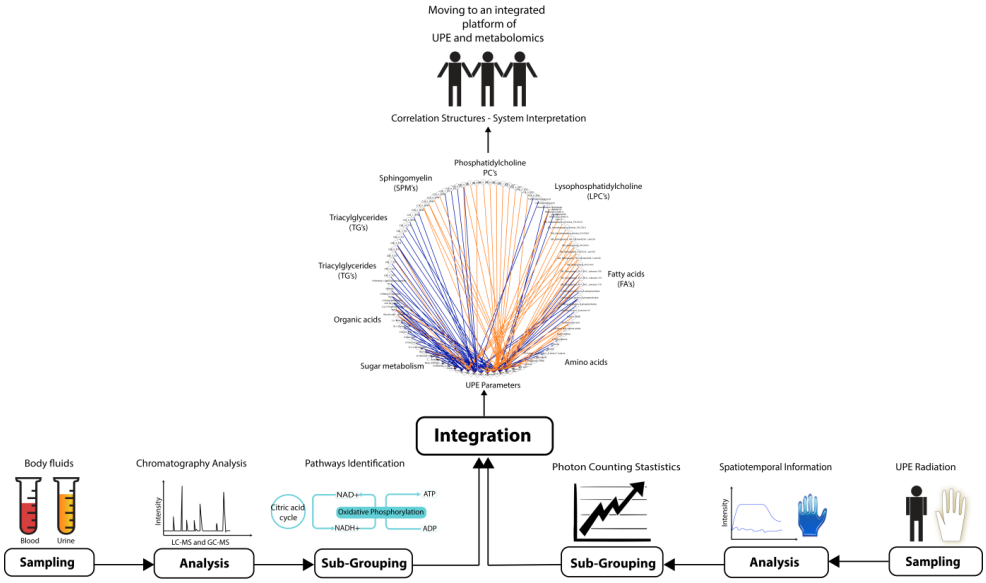

Figure 2. Overview of the experimental steps required for integrating UPE and metabolomics data in order to promote health and diagnostics. Bodily fluids (for metabolomics; left) and parts of the body (for UPE recording; right) are sampled. The samples are analyzed using chromatographic techniques (for metabolomics) and spatiotemporal analyses (for UPE). The metabolomics data are then gathered in pathways, and photon counting statistics is applied to the UPE data. Finally, the two data sets are integrated performing Spearman's rank correlations using network correlation, ultimately generating a systems-based interpretation. In this example, plasma samples of pre-diabetic subjects (44 individuals) were analyzed for the generation metabolomics data. The metabolomics study used GC-MS and LC-MS platforms to profile lipids (phosphatidylcholine, lysophosphatidylcholine, sphingomyelin, fatty acids, and triglycerides), organic acids, sugar metabolites, and amine metabolites. UPE data was acquired from the subjects' hands generating 13 parameters after applying

photon count statistics. Spearman's rank correlations were calculated between UPE parameters and various classes of compounds acquired from the metabolomics analysis. The correlation was filtered using $|r| > 0.3$ and subsequently built the correlation network using CytoScape software (MetScape plugin). Blue lines represent negative correlations, and orange lines represent positive correlations.

Overall, the integrated platform illustrates that combining UPE and metabolomics data is feasible and has high potential for both measuring specific and complex information. Specifically, integrating UPE with metabolomics contributes to our understanding of dynamic changes and provides essential insight into the underlying biochemistry, which enables to put the biochemistry information (detailed field) into a broader context and higher level of complexity. This combined approach may well be the key to realizing strategies designed to promote health.

CONCLUDING REMARKS AND PERSPECTIVES

Here, we indicate the potential of integrating UPE and metabolomics as a novel technology approach in order to move our healthcare system in the direction of promoting health in a proactive manner. Importantly, this integrated approach combining UPE and metabolomics can provide multi-scale information regarding key biological processes. The clear advantage of this approach is that it will improve our understanding of dynamic higher organizational levels while increasing our understanding of the underlying biochemistry at other levels. This might reveal the regulatory connection between different time scales as occurs from the cellular to the organism level.

The integrated information regarding metabolic activity and complex dynamicity could possibly further provide a rapid, robust readout of the biopsychosocial environment. In addition, combining UPE with metabolomics technology in an integrated platform for diagnosing both health and disease can provide an essential first step in the direction of systems-based thinking in personalized medicine, thereby crossing the boundaries of our current healthcare system by shifting diagnostic focus to higher organizational levels.

ACKNOWLEDGMENTS

RB was supported by the "Science without Borders" program of the Brazilian National Council for Scientific and Technological Development - CNPq (Conselho Nacional de Desenvolvimento Científico e Tecnológico) in the form of a research fellowship awarded for PhD training in the Netherlands (fellowship number 230827/2012-8). MH was supported by the Chinese Scholarship Council (scholarship number 20108220166). RB and MH thanks CNPq and the Chinese Scholarship Council for the scholarship awarded.

REFERENCES

1 Choi, B. C., Hunter, D. J., Tsou, W. & Sainsbury, P. Diseases of comfort: primary cause of death in the 22nd century. *J Epidemiol Community Health* **59**, 1030-1034, (2005).
2 Hunter, D. J. Health needs more than health care: the need for a new paradigm. *Eur J Public Health* **18**, 217-219, (2008).
3 Puska, P. What are the drivers of the new paradigm? *Eur J Public Health* **18**, 219, (2008).
4 Layard, R. *Happiness: Lessons from a new science*. (Penguin Press, 2005).
5 Hood, L. & Friend, S. H. Predictive, personalized, preventive, participatory (P4) cancer medicine. *Nat Rev Clin Oncol* **8**, 184-187, (2011).
6 van der Greef, J. *et al.* Systems biology-based diagnostic principles as pillars of the bridge between Chinese and Western medicine. *Planta Med* **76**, 2036 (2010).
7 Academic Consortium for Integrative Medicine & Health (2016). Available on line at http://www.imconsortium.org/
8 Muehsam, D. & Ventura, C. Life rhythm as a symphony of oscillatory patterns: electromagnetic energy and sound vibration modulates gene expression for biological signaling and healing. *Glob Adv Health Med* **3**, 40-55 (2014).
9 Sterling, P. Allostasis: a model of predictive regulation. *Physiol Behav* **106**, 5-15, (2012).
10 van der Greef, J., van Wietmarschen, H., van Ommen, B. & Verheij, E. Looking back into the future: 30 years of metabolomics at TNO. *Mass Spectrom Rev* **32**, 399-415 (2013).
11 Most, E. I., Scheltens, P. & Van Someren, E. J. Prevention of depression and sleep disturbances in elderly with memory-problems by activation of the biological clock with light-a randomized clinical trial. *Trials* **11**, 19, (2010).
12 Van Wijk, R., Van Wijk, E. P., van Wietmarschen, H. A. & van der Greef, J. Towards whole-body ultra-weak photon counting and imaging with a focus on human beings: a review. *J Photochem Photobiol B* **139**, 39-46, (2014).
13 Bajpai, R. P., Van Wijk, E. P., Van Wijk, R. & van der Greef, J. Attributes characterizing spontaneous ultra-weak photon signals of human subjects. *J Photochem Photobiol B* **129**, 6-16, (2013).
14 de Mello Gallep, C. Ultraweak, spontaneous photon emission in seedlings: toxicological and chronobiological applications. *Luminescence* **29**, 963-968, (2014).
15 Cifra, M. & Pospisil, P. Ultra-weak photon emission from biological samples: definition, mechanisms, properties, detection and applications. *J Photochem Photobiol B* **139**, 2-10, (2014).
16 Pospisil, P., Prasad, A. & Rac, M. Role of reactive oxygen species in ultra-weak photon emission in biological systems. *J Photochem Photobiol B* **139**, 11-23, (2014).
17 Van Wijk, R. *Light in Shaping Life: Biophotons in Biology and Medicine*. (Boekenservice. nl, 2014).
18 German, J. B., Hammock, B. D. & Watkins, S. M. Metabolomics: building on a century of biochemistry to guide human health. *Metabolomics* **1**, 3-9, (2005).
19 Ramautar, R., Berger, R., van der Greef, J. & Hankemeier, T. Human metabolomics: strategies to understand biology. *Curr Opin Chem Biol* **17**, 841-846, (2013).
20 Beger, R. D. *et al.* Metabolomics enables precision medicine: "A White Paper, Community Perspective". *Metabolomics* **12**, 149, (2016).
21 Oltvai, Z. N. & Barabasi, A. L. Systems biology. Life's complexity pyramid. *Science* **298**, 763-764, (2002).
22 Adachi, Y., Kindzelskii, A. L., Ohno, N., Yadomae, T. & Petty, H. R. Amplitude and frequency modulation of metabolic signals in leukocytes: synergistic role of IFN-gamma in IL-6- and IL-2-mediated cell activation. *J Immunol* **163**, 4367-4374 (1999).
23 Lindstrom, B. & Eriksson, M. Salutogenesis. *J Epidemiol Community Health* **59**, 440-442, (2005).

24 Antonovsky, A. *The sense of coherence as a determinant of health*. (John Wiley, 1984).
25 van der Greef, J., Hankemeier, T. & McBurney, R. N. Metabolomics-based systems biology and personalized medicine: moving towards n=1 clinical trials? *Pharmacogenomics* **7**, 1087-1094, (2006).
26 Bircher, J. Towards a dynamic definition of health and disease. *Med Health Care Philos* **8**, 335-341, (2005).
27 Lancet, T. What is health? The ability to adapt. *The Lancet* **373**, 781 (2009).
28 Huber, M. *et al.* How should we define health? *BMJ* **343**, 1-3 (2011).
29 Awofeso, N. Re-defining 'Health'. *B World Health Organ* **83**, 802 (2005).
30 van Ommen, B., van der Greef, J., Ordovas, J. M. & Daniel, H. Phenotypic flexibility as key factor in the human nutrition and health relationship. *Genes Nutr* **9**, 423, (2014).
31 Wopereis, S. *et al.* Metabolic profiling of the response to an oral glucose tolerance test detects subtle metabolic changes. *PLoS One* **4**, e4525, (2009).
32 van der Greef, J. *et al.* The art and practice of systems biology in medicine: mapping patterns of relationships. *J Proteome Res* **6**, 1540-1559, (2007).
33 Snyderman, R. Personalized health care: from theory to practice. *Biotechnol J* **7**, 973-979, (2012).
34 Devaraj, B., Usa, M. & Inaba, H. Biophotons: Ultraweak light emission from living systems. *Curr Opin Solid St M* **2**, 188-193, (1997).
35 Schwabl, H. & Klima, H. Spontaneous ultraweak photon emission from biological systems and the endogenous light field. *Forsch Komplementarmed Klass Naturheilkd* **12**, 84-89, (2005).
36 Wijk, R. V. & Wijk, E. P. An introduction to human biophoton emission. *Forsch Komplementarmed Klass Naturheilkd* **12**, 77-83, (2005).
37 Kobayashi, M. *et al.* In vivo imaging of spontaneous ultraweak photon emission from a rat's brain correlated with cerebral energy metabolism and oxidative stress. *Neurosci Res* **34**, 103-113 (1999).
38 Van Wijk, R., Van Wijk, E. P., Wiegant, F. A. & Ives, J. Free radicals and low-level photon emission in human pathogenesis: state of the art. *Indian J Exp Biol* **46**, 273-309 (2008).
39 Ives, J. A. *et al.* Ultraweak photon emission as a non-invasive health assessment: a systematic review. *PLoS One* **9**, e87401, (2014).
40 Sauermann, G., Mei, W. P., Hoppe, U. & Stab, F. Ultraweak photon emission of human skin in vivo: influence of topically applied antioxidants on human skin. *Methods Enzymol* **300**, 419-428 (1999).
41 Cifra, M., Van Wijk, E., Koch, H., Bosman, S. & Van Wijk, R. Spontaneous ultra-weak photon emission from human hands is time dependent. *Radioengineering* **16**, 15-19 (2007).
42 Cohen, S. & Popp, F. A. Low-level luminescence of the human skin. *Skin Res Technol* **3**, 177-180, (1997).
43 Kobayashi, M., Kikuchi, D. & Okamura, H. Imaging of ultraweak spontaneous photon emission from human body displaying diurnal rhythm. *PLoS One* **4**, e6256, (2009).
44 Van Wijk, E. P., Van Wijk, R. & Cifra, M. in *European Conference on Biomedical Optics.* 66331J-66331J-66339 (International Society for Optics and Photonics, 2007).
45 Wijk, E. P. & Wijk, R. V. Multi-site recording and spectral analysis of spontaneous photon emission from human body. *Forsch Komplementarmed Klass Naturheilkd* **12**, 96-106, (2005).
46 Van Wijk, E. P., Ackerman, J. & Van Wijk, R. Effect of meditation on ultraweak photon emission from hands and forehead. *Forsch Komplementarmed Klass Naturheilkd* **12**, 107-112 (2005).
47 Van Wijk, E. P., Koch, H., Bosman, S. & Van Wijk, R. Anatomic characterization of human ultra-weak photon emission in practitioners of transcendental meditation(TM) and control subjects. *J Altern Complement Med* **12**, 31-38, (2006).

48 Van Wijk, E. P., Ludtke, R. & Van Wijk, R. Differential effects of relaxation techniques on ultraweak photon emission. *J Altern Complement Med* **14**, 241-250, (2008).
49 Cohen, S. & Popp, F. in *Biophotons*, 183-191 (Springer, 1998).
50 Cohen, S. & Popp, F. A. Biophoton emission of human body. *Indian J Exp Biol* **41**, 440-445, (2003).
51 Devaraj, B. *et al.* in *Opt Within Life Sci* 3-6 (Elsevier Amsterdam, 1994).
52 Jung, H. H. *et al.* Left-right asymmetry of biophoton emission from hemiparesis patients. *Indian J Exp Biol* **41**, 452-456, (2003).
53 Yang, J. M. *et al.* Left-right and Yin-Yang balance of biophoton emission from hands. *Acupunct Electrother Res* **29**, 197-211 (2004).
54 Bajpai, R. P. Squeezed state description of spectral decompositions of a biophoton signal. *Physics Letters A* **337**, 265-273, (2005).
55 Kobayashi, M., Devaraj, B. & Inaba, H. Observation of super-Poisson statistics of bacterial (Photobacterium phosphoreum) bioluminescence during the early stage of cell proliferation. *Physical Review E* **57**, 2129-2133, (1998).
56 Kobayashi, M. & Inaba, H. Photon statistics and correlation analysis of ultraweak light originating from living organisms for extraction of biological information. *Appl Opt* **39**, 183-192 (2000).
57 Van Wijk, R., Van Wijk, E. P. & Bajpai, R. P. Photocount distribution of photons emitted from three sites of a human body. *J Photochem Photobiol B* **84**, 46-55, (2006).
58 Draisma, H. H. *et al.* Similarities and differences in lipidomics profiles among healthy monozygotic twin pairs. *Omics* **12**, 17-31, (2008).
59 Koek, M. M., Muilwijk, B., van der Werf, M. J. & Hankemeier, T. Microbial metabolomics with gas chromatography/mass spectrometry. *Anal Chem* **78**, 1272-1281, (2006).
60 van Wietmarschen, H. A., van der Greef, J., Schroen, Y. & Wang, M. Evaluation of symptom, clinical chemistry and metabolomics profiles during Rehmannia six formula (R6) treatment: an integrated and personalized data analysis approach. *J Ethnopharmacol* **150**, 851-859, (2013).
61 Xia, J., Psychogios, N., Young, N. & Wishart, D. S. MetaboAnalyst: a web server for metabolomic data analysis and interpretation. *Nucleic Acids Res* **37**, W652-660, (2009).
62 Van Wijk, E. P., Van Wijk, R., Bajpai, R. P. & van der Greef, J. Statistical analysis of the spontaneously emitted photon signals from palm and dorsal sides of both hands in human subjects. *J Photochem Photobiol B* **99**, 133-143 (2010).
63 Shannon, P. *et al.* Cytoscape: a software environment for integrated models of biomolecular interaction networks. *Genome Res* **13**, 2498-2504, (2003).
64 Gao, J. *et al.* Metscape: a Cytoscape plug-in for visualizing and interpreting metabolomic data in the context of human metabolic networks. *Bioinformatics* **26**, 971-973, (2010).
65 Tarusov, B., Polivoda, A. & Zhuravlev, A. [Study on ultra-weak spontaneous luminescence of animal cells.]. *Biofizika* **6**, 490-492 (1960).
66 Tarusov, B. N., Polivoda, A. I., Zhuravlev, A. I. & Sekamova, E. N. [Ultraweak spontaneous luminescence in animal tissue]. *Tsitologiia* **4**, 696-699 (1962).
67 Barenboĭm, G. M., Domanskiĭ, A. N. & Turoverov, K. K. *Luminescence of biopolymers and cells*. (Plenum, New York, 1969).

Chapter 3

Tracking biochemical changes correlated with ultra-weak photon emission using metabolomics

Based on

Rosilene Cristina Rossetto Burgos, Kateřina Červinková, Tom van der Laan, Rawi Ramautar, Eduard P.A. Van Wijk, Michal Cifra, Slavik Koval, Ruud Berger, Thomas Hankemeier, Jan van der Greef

Tracking biochemical changes correlated with ultra-weak photon emission using metabolomics

Journal of Photochemistry and Photobiology B: Biology **163**, 237-245, (2016)

doi:10.1016/j.jphotobiol.2016.08.030

ABSTRACT

Ultra-weak photon emission (UPE) is light emitted spontaneously by biological systems without the use of specific luminescent complexes. UPE is emitted in the near-UV/UV-Vis/near-IR spectra during oxidative metabolic reactions; however, the specific pathways involved in UPE remain poorly understood. Here, we used HL-60 cells, a human promyelocytic cell line that is often used to study respiratory burst, as a model system to measure UPE kinetics together with metabolic changes. HL-60 cells were differentiated into neutrophil-like cells by culturing in all-trans-retinoic acid for 7 days. We then used a targeted metabolomics approach with capillary electrophoresis-mass spectrometry to profile intracellular metabolites in HL-60 cells and to investigate the biochemical changes based on the measured UPE profile. Our analysis revealed that the levels of specific metabolites, including putrescine, creatine, β-alanine, methionine, hydroxyproline, serine, and S-adenosylmethionine, were significantly altered in HL-60 cells after inducing respiratory burst. A comparison with recorded UPE data revealed that the changes in putrescine, glutathione, sarcosine, creatine, β-alanine, methionine, and hydroxyproline levels were inversely correlated with the change in UPE intensity. These results suggest that these metabolic pathways, particular the methionine pathway, may play a role in the observed changes in UPE in HL-60 cells and therefore demonstrate the potential for using UPE to monitor metabolic changes.

INTRODUCTION

Ultra-weak photon emission (UPE) is a biological phenomenon in which light is emitted spontaneously from living tissue without the need for external stimulation by light, specific bioluminescent complexes, or exogenous luminescent probes[1-3]. This weak light — which is emitted in the UVA/Vis range and can reach the near-IR spectrum (350–1300 nm) — is believed to result from the radiative transition of excited electron states that form as a consequence of reactions between biomolecules and reactive oxygen species (ROS)[1,4,5]. ROS are produced in all living cells that undergo oxidative respiration. Several studies have indicated that ROS play a role in UPE-generating reactions mediated by mitochondrial oxidative metabolism[6-8] and/or non-mitochondrial enzymes (for example, the NOx family of enzymes)[9-11]. Because oxidative reactions and ROS are known to underlie UPE[5,12,13], it is conceivable that biochemical changes and metabolic pathways can be measured in order to improve our understanding of UPE in living organisms.

Oxidative metabolism is comprised of several specific interconnected pathways, including the TCA cycle, oxidative phosphorylation, and glycolysis. Importantly, amino acids and nucleosides are the downstream end-products of the central carbon metabolism pathway (energy and mitochondrial electron transport)[14] and therefore may also be related to UPE. Furthermore, sulfur-containing amino acids have putative antioxidant properties[15].

Recently, Hossain *et al.* examined whether UPE can be correlated with proteomics data using stress alleviation in soybeans[16-18]. However, because the precise pathways that underlie UPE are not currently known, only a limited causal relationship can be established between UPE and the concentration of protein substrates. The principal challenge with respect to mechanistic studies of UPE is that even though the compounds that undergo radiative transition (e.g., singlet oxygen and triplet excited carbonyls) have been identified, these findings cannot be placed in the context of a metabolic pathway. Therefore, metabolomics seems to be a suitable tool for interpreting the molecular mechanisms underlying UPE.

Metabolomics is a powerful method used to detect perturbations in the metabolome (i.e., the comprehensive set of endogenous metabolites) that reflect metabolic changes downstream of changes in the genome, transcriptome, and/or proteome; thus, metabolomics provides a representative biochemical “snapshot” of a given organism both in health and in the disease state[19-21]. Therefore, metabolomics is considered an advanced biochemical approach capable of measuring target/non-target metabolites in a single sample analysis[22,23]. Within the field of metabolomics, a wide range of contemporary analytical techniques with

complementary separation methods are used to profile low molecular weight compounds in various biological samples. Here, we used capillary electrophoresis time-of-flight mass spectrometry (CE-TOF-MS) to generate a metabolic profile of amino acids and nucleosides; this technique is well-suited for the analysis of highly polar and/or charged compounds in a variety of biological samples[24-27]. In addition, CE-MS has been used previously to analyze intracellular metabolites in extracts obtained from a variety of cell lines[28-31].

With respect to the biological study of UPE, HL-60 cells were differentiated into neutrophil-like cells[32], and respiratory burst was induced. This provides a suitable model, as these processes are directly related to ROS balance. HL-60 cells can differentiate into neutrophil-like cells via the granulocytic pathway under specific culture conditions and by treatment with all-*trans*-retinoic acid (ATRA)[33]. Moreover, similar to human neutrophils, differentiated HL-60 cells express genes that encode subunits of NADPH oxidase[10], the primary function of which is to catalyze the production of superoxide anion radicals ($O_2^{\cdot-}$). NADPH serves as an electron donor by reducing molecular oxygen, and NADPH subunits translocate from the cytosol to the plasma membrane, where they bind other subunits and form a functional multi-component electron transfer system[34,35]. This process requires the rapid consumption of molecular oxygen (O_2) and leads to the cellular release of ROS, primarily $O_2^{\cdot-}$[35,36], which makes this cell line a robust model for studying UPE. Notably, isolated human neutrophils that were induced into respiratory burst using phorbol 12-myristate 13-acetate (PMA) have been studied in the context of UPE, thus representing the first study of photon emissions during respiratory burst recorded without the use of luminol enhancement[37].

ROS play a significant role in inflammatory processes[38] and in many diseases, including cancer[39], Alzheimer's disease[40], atherosclerosis[41,42], and rheumatoid arthritis[43,44]. Given the involvement of ROS in photon emissions, UPE may represent a novel tool for non-invasive diagnostic screening for diseases[7,45,46]. The diagnostic potential of UPE has been realized with respect to photon emissions from the human body[45-48]. Importantly, photon emissions can be measured continuously, thereby providing information regarding the dynamics of a biological system[49,50]. Therefore, a combination of UPE measurements with metabolomics can be used as an integrated tool to detect perturbations at the molecular level with unprecedented temporal resolution compared to standard biochemical methods.

Here, we used HL-60 cells that were differentiated into neutrophil-like cells as a model system to investigate the correlation between UPE and changes in metabolomics. Respiratory burst was induced in differentiated HL-60 cells with PMA, and the UPE profile was recorded; concurrently, the metabolomics profile was measured in extracts obtained from cells during respiratory burst. Establishing a correlation between metabolomics and

UPE data will help researchers identify the specific metabolic pathways involved in UPE and will therefore lead to a robust, non-invasive diagnostic application in which UPE measurements complement standard biochemical methods, providing a wider bandwidth in terms of dynamic readout.

METHODS

Reagents

The acute promyelocytic leukemia cell line HL-60 (CCL-240) was purchased from American Type Culture Collection (ATCC, Manassas, VA). Iscove's Modified Dulbecco's Medium (IMDM) without phenol red was obtained from Gibco-Life Technologies (Grand Island, NY). All-*trans*-retinoic acid (98% grade, R250; ATRA), phorbol 12-myristate 13-acetate (99% grade, PMA), sodium azide, and sodium chloride were purchased from Sigma-Aldrich (St. Louis, MO). Anti-mouse CD11b-PE (Clone M1/70) was obtained from eBioscience Affymetrix (Vienna, Austria). The background electrolyte (BGE; 1 M formic acid, pH 1.8), cation mix standard, and the internal standard ISTD (L-methionine sulfone) were purchased from Human Metabolome Technologies (Tsuruoka, Japan). Sodium hydroxide (1 M) was purchased from Agilent Technologies (Palo Alto, CA). Fused-silica capillaries were purchased from Polymicro Technologies (Phoenix, AZ). Milli-Q purified water was purchased from EMD Millipore (Billerica, MA).

Equipment

Photomultiplier tube (PMT)

A 2-inch PMT (series 9558B with S20 photocathode) was purchased from ET Enterprises (Sweetwater, TX). The detector was cooled to -25°C in order to reduce noise. Photon emission intensity was recorded over time (in counts/sec). A Peltier element was used inside the dark chamber to maintain the sample at 37°C. The PMT was set in a vertical position at the top of the dark chamber. Background emission (average counts/sec) was measured before each sample measurement.

Capillary electrophoresis coupled to mass spectrometry

CE-TOF-MS was performed using an Agilent CE 7100 system (Agilent Technologies) coupled to a time-of-flight mass spectrometer (Agilent 6230) via a sheath-liquid interface using an Agilent 1100 isocratic HPLC pump, an Agilent G1603A adapter kit, and an Agilent G1607A CE-ESI-MS sprayer kit (Agilent Technologies, Waldbronn, Germany). The sheath-liquid interface was a mixture of methanol, water, and formic acid (50/50/0.1, v/v/v) that was

delivered at a flow rate of 10 µl/min. An Agilent Mass Hunter Workstation was used to control the system and to acquire all data.

Cell culture

HL-60 cells were cultured in IMDM medium without phenol red supplemented with 10% fetal calf serum (v/v) and 1% penicillin/streptomycin (v/v). The cells were incubated at 37°C in 5% CO_2. Cells were seeded at 0.4 x 10^6 cells/ml and maintained at 0.4-1.5 x 10^6 cells/ml in accordance with the instructions provided by ATCC. For experiments, the cells were used during the exponential growth phase. Cell number and viability were determined using the trypan blue exclusion method with an automated cell counter (Bio-Rad). Viability was >85% on days 2, 5, 6, and 7. Cells were exposed to 1 µM ATRA (from stock DMSO solution) or control (DMSO only) on the first day of the experiments. The 1 µM ATRA solution was prepared fresh in DMSO and stored at -20°C. All experiments were performed at cell passage number 16.

Fluorescence-activated cell sorting (FACS)

Flow cytometry was performed using the neutrophil marker CD11b to monitor the differentiation of HL-60 cells. Control and ATRA-treated cells were divided into aliquots containing 10^6 cells/ml, washed in PBS, and then incubated for 20 min in the dark at 4°C with 100 µl phosphate-buffered saline (PBS) containing 0.125 µg CD11b-PE, 2% fetal bovine serum, and 0.05% sodium azide. The cells were then washed in PBS, resuspended in 1 ml PBS, and kept at 4°C until analysis, which was performed as described previously[51,52]. Negative control samples were handled using the same conditions as above, except the CD11b-PE antibody was omitted.

Experimental design

The experimental protocol is depicted in **Fig. 1**. HL-60 cells were maintained in the exponential phase as previously described[51], with slight modifications. During cell passage and density adjustment, the cells were induced to differentiate along the granulocytic pathway by including 1 µM ATRA in the medium for up to 7 days. Four flasks of original cultured cells were randomly assigned to receive ATRA (treated cells) or DMSO (non-treated control cells). Three original flasks were split into twelve flasks and therefore, treated with ATRA (the red flasks in **Fig. 1**), and one original flask was split into two flasks (the green flasks in **Fig. 1**). Each ATRA-treated flask was analyzed on a given measurement day (i.e., day 2, 5, 6, or 7; see **Fig. 1**). The flasks were incubated as described above for up to 7 days, and PMA was applied on the measurement day to induce respiratory burst, after which the

UPE profile was measured. The ATRA-treated cells were analyzed on days 2, 5, 6, and 7; the control cells were analyzed on days 2 and 7. For generating the metabolic profile, cell samples were collected at four time points (TP1, TP2, TP3, and TP4; see **Fig. 1B**), followed by extraction and analysis using CE-TOF-MS.

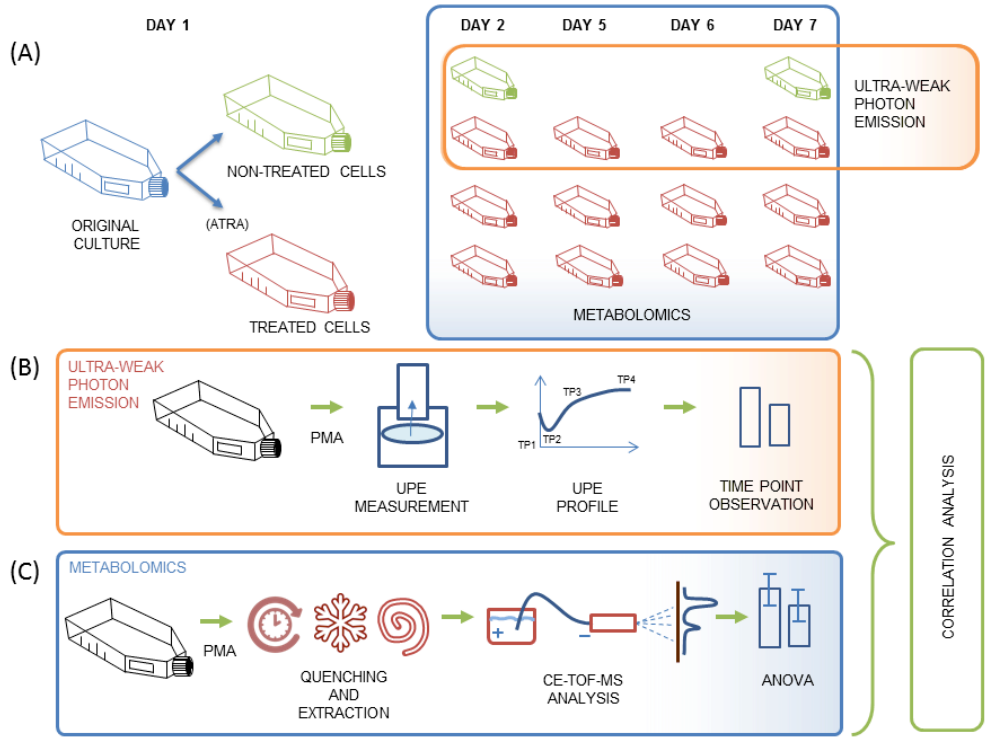

Figure 1. The experimental protocol used in the study. (A) The HL-60 cell cultures and ATRA treatment. (B) The protocol used for inducing respiratory burst and measuring UPE. (C) The protocol for metabolic profiling. In (A), the HL-60 cells were split into a total of 14 flasks; 12 of these flasks were treated with ATRA (treated cells; red), and two were treated with vehicle (non-treated cells; green). (B) On days 2, 5, 6, and 7, PMA was applied to all flasks (including control flasks) to induce respiratory burst, and UPE profile was recorded at the indicated time points (TP1 through TP4; TP1 was prior to the addition of PMA). (C) Metabolomics samples were collected at the time points shown in (B). After sample collection, liquid-liquid extraction was used to obtain cell extracts, and the metabolic profile was recorded using CE-TOF-MS. Lastly, a correlation analysis was performed between the UPE data and metabolic profiles.

Ultra-weak photon emission (UPE)

Cells were stimulated with PMA at a final concentration of 54 nM; after a small delay of approximately 30 seconds (due to the time required to transfer the sample to the measuring chamber), the UPE profile was measured. The cells were measured in the exhausted

medium in a small Petri dish positioned as close as possible to the PMT detector. Control measurements were performed on PMA-stimulated undifferentiated cells (i.e., cells that were incubated with DMSO only). The sample holder was heated to 37°C, and background activity (which averaged 17.9 counts/second) was measured before each experiment. UPE intensity was recorded with 1-second bins, and each sample measurement lasted 150 minutes.

Collection, quenching, and extraction of cell pellets for metabolomics

To collect cell pellets, each flask was split into four aliquots. One aliquot was immediately quenched for metabolomics analysis at time point 1 (TP1), without the addition of PMA. The other three aliquots were treated with PMA (to a final concentration of 54 nM), and then quenched at TP2, TP3, and TP4, which corresponded to 1, 75, and 150 minutes of PMA stimulation, respectively. ATRA-treated samples were collected in triplicate.

Quenching was performed using a standard method[53,54], with minor modifications for the suspension cell type used in this study. Aliquots containing 3 x 10^6 cells were centrifuged at 1000 rpm for 4 minutes. The supernatant (i.e., culture medium) was collected and stored on dry ice, and the cell pellet was resuspended in 1 ml 0.9% NaCl at 0-2°C. The cell suspension was centrifuged immediately, the supernatant was removed, and the cell pellets were stored at -80°C.

To measure intracellular metabolites, cell pellets were extracted in an ice bath using conventional liquid-liquid extraction (using the Bligh and Dyer method[55]). The cell pellets were resuspended in 200 µl methanol (at -20°C) and 80 µl Milli-Q water (at 4°C), followed by the addition of 1.25 µl of internal standard (ISTD; 1 mM) to each sample.

Each methanol/Milli-Q water aliquot (containing resuspended cells) was transferred to a fresh Eppendorf tube containing 200 µl chloroform. The two phases were mixed, and the polar phase was transferred to a fresh Eppendorf tube. The dried samples (i.e., the polar phase) were resuspended in 20 µl H_2O and 1.25 µl ammonium acetate (5 M) and subsequently analyzed using CE-MS. Quality control pools (containing aliquots of all samples and replicates) were prepared from 20 µl of each MeOH/H_2O sample and extracted as described above.

CE-TOF-MS experiments

Intracellular cationic metabolites were measured in ATRA-treated and non-treated cells. The methodology used to profile cationic metabolites with CE-TOF-MS is based on a procedure first described by Soga *et al.*[25-27,56,57], with slight modification. In brief, cationic metabolites

were separated using a bare fused-silica capillary (50 µm ID, 80 cm total length) with formic acid (pH 1.8) as the background electrolyte (BGE). Milli-Q water and sodium hydroxide (1 M) were used for capillary conditioning. Prior to each CE-MS run, the capillary was preconditioned by rinsing sequentially with water, sodium hydroxide, water, and BGE; each step lasted 2 min. The sheath-liquid interface was delivered at a flow rate of 1 ml/min (split 1:100). A mixture containing 60 cationic metabolites was used as a standard. The samples were injected in the hydrodynamic mode by applying a pressure of 50 millibars for 2 min (corresponding to a volume of approximately 120 nl; such a large sample volume was possible due to the dynamic pH junction). Subsequently, a plug of BGE was added at a pressure of 50 millibars for 1 min. Voltage (27 kV) was applied for 40 minutes at 25°C. Electrospray ionization-mass spectrometry (ESI-MS) was performed in the positive-ion mode. The capillary, fragmentor, and skimmer voltages were set to 4000, 100, and 50 V respectively. The nebulizer pressure was 5 psi, and drying gas was delivered at a rate of 7 l/min at 300°C. Exact mass data were acquired at a rate of 1.5 cycles/sec over a 50–1000 *m*/*z* range. Metabolites were identified based on accurate mass information and migration times obtained using standard compounds.

After CE-TOF-MS analysis, the peak area of each identified metabolite was corrected using the internal standard ISTD (L-methionine sulfone) in order to obtain the response ratio (i.e., target compound/ISTD). A sample containing pooled cell pellet extracts (i.e., a pooled quality control sample) was prepared and measured after every ten samples[58]. The reliability of the measurements was determined by calculating: *i*) the repeatability (i.e., the relative standard deviation, RSD) of each metabolite in a quality control pool; *ii*) the repeatability of academic standards; and *iii*) the repeatability between sample replicates. Metabolites that exceeded 30% of the RSD in at least one of the three analytical controls were excluded from the analysis due to technical and/or analytical variations[58,59].

Statistical analysis

The metabolite results were uploaded to the web-based tool metaboAnalyst for high-throughput analysis of the comprehensive metabolomics data[60,61]. The data were log-transformed and auto-scaled by the standard deviation in order to obtain a normal distribution[59]. First, an analysis of variance (ANOVA) was used to detect metabolites that differed significantly between the ATRA-treated cells and non-treated cells. Next, Spearman's correlation was calculated using the R statistics package in order to analyze the correlation between UPE and the metabolomics data.

RESULTS AND DISCUSSION

Ultra-weak photon emission profile

To investigate whether UPE profile is correlated with the metabolic profile, we used PMA to induce respiratory burst in differentiated (i.e., ATRA-treated) and undifferentiated (control) HL-60 cells, and then measured the metabolomics and UPE profiles over the course of 7 days. The profile that was obtained was both reproducible and well-defined. Control cells were recorded on days 2 and 7.

The UPE profiles of undifferentiated and differentiated cells on day 7 are shown in **Fig. 2A**, and the UPE profiles of differentiated cells on days 2, 5, 6, and 7 are shown in **Fig. 2B**. The initial rapid decay in the first 5-7 min of the UPE profile is due to conditioning of the sample in the dark chamber (i.e., weak illumination of the sample by external visible light during placement of the sample)[62].

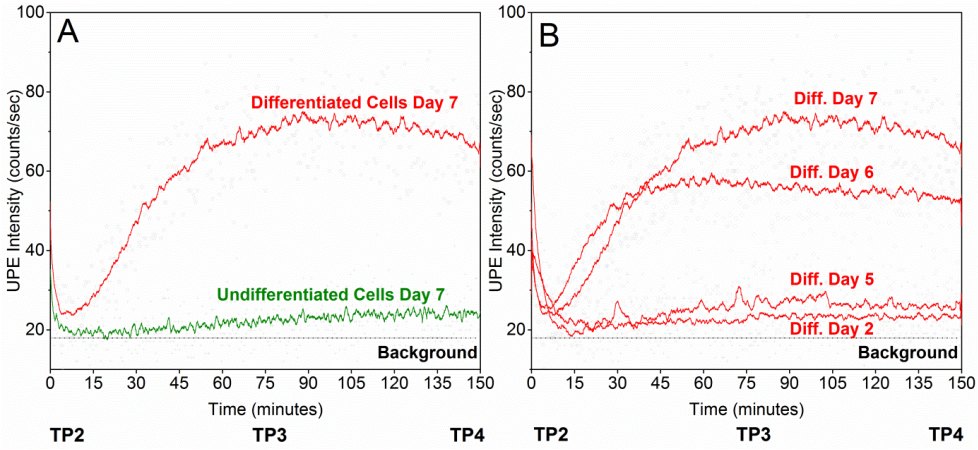

Figure 2. UPE profiles recorded from differentiated (ATRA-treated) and undifferentiated HL-60 cells on the indicated days. Cell suspensions (0.5 x 10^6 cells/ml) were recorded in the dark for 150 minutes at 37°C. The running average is based on the raw data (scatter) and represents 100 points (i.e., 100 seconds). TP1: samples measured without PMA induction; TP2, TP3, and TP4: samples measured after 1, 75, and 150 minutes of induction with PMA, respectively. Note that UPE was not measured in the TP1 samples.

Fig. 2A shows that the UPE intensity of differentiated cells increased considerably compared to undifferentiated cells, indicating that neutrophil-like cells have higher levels of photon emissions during PMA-induced respiratory burst. Neutrophils are specialized cells that produce a variety of reactive agents, including superoxide anion radicals ($O_2^{\cdot-}$), which increases UPE. The PMA-induced UPE profile increased steadily during the 7 days of ATRA treatment (**Fig. 2B**), which was likely due to the increased number of differentiated neutrophil-like cells during ATRA treatment. Thus, UPE intensity measured on days 6 and 7

(which averaged 59 photons/sec) were significantly higher than on days 2 and 5 (which averaged 24 photons/sec). On day 7, UPE intensity reached its peak value of approximately 70 photons/sec after 75 minutes of PMA stimulation (i.e., at time point 3 in **Fig. 2**).

The significant increase in UPE on days 6 and 7 in the differentiated cells is consistent with previous reports showing that cellular differentiation into neutrophil-like cells peaked after six days of culture in the presence of 1 μM ATRA[63]. Our results are also supported by FACS experiments performed on day 7, which show that approximately 80-90% of ATRA-treated cells had differentiated into neutrophil-like cells (**Supplementary Fig. S1**); in contrast, non-treated control cells contained only a small number of differentiated cells after seven days in culture, likely due to spontaneous differentiation (**Supplementary Fig. S1**). These results are consistent with the low UPE profile measured in control (non-treated) cells. Together, these results suggest that UPE qualitatively reflects the degree to which HL-60 cells are differentiated into neutrophil-like cells by ATRA. Chemiluminescence — which differs from UPE solely by the addition of an exogenous luminescent reagent (e.g., luminol) — has been used previously to evaluate the differentiation of HL-60 cells into neutrophil-like cells[9,64].

Interestingly, we found that the increase in UPE progressed slowly from day 2 to day 5, then increased rapidly from days 5 to day 6 (**Fig. 2B**).

Metabolic profiling of HL-60 cells using CE-TOF-MS

Our primary objective was to determine whether changes in the metabolic profile could be correlated with measurable changes in UPE, using HL-60 cells as a model system. Toward this end, we used CE-TOF-MS to profile the cationic metabolites contained in extracts of HL-60 cells in order to determine: *i*) whether metabolic changes occur at this level, and *ii*) whether any such changes can be correlated with a change in UPE. Under the conditions used in this study, CE-TOF-MS is well-suited for analyzing amino acids, nucleosides, and amines in cell lines. For details regarding the analytical reproducibility and detection sensitivity, we refer the reader to the work of Soga and colleagues (see also **section CE-TOF-MS Experiments**), who first developed this methodology and used it to analyze a wide range of biological samples[25-27,56,57]. To compare the metabolic profiles obtained using CE-TOF-MS with the UPE data, we designed the global workflow protocol depicted in **Fig. 1** (see **section Experimental Design**).

In total, our CE-TOF-MS analysis identified 50 compounds in extracts obtained from HL-60 cells. However, only 24 of these compounds were used for our statistical analysis, as the RSD in the peak area of these 24 metabolites was <30% (see criteria in **CE-TOF-MS Experiments section**).

With respect to our analysis of the data generated by the CE-TOF-MS experiments, we evaluated three distinct profiles. The first profile included the ATRA-treated samples prior to stimulation with PMA (i.e., TP1). The second and third profiles used ATRA-treated samples that were measured at all time four points (i.e., TP1 through TP4) and were based on the UPE profile obtained (see **Fig. 2B**). The samples obtained on days 2 and 5 were similar with respect to their UPE profile intensities; therefore, their metabolomics data were pooled into one group, yielding the second profile. Similarly, the metabolomics data obtained from days 6 and 7 were pooled into one group, yielding the third profile.

To increase our statistical power, we calculated the similarity between the time series of UPE data (see **Fig. 2B**). We calculated normalized Manhattan distances (i.e., the sum of the absolute differences between two time series) for each day of the UPE profile and obtained the distances presented in **Table 1**.

Table 1. Manhattan distances calculated for UPE data profiles.

UPE Profile Day	Second Profile		Third Profile	
	Day2	*Day5*	*Day6*	*Day7*
Day 2	-	0.17	0.76	1
Day 5		-	0.70	0.94
Day 6			-	0.35
Day 7				-

The effect of ATRA treatment: First Profile

We used ATRA to induce granulocytic differentiation of HL-60 cells (i.e., into mature functional neutrophil-like cells) via the retinoic acid receptor (RAR). Two classes of nuclear receptors (RARs and RXR) are associated with morphological changes and other events occurring at the cell surface and in the plasma membrane, cytoplasm, and nucleus[65,66]. With respect to metabolites, polyamines — particularly spermidine — is required for inducing differentiation[67]. However, in our analysis, the RSD of spermidine was >30%; therefore, this metabolite was excluded from the statistical analysis.

In our experiments, we measured the target metabolic profile (i.e., amino acids and nucleosides) in undifferentiated HL-60 cells and in HL-60 cells during ATRA-induced differentiation. With respect to the metabolic changes mediated by ATRA-induced differentiation, an ANOVA revealed nine compounds that changed significantly from day 2 through day 7 (**Fig. 3** and **Table 2**).

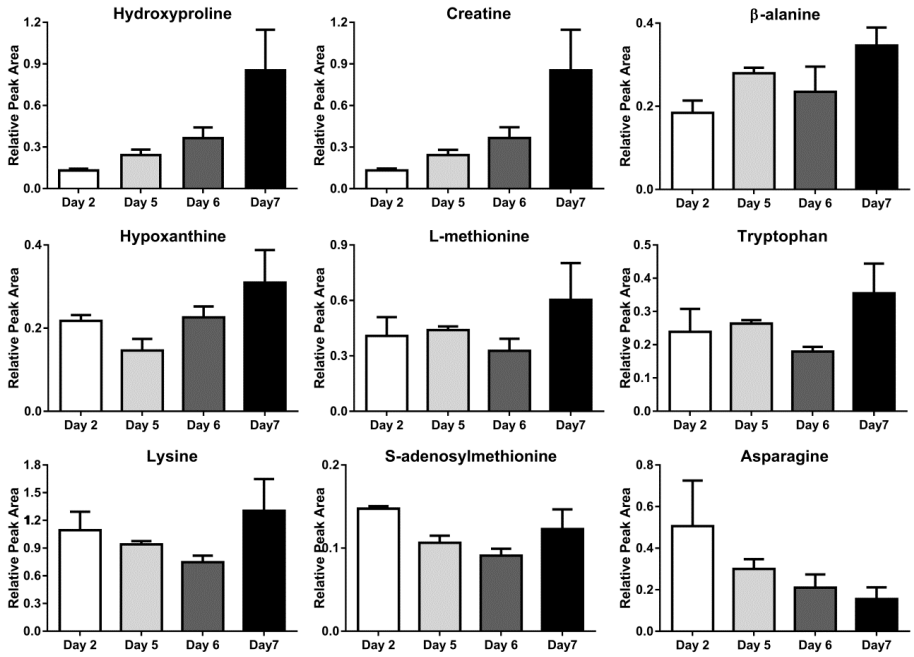

Figure 3. Metabolic profile of HL-60 cells during ATRA-induced differentiation (TP1 samples only). The data for each metabolite are presented as the mean ±SD of the relative peak area. Each day's value represents the average of three sample replicates measured at time point 1 (TP1). We performed pair-wise ANOVA analyses, and shown are the nine compounds that differed significantly (p<0.05) between at least two days; for additional information, see **Table 2**.

Table 2. Summary of the metabolic profile obtained in ATRA-treated HL-60 cells.

Compound	*p*-value	-log10(*p*)	FDR[a]	Fisher LSD[b]
Hydroxyproline	$6.51e^{-06}$	5.19	0.00	D5 - D2; D6 - D2; D7 - D2; D6 - D5; D7 - D5; D7 - D6
Creatine	$6.97e^{-06}$	5.16	0.00	D5 - D2; D6 - D2; D7 - D2; D6 - D5; D7 - D5; D7 - D6
β-alanine	0.004	2.41	0.02	D5 - D2; D7 - D2; D7 - D6
Hypoxanthine	0.002	2.62	0.01	D2 - D5; D7 - D2; D6 - D5; D7 - D5; D7 - D6
Methionine	0.046	1.33	0.10	D7 - D2; D7 - D6
Tryptophan	0.013	1.90	0.04	D7 - D2; D5 - D6; D7 - D6
Lysine	0.017	1.78	0.04	D2 - D6; D7 - D5; D7 - D6
Asparagine	0.007	2.19	0.03	D2 - D6; D2 - D7; D5 - D7
S-adenosylmethionine	0.002	2.80	0.01	D2 - D5; D2 - D6; D2 - D7; D7 - D6

a FDR: false discovery rate

b Fisher LSD: significance (p<0.05) between the **two indicated** *days (D).*

Specifically, hydroxyproline, creatine, β-alanine, hypoxanthine, methionine, tryptophan, and lysine increased during ATRA treatment, whereas asparagine decreased. Lastly, although S-adenosylmethionine (SAM) fluctuated slightly during the seven days of ATRA treatment, the

level of SAM generally decreased (**Fig. 3**). Our findings regarding the effect of cell differentiation on SAM levels is consistent with a previous study in which the authors concluded that the decrease in SAM levels in HL-60 cells during differentiation was a consequence — rather than the cause — of differentiation[68].

Analysis based on UPE profiles (days 2 and 5): Second Profile

Our ANOVA results from the second profile revealed that only one metabolite — putrescine — changed significantly during respiratory burst. Putrescine also changed significantly during the four times points (**Fig. 4** and **Table 3**). Putrescine is one of three natural polyamines. Putrescine, spermidine, and spermine play multifunctional roles in cell growth and differentiation, and several studies of HL-60 cell metabolism and differentiation revealed the significance of putrescine with respect to proliferation and apoptosis[69,70]. Our results show that the levels of putrescine decrease during PMA-induced respiratory burst.

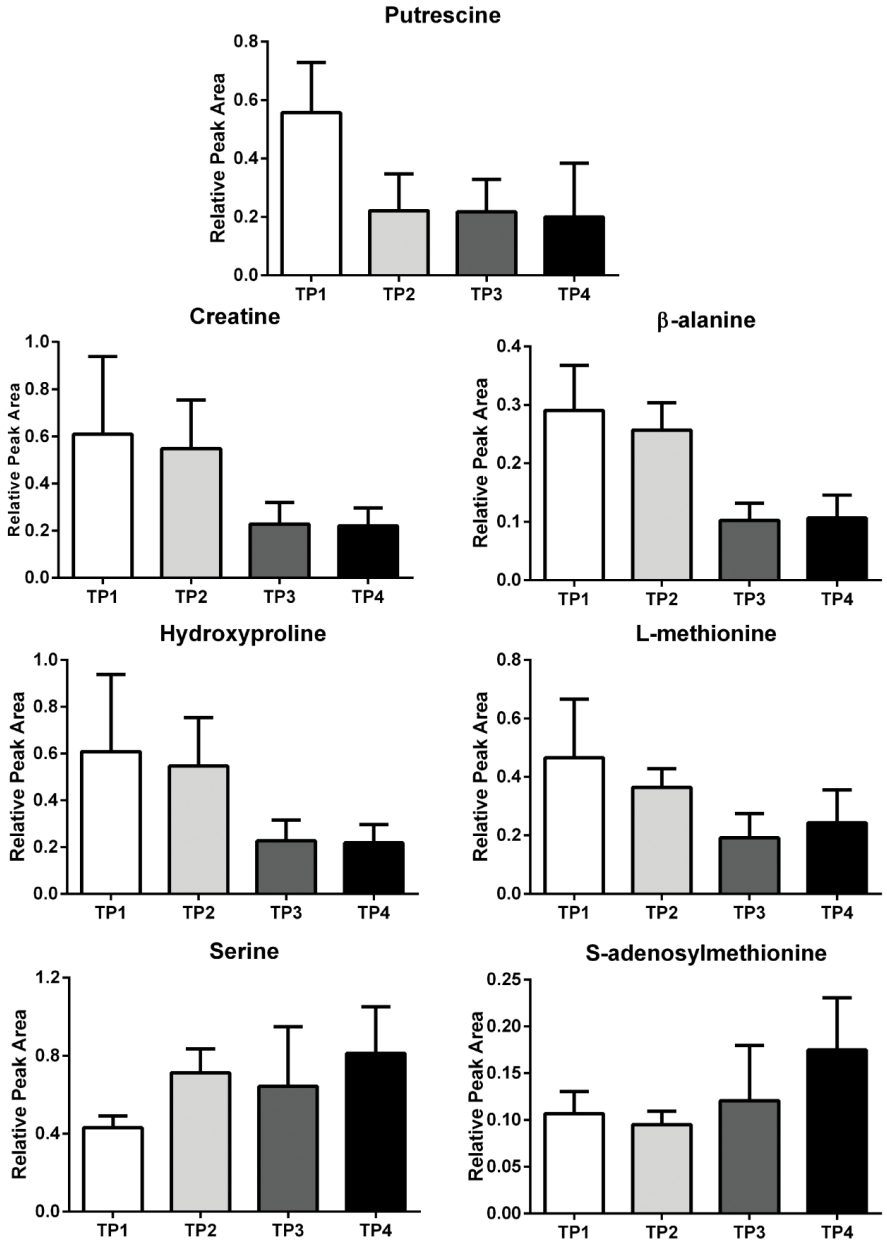

Figure 4. Summary of the metabolites that changed during respiratory burst in the second and third profiles (samples analyzed using the UPE profile similarities) at the indicated time points (TP1 through TP4). The data are presented as the mean ±SD of the relative peak area. Each time point represents the average of three sample replicates. We performed a pair-wise ANOVA at different time points, and only the compounds that differed significantly (p<0.05) between at least two time points are shown; for additional information, **see Table 3**.

Table 3. Summary of the metabolites that changed significantly over the four time points (i.e., TP1 through TP4) in the second and third profiles.

Profile Analysis	Compound	*p*-value	-log10(*p*)	FDR[a]	Fisher LSD[b]
Second Profile	Putrescine	0.009	2.04	0.16	TP1 - TP2; TP1 - TP3; TP1 - TP4
Third Profile	Creatine	0.001	3.19	0.01	TP1 - TP3; TP1 - TP4; TP2 - TP3; TP2 - TP4
Third Profile	β-alanine	$1.18e^{-06}$	5.93	0.00	TP1 - TP3; TP1 - TP4; TP2 - TP3; TP2 - TP4
Third Profile	Methionine	0.004	2.40	0.03	TP1 - TP3; TP1 - TP4; TP2 - TP3
Third Profile	Hydroxyproline	0.001	3.20	0.01	TP1 - TP3; TP1 - TP4; TP2 - TP3; TP2 - TP4
Third Profile	S-adenosylmethionine	0.038	1.42	0.12	TP4 - TP1; TP4 - TP2; TP4 - TP3
Third Profile	Serine	0.021	1.69	0.08	TP2 - TP1; TP4 - TP1

a FDR: false discovery rate

b Fisher LSD: significance (p<0.05) between the* two indicated *days (D).

Analysis based on UPE profiles (days 6 and 7): Third Profile

Based on the third analysis profile, in which UPE intensity was highest (i.e., in the samples measured on days 6 and 7), the ANOVA analysis identified six metabolites that changed significantly over the four time points (**Fig. 4** and **Table 3**). Specifically, creatine, β-alanine, methionine, and hydroxyproline decreased during PMA stimulation, whereas S-adenosylmethionine (SAM) and serine increased during PMA stimulation.

Comparing the results from the first profile with the results from the third profile revealed that four compounds — creatine, β-alanine, methionine, and hydroxyproline — increased during ATRA-induced differentiation. Thus, ATRA caused a slight increase in the intracellular concentration of these compounds, and inducing respiratory burst decreased the intracellular concentration of these compounds, thereby reflecting a switch in cellular function.

Furthermore, given the changes observed in methionine and S-adenosylmethionine, our results suggest that the methionine pathway is affected by respiratory burst. In the transmethylation pathway, methionine regeneration requires vitamin B12[71,72] and the subsequent reduction of cobalamin Co(III) to Co(I) via the folate pathway. The reduced levels of methionine in our study may be attributed to the electron species generated during respiratory burst. Indeed, this hypothesis is supported by Danishpajooh *et al*., who reported the involvement of NO species in the folate and methionine pathways[73]. However, in-depth studies including methyltransferase enzymes and tracer-based metabolomics are needed in order to further understand the role of this pathway in UPE.

Correlation between UPE and metabolomics

Next, we examined the correlation between the UPE data and metabolomics profiles. Accordingly, we performed a Spearman's rank correlation test. Because the UPE data were not distributed normally, we used the non-parametric Spearman's correlation (see **section Statistical analysis**).

For the metabolomics data, we used the same sets of sample profiles described above (i.e., the second and third profiles). We calculated the average of three sample replicates for each time point and examined the correlation between these results and the UPE values. The UPE data used in the correlation analysis were calculated using the average value measured 10 seconds before each time point and the average value measured 10 seconds after the respective time point. For TP1, we used the average of the background value that was recorded on that day. For TP2, we used the data measured at 420 seconds (rather than 60 seconds), due to the rapid decay observed at the start of this UPE measurement. For TP4, we calculated the average of the last 20 seconds. Our analysis revealed a significant correlation between the UPE data and both putrescine and glutathione in the differentiated cells combined from days 2 and 5 (the second profile). In addition, we observed a significant correlation between the UPE data and sarcosine, creatine, β-alanine, hydroxyproline, and methionine in the differentiated cells combined from days 6 and 7 (the third profile). The results of the correlation analysis are summarized in **Table 4**. Six of these seven compounds were identified previously based on our ANOVA results.

Table 4. Spearman's rank correlation between the UPE and metabolomics data.

Compound	Profile	Correlation Coefficient	*p*-value
Putrescine	Second Profile	-0.844	0.008
Glutathione	Second Profile	-0.770	0.025
Sarcosine	Third Profile	-0.910	0.002
Creatine	Third Profile	-0.742	0.035
β-alanine	Third Profile	-0.917	0.001
Hydroxyproline	Third Profile	-0.743	0.035
Methionine	Third Profile	-0.793	0.019

Next, we used the web-based tool metaboAnalyst to perform a pathway enrichment analysis. Here, we report the pathways that had a statistically significant effect on the compounds identified by our correlation analysis. The results show that the following metabolic pathways are involved: arginine, proline, glycine, serine, threonine, β-alanine metabolism, glutathione, cysteine, and methionine (**Supplementary Fig. 2**).

Oxidative metabolism underlies UPE; specifically, ROS produced during metabolism oxidize biomolecules, which leads to the generation of excited electron states and the subsequent emission of photons[5]. Thus, increased UPE intensity reflects an increased rate of oxidative reactions and increased oxidative stress. Under oxidative stress conditions, cellular antioxidant mechanisms are activated, including the production of antioxidants such as glutathione, which requires precursors such as methionine[74]. Thus, a prolonged state of oxidative stress can deplete methionine. This scenario is consistent with our finding that UPE intensity is inversely correlated with methionine levels and is consistent with findings reported by Panayiotidis *et al.*[75], who examined the correlation between oxidative stress and regulation of the methionine pathway in human lung epithelial-like cells. The transmethylation/transsulfuration metabolic pathway has a direct effect on the levels of SAM, methionine, and glutathione. SAM is the principal methyl donor in the synthesis of DNA, polyamines, RNA, and phospholipids[76]. Thus, changes in SAM levels due to oxidative metabolism can affect the methylation process, thereby depleting the aforementioned metabolites, as reported by Panayiotidis *et al*[75]. Moreover, James *et al*. reported that increased levels of oxidative stress are associated with reduced methylation capacity and reduced levels of methionine[77], and our findings are consistent with these results. In addition, perturbations in methionine levels are associated with cardiovascular disease[78], liver disease[79], and cognitive impairment[80,81].

Our correlation analysis revealed that the dynamic behavior of UPE was fundamental to our ability to monitor biochemical changes. Specifically, we found that UPE was significantly correlated with changes in amino acids and nucleosides. This finding indicates that UPE provides important biological information at the molecular level; therefore, UPE might be a used as a dynamic parameter together with metabolomics for tracking biochemical changes in biological systems.

CONCLUSIONS

Here, we report the results of the first integrated study using differentiated HL-60 cells as a model system for investigating whether changes in ultra-weak photon emission are correlated with changes in the metabolic profile. Specifically, HL-60 cells were differentiated into neutrophil-like cells and induced to undergo respiratory burst. The temporal UPE profile was recorded during respiratory burst, and cationic metabolites were measured in cell extracts and used to create a metabolomics profile. Our results revealed that several metabolites are significantly correlated with changes in UPE. Although these findings suggest that the methionine pathway plays a role in UPE, additional experiments are needed in order to elucidate the precise role of methionine metabolism in UPE. Therefore, future

studies should use analytical platforms that include additional metabolites, including metabolites that are associated with oxidative stress, oxylipins, and cellular energy levels, thereby providing a more comprehensive metabolic profile.

In summary, we provide the first experimental evidence that measuring UPE can be used to study metabolic profiles. Specifically, we found that the concentration profiles of putrescine, glutathione, sarcosine, creatine, and β-alanine were significantly correlated with the UPE signal, suggesting that the methionine pathway plays a key role in UPE. These results pave the way for future research regarding metabolic pathways that underlie UPE, and they provide important information regarding the potential use of UPE as a diagnostic tool.

ACKNOWLEDGMENTS

We thank Ondřej Kučera and Cristiano de Mello Gallep for valuable comments and detailed feedback regarding the manuscript. R.C.R.B. was supported by the Brazilian Scholarship Program “Science without Borders” of the Brazilian National Council for Scientific and Technological Development (Conselho Nacional de Desenvolvimento Científico e Tecnológico, fellowship no. 230827/2012-8). K.Č. and M.C. were supported by the Czech Science Foundation (grant no. GP13-29294S).

REFERENCES

1 Cifra, M. & Pospisil, P. Ultra-weak photon emission from biological samples: definition, mechanisms, properties, detection and applications. *J Photochem Photobiol B* **139**, 2-10, (2014).
2 Devaraj, B., Usa, M. & Inaba, H. Biophotons: Ultraweak light emission from living systems. *Curr Opin Solid St M* **2**, 188-193, (1997).
3 Schwabl, H. & Klima, H. Spontaneous ultraweak photon emission from biological systems and the endogenous light field. *Forsch Komplementarmed Klass Naturheilkd* **12**, 84-89, (2005).
4 Popp, F.-A. Properties of biophotons and their theoretical implications. *Indian J Exp Biol* **41**, 391-402 (2003).
5 Pospisil, P., Prasad, A. & Rac, M. Role of reactive oxygen species in ultra-weak photon emission in biological systems. *J Photochem Photobiol B* **139**, 11-23, (2014).
6 Galantsev, V. P., Kovalenko, S. G., Moltchanov, A. A. & Prutskov, V. I. Lipid peroxidation, low-level chemiluminescence and regulation of secretion in the mammary gland. *Experientia* **49**, 870-875 (1993).
7 Rastogi, A. & Pospisil, P. Ultra-weak photon emission as a non-invasive tool for the measurement of oxidative stress induced by UVA radiation in Arabidopsis thaliana. *J Photoch Photobio B* **123**, 59-64, (2013).
8 Birtic, S. *et al.* Using spontaneous photon emission to image lipid oxidation patterns in plant tissues. *Plant J* **67**, 1103-1115, (2011).
9 Ashkenazi, A. & Marks, R. Luminol-dependent chemiluminescence of human phagocyte cell lines: comparison between DMSO differentiated PLB 985 and HL 60 cells. *Luminescence* **24**, 171-177 (2009).
10 Bedard, K. & Krause, K. H. The NOX family of ROS-generating NADPH oxidases: physiology and pathophysiology. *Physiol Rev* **87**, 245-313, (2007).

11 Bylund, J., Björnsdottir, H., Sundqvist, M., Karlsson, A. & Dahlgren, C. in *Neutrophil Methods and Protocols* Vol. 1124 *Methods in Molecular Biology* (eds Mark T. Quinn & Frank R. DeLeo) Ch. 21, 321-338 (Humana Press, 2014).

12 Kobayashi, M. *et al.* In vivo imaging of spontaneous ultraweak photon emission from a rat's brain correlated with cerebral energy metabolism and oxidative stress. *Neurosci Res* **34**, 103-113 (1999).

13 Van Wijk, R., Van Wijk, E. P., Wiegant, F. A. & Ives, J. Free radicals and low-level photon emission in human pathogenesis: state of the art. *Indian J Exp Biol* **46**, 273-309 (2008).

14 Noor, E., Eden, E., Milo, R. & Alon, U. Central Carbon Metabolism as a Minimal Biochemical Walk between Precursors for Biomass and Energy. *Mol Cell* **39**, 809-820, (2010).

15 Atmaca, G. Antioxidant Effects of Sulfur-Containing Amino Acids. *Yonsei Med J* **45**, 776-788 (2004).

16 Komatsu, S., Kamal, A. H., Makino, T. & Hossain, Z. Ultraweak photon emission and proteomics analyses in soybean under abiotic stress. *Biochim Biophys Acta* **1844**, 1208-1218, (2014).

17 Hossain, Z., Makino, T. & Komatsu, S. Proteomic study of beta-aminobutyric acid-mediated cadmium stress alleviation in soybean. *J Proteomics* **75**, 4151-4164, (2012).

18 Khatoon, A., Rehman, S., Hiraga, S., Makino, T. & Komatsu, S. Organ-specific proteomics analysis for identification of response mechanism in soybean seedlings under flooding stress. *J Proteomics* **75**, 5706-5723, (2012).

19 Leon, Z., Garcia-Canaveras, J. C., Donato, M. T. & Lahoz, A. Mammalian cell metabolomics: experimental design and sample preparation. *Electrophoresis* **34**, 2762-2775, (2013).

20 Mathew, A. K. & Padmanaban, V. C. Metabolomics: The apogee of the omics trilogy. *Int J Pharm Pharm Sci* **5**, 45-48 (2013).

21 Ramautar, R., Berger, R., van der Greef, J. & Hankemeier, T. Human metabolomics: strategies to understand biology. *Curr Opin Chem Biol* **17**, 841-846, (2013).

22 Kaddurah-Daouk, R., Kristal, B. S. & Weinshilboum, R. M. Metabolomics: a global biochemical approach to drug response and disease. *Annu Rev Pharmacol Toxicol* **48**, 653-683 (2008).

23 Kaddurah-Daouk, R. & Krishnan, K. R. R. Metabolomics: a global biochemical approach to the study of central nervous system diseases. *Neuropsychopharmacology* **34**, 173-186 (2009).

24 Kami, K. *et al.* Metabolomic profiling of lung and prostate tumor tissues by capillary electrophoresis time-of-flight mass spectrometry. *Metabolomics* **9**, 444-453, (2013).

25 Soga, T. *et al.* Differential metabolomics reveals ophthalmic acid as an oxidative stress biomarker indicating hepatic glutathione consumption. *J Biol Chem* **281**, 16768-16776, (2006).

26 Soga, T. *et al.* Quantitative metabolome analysis using capillary electrophoresis mass spectrometry. *J Proteome Res* **2**, 488-494, (2003).

27 Tanaka, S. *et al.* Pilot study of changes in salivary metabolic profiles induced by template therapy. *In Vivo* **26**, 1015-1020 (2012).

28 Uetaki, M., Tabata, S., Nakasuka, F., Soga, T. & Tomita, M. Metabolomic alterations in human cancer cells by vitamin C-induced oxidative stress. *Sci Rep* **5**, 13896, (2015).

29 Kitajima, T., Jigami, Y. & Chiba, Y. Cytotoxic mechanism of selenomethionine in yeast. *J Biol Chem* **287**, 10032-10038, (2012).

30 Simó, C., Ibáñez, C., Gómez-Martínez, Á., Ferragut, J. A. & Cifuentes, A. Is metabolomics reachable? Different purification strategies of human colon cancer cells provide different CE-MS metabolite profiles. *Electrophoresis* **32**, 1765-1777 (2011).

31 Kitagawa, M., Ikeda, S., Tashiro, E., Soga, T. & Imoto, M. Metabolomic identification of the target of the filopodia protrusion inhibitor glucopiericidin A. *Chem Biol* **17**, 989-998, (2010).

32 Birnie, G. D. The HL60 cell line: a model system for studying human myeloid cell differentiation. *Br J Cancer Suppl* **9**, 41-45 (1988).

33 Sham, R. L., Phatak, P. D., Belanger, K. A. & Packman, C. H. Functional properties of HL60 cells matured with all-trans-retinoic acid and DMSO: differences in response to interleukin-8 and fMLP. *Leuk Res* **19**, 1-6 (1995).

34 Babior, B. M. NADPH oxidase: an update. *Blood* **93**, 1464-1476 (1999).

35 Dahlgren, C. & Karlsson, A. Respiratory burst in human neutrophils. *J Immunol Methods* **232**, 3-14 (1999).

36 Uhlinger, D. J., Tyagi, S. R., Inge, K. L. & Lambeth, J. D. The respiratory burst oxidase of human neutrophils. Guanine nucleotides and arachidonate regulate the assembly of a multicomponent complex in a semirecombinant cell-free system. *J Biol Chem* **268**, 8624-8631 (1993).

37 van Wijk, E., van der Greef, J. & van Wijk, R. Photon count statistics in leukocyte cell dynamics. *Journal of Physics: Conference Series* **329**, 12-21 (IOP Publishing, 2011).

38 Chapple, I. L. Reactive oxygen species and antioxidants in inflammatory diseases. *J Clin Periodontol* **24**, 287-296 (1997).

39 Liou, G.-Y. & Storz, P. Reactive oxygen species in cancer. *Free Radic Res* **44**, 479-496 (2010).

40 Perry, G., Castellani, R. J., Hirai, K. & Smith, M. A. Reactive oxygen species mediate cellular damage in Alzheimer disease. *J Alzheimers Dis* **1**, 45-55 (1998).

41 Mügge, A. The role of reactive oxygen species in atherosclerosis. *Zeitschrift fur Kardiologie* **87**, 851-864 (1998).

42 Halliwell, B. Free radicals, reactive oxygen species and human disease: a critical evaluation with special reference to atherosclerosis. *Br J Exp Pathol* **70**, 737-757 (1989).

43 Bauerova, K. & Bezek, S. Role of reactive oxygen and nitrogen species in etiopathogenesis of rheumatoid arthritis. *Gen Physiol Biophys* **18**, 15-20 (2000).

44 van Wijk, E., Kobayashi, M., van Wijk, R. & van der Greef, J. Imaging of ultra-weak photon emission in a rheumatoid arthritis mouse model. *PLoS One* **8**, e84579, (2013).

45 Van Wijk, R., Van Wijk, E. P., van Wietmarschen, H. A. & van der Greef, J. Towards whole-body ultra-weak photon counting and imaging with a focus on human beings: a review. *J Photochem Photobiol B* **139**, 39-46, (2014).

46 Ives, J. A. *et al.* Ultraweak photon emission as a non-invasive health assessment: a systematic review. *PLoS One* **9**, e87401, (2014).

47 Van Wijk, R., Van Wijk, E. P., Schroen, Y. & van der Greef, J. Imaging human spontaneous photon emission: historic development, recent data and perspectives. *Trends Photochem. Photobiol* **15**, 27-40 (2013).

48 Bajpai, R. P., Van Wijk, E. P., Van Wijk, R. & van der Greef, J. Attributes characterizing spontaneous ultra-weak photon signals of human subjects. *J Photochem Photobiol B* **129**, 6-16, (2013).

49 Cifra, M., Van Wijk, E., Koch, H., Bosman, S. & Van Wijk, R. Spontaneous ultra-weak photon emission from human hands is time dependent. *RADIOENGINEERING* **16**, 15 (2007).

50 Van Wijk, E. P., Van Wijk, R. & Cifra, M. in *European Conference on Biomedical Optics.* 66331J-66331J-66339 (International Society for Optics and Photonics).

51 Batista, E. L., Jr., Warbington, M., Badwey, J. A. & Van Dyke, T. E. Differentiation of HL-60 cells to granulocytes involves regulation of select diacylglycerol kinases (DGKs). *J Cell Biochem* **94**, 774-793, (2005).

52 Krance, S. *Glutathione homeostasis during terminal human leukemia-60 (HL-60) cell differentiation*, <http://hdl.handle.net/1802/6613> (2008).

53 Dietmair, S., Timmins, N. E., Gray, P. P., Nielsen, L. K. & Kromer, J. O. Towards quantitative metabolomics of mammalian cells: development of a metabolite extraction protocol. *Anal Biochem* **404**, 155-164, (2010).

54 Tran, T. T. *et al.* Development of quenching and washing protocols for quantitative intracellular metabolite analysis of uninfected and baculovirus-infected insect cells. *Methods* **56**, 396-407, (2012).

55 Bligh, E. G. & Dyer, W. J. A rapid method of total lipid extraction and purification. *Can J Biochem Physiol* **37**, 911-917 (1959).

56 Hirayama, A. *et al.* Quantitative metabolome profiling of colon and stomach cancer microenvironment by capillary electrophoresis time-of-flight mass spectrometry. *Cancer Res* **69**, 4918-4925, (2009).

57 Ohashi, Y. *et al.* Depiction of metabolome changes in histidine-starved Escherichia coli by CE-TOFMS. *Mol BioSyst* **4**, 135-147, (2008).

58 Godzien, J., Alonso-Herranz, V., Barbas, C. & Armitage, E. G. Controlling the quality of metabolomics data: new strategies to get the best out of the QC sample. *Metabolomics* **11**, 518-528 (2015).

59 van den Berg, R. A., Hoefsloot, H. C., Westerhuis, J. A., Smilde, A. K. & van der Werf, M. J. Centering, scaling, and transformations: improving the biological information content of metabolomics data. *BMC Genomics* **7**, 142, (2006).

60 Xia, J., Mandal, R., Sinelnikov, I. V., Broadhurst, D. & Wishart, D. S. MetaboAnalyst 2.0--a comprehensive server for metabolomic data analysis. *Nucleic Acids Res* **40**, W127-133, (2012).

61 Xia, J. G., Sinelnikov, I. V., Han, B. & Wishart, D. S. MetaboAnalyst 3.0-making metabolomics more meaningful. *Nucleic Acids Res* **43**, W251-W257, (2015).

62 Prasad, A. & Pospisil, P. Ultraweak photon emission induced by visible light and ultraviolet A radiation via photoactivated skin chromophores: in vivo charge coupled device imaging. *J Biomed Opt* **17**, 085004, (2012).

63 Breitman, T. R., Selonick, S. E. & Collins, S. J. Induction of differentiation of the human promyelocytic leukemia cell line (HL-60) by retinoic acid. *Proc Natl Acad Sci U S A* **77**, 2936-2940 (1980).

64 Thompson, B. Y., Sivam, G., Britigan, B. E., Rosen, G. M. & Cohen, M. S. Oxygen metabolism of the HL-60 cell line: comparison of the effects of monocytoid and neutrophilic differentiation. *J Leukoc Biol* **43**, 140-147 (1988).

65 Tsiftsoglou, A. S. & Robinson, S. H. Differentiation of leukemic cell lines: A review focusing on murine erythroleukemia and human hl-60 cells. *Int J Cell Cloning* **3**, 349-366 (1985).

66 Zhang, J.-W., Gu, J., Wang, Z.-Y., Chen, S.-J. & Chen, Z. Mechanisms ofall-trans retinoic acid-induced differentiation of acute promyelocytic leukemia cells. *J Biosci* **25**, 275-284 (2000).

67 Kufe, D. W., Griffin, J., Mitchell, T. & Shafman, T. Polyamine requirements for induction of HL-60 promyelocyte differentiation by leukocyte-conditioned medium and phorbol ester. *Cancer Res* **44**, 4281-4284 (1984).

68 Chiba, P., Wallner, C. & Kaiser, E. S-adenosylmethionine metabolism in HL-60 cells: effect of cell cycle and differentiation. *Biochim Biophys Acta* **971**, 38-45 (1988).

69 Huberman, E., Weeks, C., Herrmann, A., Callaham, M. & Slaga, T. Alterations in Polyamine Levels Induced by Phorbol Diesters and Other Agents That Promote Differentiation in Human Promyelocytic Leukemia-Cells. *P Natl Acad Sci Biol* **78**, 1062-1066, (1981).

70 Schipper, R. G., Penning, L. C. & Verhofstad, A. A. Involvement of polyamines in apoptosis. Facts and controversies: effectors or protectors? *Semin Cancer Biol* **10**, 55-68, (2000).

71 Finkelstein, J. D. Methionine metabolism in mammals. *J Nutr Biochem* **1**, 228-237, (1990).

72 Finkelstein, J. D. & Martin, J. J. Homocysteine. *Int J Biochem Cell Biol* **32**, 385-389 (2000).

73 Danishpajooh, I. O. *et al.* Nitric oxide inhibits methionine synthase activity in vivo and disrupts carbon flow through the folate pathway. *J Biol Chem* **276**, 27296-27303 (2001).
74 Lu, S. C. Regulation of glutathione synthesis. *Mol Aspects Med* **30**, 42-59 (2009).
75 Panayiotidis, M. I., Stabler, S. P., Allen, R. H., Pappa, A. & White, C. W. Oxidative stress-induced regulation of the methionine metabolic pathway in human lung epithelial-like (A549) cells. *Mutat Res* **674**, 23-30 (2009).
76 Mosharov, E., Cranford, M. R. & Banerjee, R. The quantitatively important relationship between homocysteine metabolism and glutathione synthesis by the transsulfuration pathway and its regulation by redox changes. *Biochemistry* **39**, 13005-13011 (2000).
77 James, S. J. *et al.* Metabolic biomarkers of increased oxidative stress and impaired methylation capacity in children with autism. *Am J Clin Nutr* **80**, 1611-1617 (2004).
78 Wilcken, D. & Wilcken, B. The pathogenesis of coronary artery disease. A possible role for methionine metabolism. *J Clin Investig* **57**, 1079 (1976).
79 Finkelstein, J. D. Methionine metabolism in liver diseases. *Am J Clin Nutr* **77**, 1094-1095 (2003).
80 Miller, A. L. The methionine-homocysteine cycle and its effects on cognitive diseases.(Homocysteine & Cognitive). *Altern Med Rev* **8**, 7-20 (2003).
81 Tchantchou, F. & Shea, T. B. Folate deprivation, the methionine cycle, and Alzheimer's disease. *Vitam Horm* **79**, 83-97 (2008).

SUPPLEMENTARY INFORMATION

Supplementary Figure S1. Flow cytometry recorded on day 7 in undifferentiated (control) and differentiated (ATRA-treated) HL-60 cells. (A) Flow cytometry results of undifferentiated cells measured without CD11b-PE staining. (B) Flow cytometry results of undifferentiated cells stained with CD11b-PE. (C) Flow cytometry results of differentiated cells measured without CD11b-PE staining. (D) Flow cytometry results of differentiated cells stained with CD11b-PE.

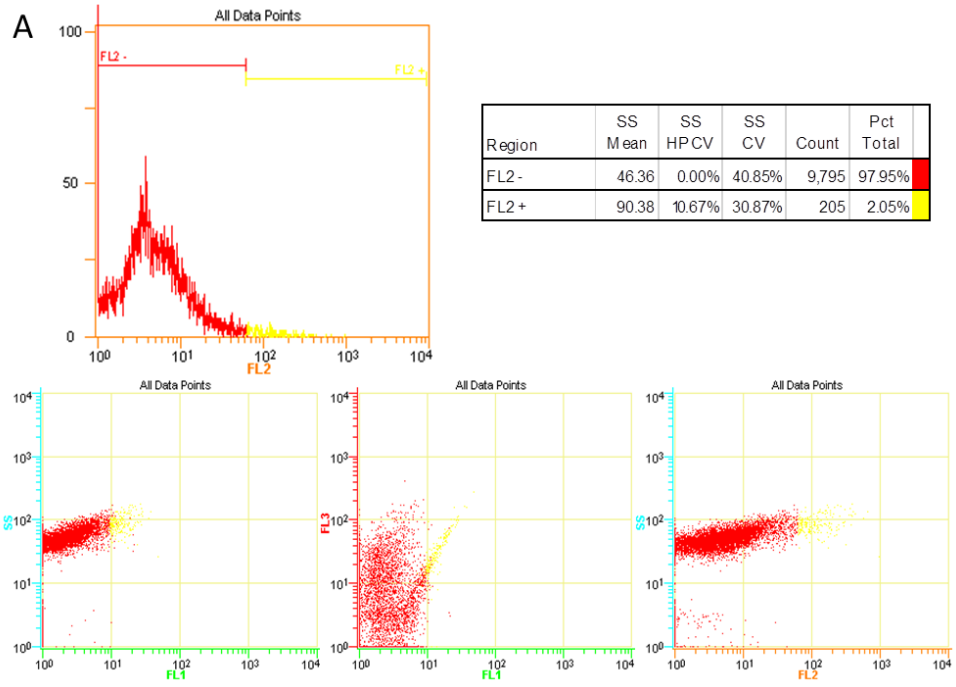

Region	SS Mean	SS HPCV	SS CV	Count	Pct Total
FL2 -	46.36	0.00%	40.85%	9,795	97.95%
FL2 +	90.38	10.67%	30.87%	205	2.05%

B

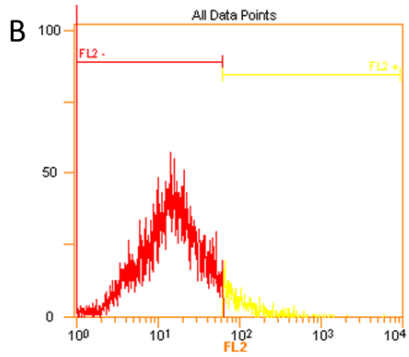

Region	SS Mean	SS HPCV	SS CV	Count	Pct Total
FL2 -	46.86	24.72%	36.65%	9,142	91.42%
FL2 +	70.49	31.23%	40.71%	858	8.58%

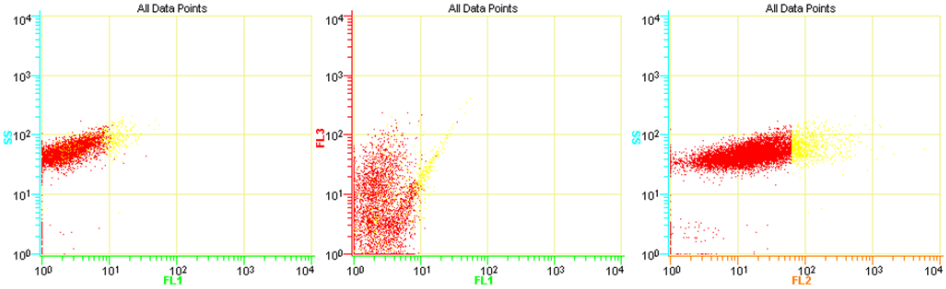

C

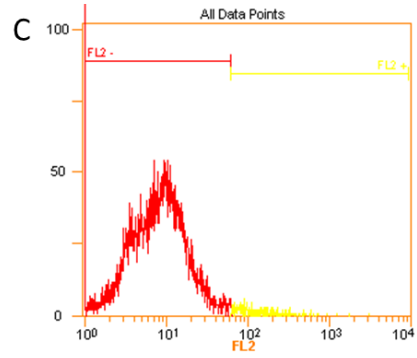

Region	SS Mean	SS HPCV	SS CV	Count	Pct Total
FL2 -	42.10	17.85%	35.90%	9,697	96.97%
FL2 +	91.54	11.26%	37.41%	303	3.03%

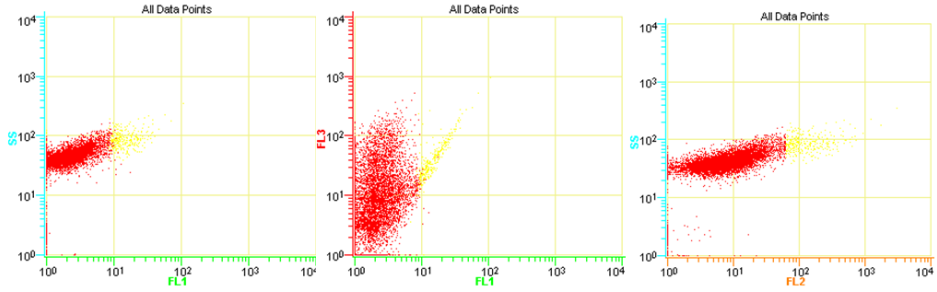

D

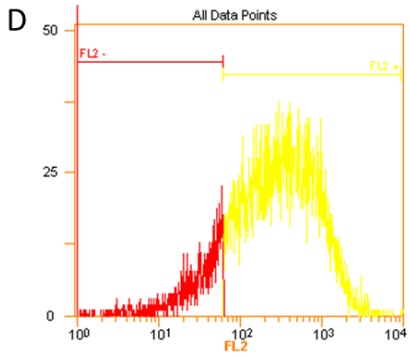

Region	SS Mean	SS HPCV	SS CV	Count	Pct Total
FL2 -	43.58	0.00%	49.77%	1,559	15.59%
FL2 +	45.72	17.86%	37.39%	8,441	84.41%

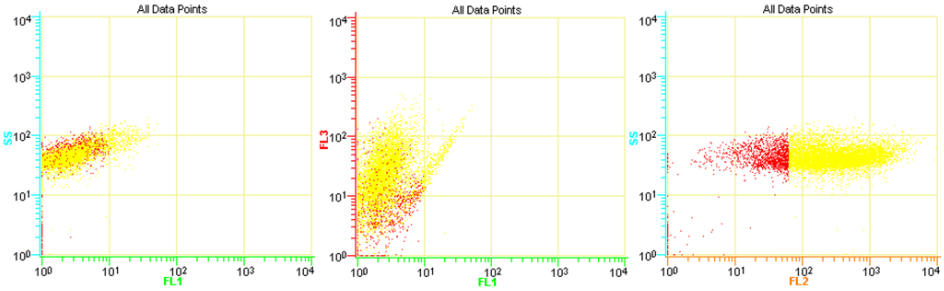

Supplementary Figure S2. Pathway results obtained for the metabolites identified in the correlation analysis. The number of hits indicates the number of compounds of interest in the indicated pathway, and the pathway impact is calculated as the ratio of the number of hits to the total number of compounds in the pathway.

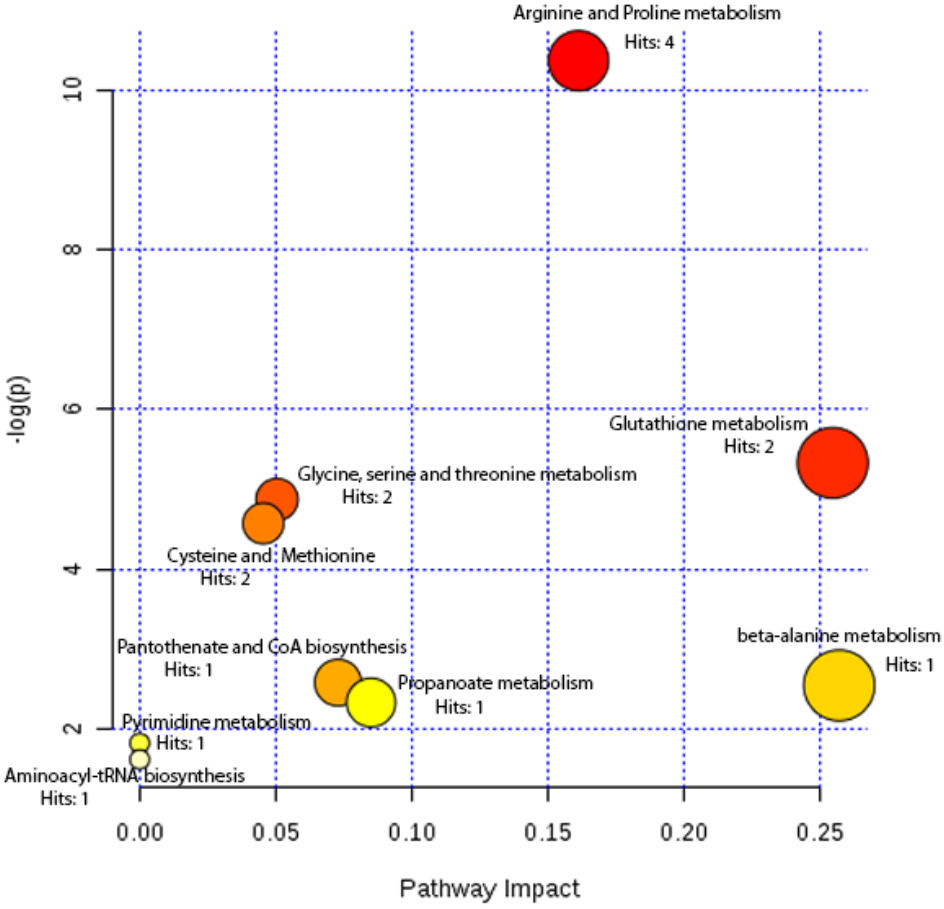

Chapter 4

Ultra-weak photon emission as a dynamic tool for monitoring oxidative stress metabolism

Based on

Rosilene Cristina Rossetto Burgos, Johannes Cornelius Schoeman, Lennart Jan van Winden, Kateřina Červinková, Rawi Ramautar, Eduard P.A. van Wijk, Michal Cifra, Ruud Berger, Thomas Hankemeier and Jan van der Greef

Ultra-weak photon emission as a dynamic tool for monitoring oxidative stress metabolism

Scientific Reports **7**:1229, (2017)

doi:10.1038/s41598-017-01229-x

ABSTRACT

In recent years, excessive oxidative metabolism has been reported as a critical determinant of pathogenicity in many diseases. The advent of a simple tool that can provide a physiological readout of oxidative stress would be a major step towards monitoring this dynamic process in biological systems, while also improving our understanding of this process. Ultra-weak photon emission (UPE) has been proposed as a potential tool for measuring oxidative processes due to the association between UPE and reactive oxygen species. Here, we used HL-60 cells as an *in vitro* model to test the potential of using UPE as readout for dynamically monitoring oxidative stress after inducing respiratory burst. In addition, to probe for possible changes in oxidative metabolism, we performed targeted metabolomics on cell extracts and culture medium. Lastly, we tested the effects of treating cells with the NADPH oxidase inhibitor diphenyleneiodonium chloride (DPI). Our results show that UPE can be used as readout for measuring oxidative stress metabolism and related processes.

INTRODUCTION

Respiratory burst is one of the first defence mechanisms used by specialised cells such as neutrophils in response to invading pathogens[1-3]. This process uses the rapid consumption of molecular oxygen (O_2) to produce high levels of intracellular reactive oxygen species (ROS) for killing invading pathogens[1-3]. Under homeostatic conditions, ROS are produced by mitochondria as a product of cellular metabolism[4]; however, during respiratory burst NADPH oxidase plays a central role in ROS production for cellular defence[5,6]. The primary function of NADPH oxidase is the production of superoxide radicals ($O_2^{\cdot -}$)[7,8], which serve as the initial substrate in the generation of a diverse variety of ROS species, including hydrogen peroxide (H_2O_2) and hydroxyl radicals ($OH^{\cdot}$).

Physiologically, ROS have a hormetic effect – at relatively low concentrations, ROS have beneficial properties, which include maintaining cellular redox biology and facilitating signaling[9], whereas at high concentrations, ROS cause oxidative stress that can damage nucleic acids, proteins, and lipids. Studies have shown that oxidative stress contributes to the pathogenesis of many diseases and conditions, including chronic inflammation[10], various types of cancers[11], Alzheimer's disease[12], and cardiovascular disease[13]. Moreover, the aforementioned studies revealed a clear association between ROS production and NADPH oxidase, thereby providing insight into the underlying ROS-based physiological processes. In recent years, several NADPH inhibitors have been investigated as candidate therapies for ROS-related pathology[14,15], and measuring these oxidation reactions and related biomolecules can provide a readout of cellular oxidative stress[16]. ROS production has been analysed using various techniques, including photometry, luminometry, flow cytometry, and precipitation reactions[17]. However, all of these techniques provide a measure at only a single time point; moreover, these techniques are cell-dependent, laborious, and not necessarily feasible for diagnostic purposes. In contrast, ultra-weak photon emission (UPE) is a promising new tool that could be used to monitor oxidative processes. Indeed, the feasibility of using UPE as a tool for monitoring health and disease has been examined in several studies[18-20].

Ultra-weak photons are emitted spontaneously by many biological systems[21,22]. UPE is characterised as non-thermal radiation in the near-ultraviolet to visible region (100-800 nm) of the electromagnetic spectrum, possibly reaching the near-infrared region (801-1300 nm). UPE is generated by the transition of electrons from an excited state to the ground state; excited electron states (e.g. triplet carbonyls, singlet oxygen, etc.) are produced by the oxidation of biomolecules by ROS[21,23]. Thus, UPE is a potential new tool for monitoring dynamic biological processes that involve ROS, including ROS-related diseases[24,25], as well

as processes related to oxidative stress metabolism. A clear advantage of UPE is that it provides spatiotemporal information; in addition, UPE is non-damaging, non-invasive, label-free, and relatively cost-effective.

Because UPE can reflect complex molecular processes, it can be combined with other technologies such as metabolomics, thereby providing valuable insight into the biochemical processes probed using UPE[26]. Recently, we used metabolomics to identify several metabolites correlated with UPE[27]. Moreover, metabolomics is a powerful approach that can be applied to numerous biological studies due to the ability to detect many hundreds of metabolites in a single biological sample, thereby providing a 'phenotypic' readout of other 'omics'. Previous reports suggest that lipid peroxidation of linoleic acid in cell membranes can strongly affect UPE emission[18,28]. In this respect, the products of lipid and protein oxidation are closely related to UPE. For example, compounds related to the arachidonic acid pathway (e.g. isoprostanes, prostaglandins, and lysosphingolipids) are key signalling compounds in biological systems and are often related to oxidative stress and/or inflammatory processes[29,30]. In addition, previous studies demonstrated the relationship between these metabolites and low-level chemiluminescence and electronically excited species[31-34].

Here, we evaluated the feasibility of using UPE as a dynamic tool for monitoring oxidative stress metabolism and related processes. A metabolomics approach was also used to gain insight into the biochemical processes probed using UPE. We used differentiated neutrophil-like HL-60 cells as an *in vitro* model. Respiratory burst was induced by treating the cells with phorbol 12-myristate 13-acetate (PMA)[35,36]; in response to PMA, these cells produce large quantities of ROS, which were monitored in real-time using UPE. A targeted metabolomics approach was then used to analyse metabolites related to oxidative stress and inflammation (e.g. prostaglandins and isoprostanes) in HL-60 cell extracts and culture medium. Moreover, we measured the effects of treating cells with the NADPH oxidase inhibitor diphenyleneiodonium chloride (DPI).

METHODS

Cell culture and experimental design

All experiments with human cell lines were performed in accordance with approved guidelines, and all experimental protocols were approved in accordance with the regulations established by the Institute of Photonics and Electronics, Czech Academy of Sciences. The acute promyelocytic leukaemia cell line HL-60 (catalogue number CCL-240; lot number 62690063; ATCC, Manassas, VA) were cultured in Iscove's Modified Dulbecco's Medium

(IMDM) without phenol red (Gibco-Life Technologies, Grand Island, NY) supplemented with 10% (v/v) fetal calf serum and 1% (v/v) penicillin/streptomycin (Sigma-Aldrich, St. Louis, MO) in an incubator at 37°C in 5% CO_2. The cells were seeded at 2 x 10^5 cells/ml and maintained in the exponential growth phase in accordance with the instructions provided by ATCC. Cell number and viability were measured using the trypan blue exclusion method with an automated cell counter (Bio-Rad Laboratories, Hercules, CA). Cell viability was >85%. UPE and metabolomics measurements were performed at cell passage number 28. We have used the experimental design as described previously[27], with minor modifications. In brief, when the cells were split and adjusted for cell density, 1 µM all-*trans* retinoic acid (ATRA; 98% grade, catalogue number R250, Sigma-Aldrich) was added to the cells in order to induce differentiation via the granulocytic pathway; control cells received the same volume of vehicle. The cells were then incubated for up to 7 days, and UPE and metabolomics experiments were performed on days 2 and 7. Prior to any UPE measurement and/or sample collection for metabolomics, the culture medium was replaced with fresh IMDM (without supplementation), and the cells were counted. Where indicated, cells were stimulated with phorbol 12-myristate 13-acetate (PMA; 98% grade, Sigma-Aldrich) in the presence or absence of diphenyleneiodonium chloride (DPI; Cayman Chemicals, Ann Arbor, MI). A small aliquot of the cell suspension was used for UPE measurements. Based on the UPE profile, four time points were used for the metabolomics study; aliquots containing of 12 x 10^6 cells were used for each time point. TP1 samples were collected prior to PMA induction; TP2, TP3, and TP4 samples were collected 60, 4500, and 9000 seconds, respectively, after PMA induction (see **Supplementary Fig. S1**).

Ultra-weak photon emission (UPE)

UPE was measured using a module H7360-01 photomultiplier tube (PMT; Hamamatsu Photonics, Hamamatsu, Japan), which is sensitive to wavelengths of 300-650 nm and has a dark count of approximately 13 counts per second. UPE was measured from HL-60 cells suspended in IMDM without any supplementation. The cell suspension (3 ml containing 1.5 x 10^6 cells/ml) was transferred to a small Petri dish, which was then placed in the PMT dark chamber at 37°C. The Petri dish was positioned as close as possible to the PMT detector using a sample holder. A background measurement was taken before each sample measurement. To stimulate the respiratory burst in cells, PMA was applied at a concentration of 54 nM, and the UPE profile was recorded for 9000 seconds. DPI was applied at a concentration of 0.9 µM prior to PMA (54 nM) stimulation in independent cell suspensions after which the UPE profile was recorded for 9000 seconds. There was a brief delay of approximately 30 seconds between PMA application and the start of the UPE measurement

due to placing the samples in the PMT dark chamber. Control cells (i.e. cells that were not cultured in ATRA) were measured using the same conditions.

Collection, quenching, and extraction of cell pellets and culture medium for metabolomics

Sample collection and quenching

Aliquots of suspension cells were centrifuged for 4 minutes at 0.2 rcf at room temperature. The supernatant (containing the culture medium) was collected and stored at -80°C. The pellets (containing the cells) were quenched in 0.9% (w/v) sodium chloride solution (Sigma-Aldrich) at 0-2°C. The cell aliquots were then centrifuged for 4 minutes at 0.2 rcf at room temperature. The supernatant was discarded, and the cell pellets were stored at -80°C.

Extraction

The medium and cell pellets were extracted using a liquid-liquid extraction protocol as described below.

<u>*Cell pellets*</u> – First, each cell pellet was suspended in 500 µl citric acid (Merck, Darmstadt, Germany), 5 µl antioxidant containing 0.4 mg/ml butylated hydroxytoluene (BHT; Sigma-Aldrich) and 0.4 mg/ml ethylenediaminetetraacetic acid (EDTA; Sigma-Aldrich), 10 µl internal standard mix (ISTD) comprised of deuterated compounds (Cayman Chemicals), and 1 ml n-butanol (Boom B.V., Meppel, the Netherlands):ethyl acetate (Biosolve B.V., Valkenswaard, the Netherlands). The cell suspension was shaken in a bullet blender (Next Advance, Averill Park, NY) to mix the organic phase and lyse the cells. The suspension was then centrifuged for 10 minutes at 16.1 rcf at 4°C, and 900 µl of the organic phase was collected from each sample. The remaining mixture was subjected to a second extraction round with 400 µl n-butanol (saturated in Milli-Q water from EMD Millipore, Billerica, MA) and 400 µl of ethyl acetate. The mixture was then shaken and centrifuged, and 800 µl of the organic phase was collected and added to the first-round organic phase sample. Finally, the organic phase was dried in a CentriVap centrifugal concentrator. The dried samples were resuspended in 30 µl injection solution consisting of 70% MeOH (Biosolve B.V.) in Milli-Q water and transferred to a glass vial suitable for use in the LC system.

<u>*Medium samples*</u> – Medium samples (800 µl total) were divided into two 400-µl aliquots to increase the concentration of extracellular metabolites. First, we added 400 µl citric acid, 5 µl antioxidant (0.4 mg/ml BHT and 0.4 mg/ml EDTA), 6 µl ISTD mix, and 1 ml butanol:ethyl acetate to each aliquot. The samples were then shaken using a bullet blender, centrifuged

for 10 minutes at 16.1 rcf at 4°C, and 950 µl of the organic phase was collected. The remaining mixture was subjected to a second extraction round with 500 µl butanol saturated in Milli-Q water and 500 µl of ethyl acetate. The mixture was then shaken and centrifuged for 10 minutes at 16.1 rcf at 4°C; 950 µl of the organic phase was collected and added to the first-round organic phase sample. The organic phase was dried using a CentriVap centrifugal concentrator. The dried samples were resuspended in 30 µl injection solution (70% MeOH in Milli-Q water) and transferred to a glass vial suitable for use in the LC system.

Liquid chromatography–mass spectrometry (LC-MS) analysis

For metabolomics, a model LCMS-8050 liquid chromatograph-mass spectrometer (Shimadzu, Tokyo, Japan) and an ACQUITY BEH C18 column (50 mm x 2.1 mm, 1.7 µm; Waters, Milford, MA) maintained at 40°C was used for reverse-phase LC separation. Electrospray ionisation was used as an ionisation source. The mobile phase A consisted of H_2O containing 0.1% acetic acid. The mobile phase B contained 75% acetonitrile, 25% MeOH, and 0.1% acetic acid (Sigma-Aldrich). The mobile phase C contained 100% isopropanol. The temperature of the column was set at 40°C, and the temperature of the autosampler was set at 5°C. The injection volume and flow rate were 10 µl and 0.7 ml/min, respectively. After each measurement, peak detection and integration of the raw data were processed and analysed using the Shimadzu Lab Solutions software program, version 5.65. Pooled cell pellet extracts and pooled medium samples were prepared and measured after every ten samples in order to verify reliability of the measurements. Any metabolites detected in the pooled samples that exceeded 30% of the relative standard deviation due to technical and/or analytical variations were excluded from analysis.

Statistical analysis

UPE data were analysed using GraphPad Prism (GraphPad Software, Inc., La Jolla, CA). The two-tailed paired Student's *t*-test was used to compare individual groups. The metabolic results (i.e. response ratio) were uploaded to the MetaboAnalyst website (http://www.metaboanalyst.ca)[37,38] and tested for statistical significance. To obtain data with a normal distribution, the metabolomics data were log-transformed and auto-scaled. We analysed the following parameters: *i*) the variance between the four time points (i.e. TP1, TP2, TP3, and TP4) relative to PMA stimulation was analysed using a two-way ANOVA (two-tailed); *ii*) the variance between the four time points in cells treated with DPI and PMA were analysed using a two-way ANOVA (two-tailed); and *iii*) Spearman's correlation coefficient (two-tailed) was used to analyse the relationship between the UPE data and metabolic profile. Spearman's correlations were done independently for the PMA and DPI+PMA

groups, correlating their averaged metabolite levels to their respective averaged UPE profiles over the four TPs measured. Differences with a *p*-value <0.05 were considered significant.

RESULTS

Ultra-weak photon emission (UPE)

HL-60 cells were differentiated into neutrophil-like cells by incubation in all-*trans* retinoic acid (ATRA) for up to 7 days. Next, we induced respiratory burst by treating the cells with PMA. After PMA induction we measured the dynamic UPE profile for 9000 seconds (**Fig. 1**). **Fig. 1A** shows control experiments recorded under the same conditions and **Fig. 1B** presents the UPE profile of differentiated cells on Day 7 induced by PMA in the presence or absence of DPI. **Fig. 1C** illustrates the paired t-test performed (*n=5*).

Cells treated with ATRA for only 2 days had no response to PMA stimulation. In contrast, cells treated with ATRA for 7 days had a robust increase in UPE in response to PMA due to a high amount of ROS generated. This profile is in agreement with our previous work[27]. Treating the differentiated cells with the NADPH oxidase inhibitor DPI significantly reduced ($p < 0.0001$) the UPE response, substantiating the biochemical link between ROS and UPE. Furthermore, this inhibition was also observed in undifferentiated cells (see **Fig. 1A)** due to a small percentage of cells spontaneously differentiating into neutrophils-like cells[27].

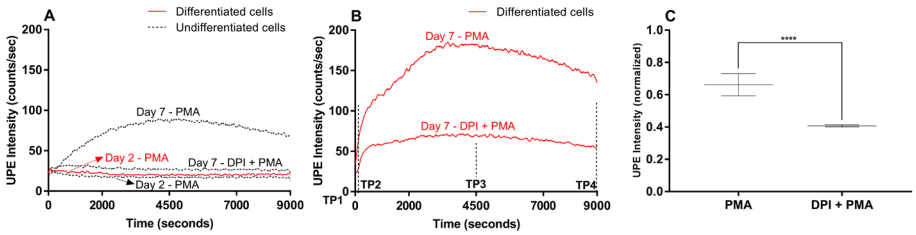

Figure 1. Dynamic UPE measurement of HL-60 cells treated with ATRA for 2 or 7 days to differentiate the cells into neutrophil-like cells. The lines (red - differentiated cells and black - undifferentiated cells) represent the moving UPE average of 100 points. **(A)** Control measurements. **(B)** The UPE profile of differentiated cells (day 7) was recorded after stimulation with PMA in the absence or presence of DPI. **(C)** Summary of peak UPE intensity measured in HL-60 cell treated for 7 days with ATRA after stimulation with PMA in the absence or presence of DPI. The data are represented as the mean ± SD (n=5) of the normalized maximum peak intensity. Student's paired *t*-test with **** $p<0.0001$.

Metabolic profiling of isoprostanes, prostaglandins and lysosphingolipids

Next, to measure the biochemical changes related to oxidative metabolism, we performed targeted metabolomics of compounds related to oxidative stress and inflammation, including prostaglandins, isoprostanes, nitro-fatty acids, and lysosphingolipids. We used our previously reported approach[27] (see also **Supplementary Fig. S1**), and DPI treatment was included in order to determine which metabolic pathways may be involved in this process.

Based on the dynamic UPE profiles (see **Fig. 1B** and **Supplementary Fig. S1**), cell lysates (to measure intracellular metabolites) and culture medium samples (to measure extracellular metabolites) were obtained at four time points relative to PMA stimulation and analysed using targeted metabolomics. TP1 corresponds to the basal condition (i.e. prior to the addition of PMA), and TP2, TP3 and TP4 correspond to 60, 4500 and 9000 seconds after PMA stimulation, respectively. To measure the metabolic profiles indicative of oxidative stress and inflammation, we used a custom-built liquid chromatography–mass spectrometry platform[39]. A total of 10 and 11 metabolites were detected in the cell lysates and culture medium samples, respectively; 7 metabolites were detected in both samples (**Supplementary Table S1**).

Intracellular metabolites

Among the 10 intracellular metabolites measured in the cell lysates, only 8-iso-PGE_2, 8-iso-PGE_1, PGE_1 and sphinganine C18:0 increased significantly in response to PMA stimulation, and sphingosine C18:1 significantly decreased in response to PMA stimulation shown in **Fig. 2** and **Supplementary Table S2**. PGE_2 did display an increasing trend over the four time points. We also found a significant correlation between the recorded UPE data and the metabolites measured (see **Supplementary Table S2**).

Pre-treating the cells with DPI significantly decreased the PMA-induced responses of 8-iso-PGE_2, 8-iso-PGE_1 and PGE_1. In addition, the PMA-induced response of sphingosine increased, whereas sphinganine C18:0 had no response (see **Fig. 2**).

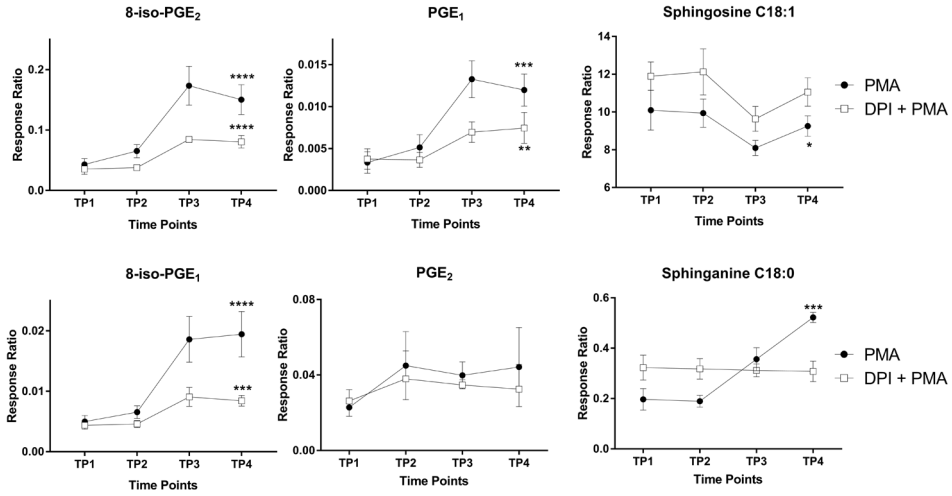

Figure 2. HL-60 cells were treated with ATRA for 7 days, after which respiratory burst was induced with PMA in the presence or absence of DPI. Cell lysates were collected at the indicated time points, and intracellular metabolites were measured. We performed intragroup ANOVA analysis over the four time points to identify significant changes in metabolite levels. Data are plotted as the mean ± SD (n=3). ANOVA with **p*<0.05, ***p*<0.01, ****p*<0.001, and *****p*<0.0001.

Extracellular metabolites

Next, we examined the extracellular metabolites measured from the culture medium during PMA-induced respiratory burst. Among the 11 compounds detected (see **Supplementary Table S1)**, only PGE_2, PGD_2, (±)5-iPF2α-IV, and 8-12-iPF2α-IV increased significantly during respiratory burst (**Fig. 3** and **Supplementary Table S3**). Interestingly, treating the cells with DPI also increased the extracellular levels of all four compounds. Spearman's correlation showed a high correlation coefficient (r>0.6) to the extracellular metabolite levels and the measured UPE intensity. However, the *p-values* were not significant ($p > 0.05$).

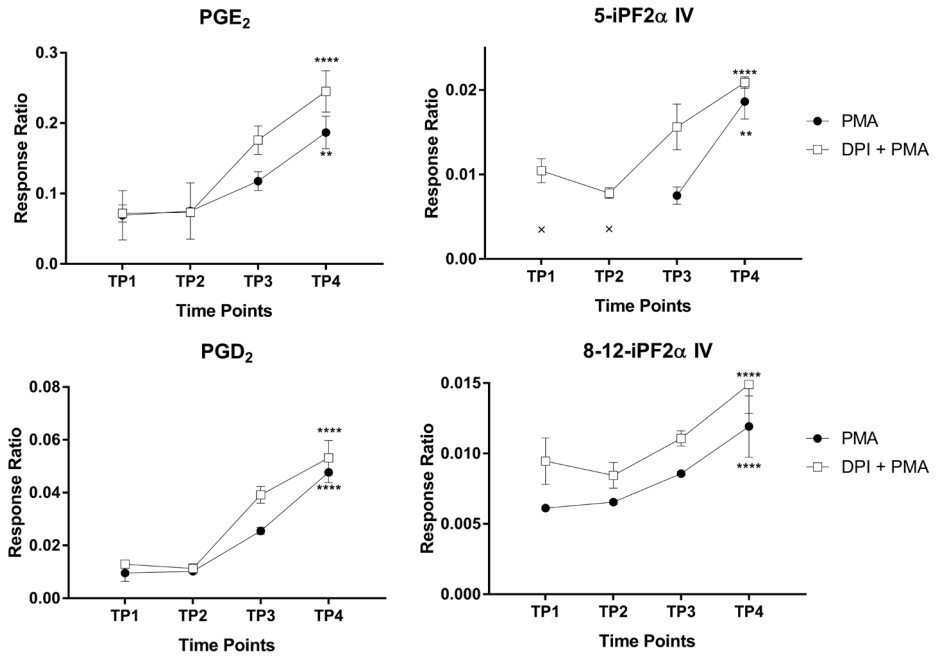

Figure 3. HL-60 cells were treated with ATRA for 7 days, after which respiratory burst was induced with PMA in the presence or absence of DPI. Culture medium was collected at the indicated time points, and extracellular metabolites were measured. We performed intragroup ANOVA analysis over the four time points to identify significant changes in metabolite levels. Data are plotted as the mean ± SD (n=3/group). ANOVA with $^{**}p<0.01$ and $^{****}p<0.0001$. The data points indicated with an "x" in the top-right panel were below the metabolite's limit of detection.

DISCUSSION

Treating HL-60 cells with ATRA causes the cells to differentiate into neutrophil-like cells[35]. Neutrophils are specialised cells capable of producing high amounts of ROS. In addition, the differentiation of HL-60 cells into neutrophil-like cells is associated with morphological changes, as well as metabolic changes that occur at the cell surface and in the nucleus[35,40,41]. We used PMA to induce respiratory burst, thereby activating protein kinase C (PKC). PKC phosphorylates the cytosolic NADPH oxidase subunit $p47^{PHOX}$, contributing to assembly of the NADPH oxidase complex[42-44]. The function of NADPH oxidase is to extract electrons from NADPH, transferring the electrons to oxygen, thereby forming $O_2^{\bullet-}$ in the cytosol and extracellular space; this ultimately leads to the generation of other ROS species[5-7]. Here, we found that UPE can be used to establish the link between respiratory burst and increased levels of ROS in response to PMA stimulation (**Fig. 4**).

The NADPH oxidase inhibitor DPI binds specifically to the flavoprotein subunit (a polypeptide in the plasma membrane), thereby blocking the flow of electrons in the NADPH oxidase complex[5,6,45-47]. DPI has also been used to inhibit mitochondrial ROS production[48]. In our study, DPI significantly decreased the UPE signal in PMA-stimulated differentiated HL-60 cells. Interestingly, DPI also acts by suppressing $O_2^{\cdot-}$ production, H_2O_2 production, and mitochondrial processes such as NADH-ubiquinone oxidoreductase (complex I)[45,46,48] (see **Fig. 4**). In our study, we used DPI at its reported IC_{50} value(0.9 μM)[46]. At this concentration, DPI caused a 50-60% decrease in the UPE signal, suggesting residual electron transport flow, likely due to residual NADPH oxidase activity and the relatively low levels of photon emissions from mitochondrial activity.

With respect to intracellular metabolites, isoprostanes such as 8-iso-PGE_2 and 8-iso-PGE_1 are non-enzymatic products produced by the auto-oxidation of arachidonic acid by free radicals; thus, these metabolites are useful markers of oxidative stress[30]. In biological processes involving ROS, polyunsaturated fatty acids (PUFAs) – particularly arachidonic acid – are susceptible to oxidation by free radicals. PUFAs also serve as a precursor for cyclooxygenase-mediated oxidation, producing thromboxanes, prostacyclins, and prostaglandins[30,49,50].

Although the production of the isoprostane 8-iso-PGE_1 is poorly understood, one study reported that E_1-isoprostane is produced in plants by oxidation, with α-linoleic acid as the substrate[51]. Similarly, little is known regarding the production and biological role of 8-iso-PGE_2. In a previous *in vivo* study with rats, 8-iso-PGE_2 was identified as a non-enzymatic product of free radical–catalysed lipid peroxidation, ultimately exerting potent biological activity (in this case, renal vasoconstriction)[52]. Another biological role of 8-iso-PGE_2 is the ability to inhibit platelet aggregation[53]. Thus, 8-iso-PGE_2 appears to act as a signalling molecule with a wide range of biological functions.

The prostaglandins PGE_1 and PGE_2 have been well characterised and mediate a variety of biological processes, including vasodilation[54], platelet aggregation[55], and adaptive crosstalk activation[56]. Here, we found that the intracellular levels of both 8-iso-PGE_2 and 8-iso-PGE_1 are increased during respiratory burst in differentiated HL-60 cells; therefore, these metabolites are presumably products of ROS oxidation mediated by NADPH oxidase and mitochondrial electron transport. Moreover, pre-treating cells with DPI significantly reduced the intracellular levels of isoprostanes and prostaglandins (see **Fig. 2**). Taken together, our results show that DPI treatment significantly decreases the intracellular levels of 8-iso-PGE_1, 8-iso-PGE_2, and PGE_1, thereby showing a clear correlation with UPE intensity.

Sphingosine and sphinganine are lysosphingolipids that serve as precursors for ceramide and/or sphingosine-1-phosphate, both of which are involved in various signalling pathways, including cell proliferation, differentiation, and apoptosis[57]. In addition, both sphingosine and sphinganine can inhibit PKC activity[58,59] (see **Fig. 4**). PKC phosphorylates $p47^{PHOX}$, a key component of NADPH oxidase (see **Fig. 4**), and therefore contributes to the activation of respiratory burst by inducing flavoenzyme[46]. Our finding of increased levels of sphinganine, however, suggests that PKC activity has an inhibitory role, acting as a negative regulator of respiratory burst. During respiratory burst, sphingosine C18:1 decreased significantly (see **Fig. 2**). Previous studies found that sphingosine is converted to *N*,*N*-dimethyl sphingosine (DMS), which has an even stronger inhibitory effect on PKC[60]. This may explain the decrease in sphingosine C18:1; however, DMS was not included in our analysis.

E-series prostaglandins play a role in cell signalling by activating E2 and E4 prostanoid receptors located on the neutrophils[49]. In a negative feedback mechanism, receptor E2 and E4 activation increases intracellular levels of cAMP inhibiting neutrophil extracellular traps[61] and the respiratory burst[62]. This may explain the increased extracellular levels of E-series prostaglandins, including PGE_2 as a protective mechanism.

PGD_2 has both pro-inflammatory and anti-inflammatory properties and is considered one of the major mediators of the mast cell allergic response and can serve as a potent eosinophil chemoattractant[63,64]. During respiratory burst, PGD_2 is rapidly metabolised through enzymatic and non-enzymatic pathways to 11-epi-PGF2α, dihydro-15-keto-PGD_2, and PGJ_2 in order to attract eosinophils to inflammatory sites[63]. However, PGJ_2 was not included among the metabolites analysed in the current study. Thus, PGD_2 may be produced during respiratory burst in order to attract other immune cells (e.g. eosinophils), thereby further stimulating the immune response at the site of inflammation. We hypothesise that ROS generated by NADPH oxidase during respiratory burst induces lipid peroxidation in the cell membrane. Thus, prostaglandins and isoprostanes are secreted into the extracellular space during membrane repair (see **Fig. 4**). Although our analysis revealed significant PMA-induced changes in PGE_2, PGD_2, (±)5-iPF2α-IV, and 8-12-iPF2α-IV in the medium, DPI had the same effect, with slightly increased levels.

Taken together, these results suggest that UPE is correlated only with intracellular signalling metabolic intermediates. These findings strongly support the notion that UPE is linked to intracellular metabolism. Another explanation for the results of our analysis of extracellular metabolites is that the time course of respiratory burst (measured up to 9000 seconds) was too short for studying the flow of metabolites from the cytoplasm to the extracellular medium.

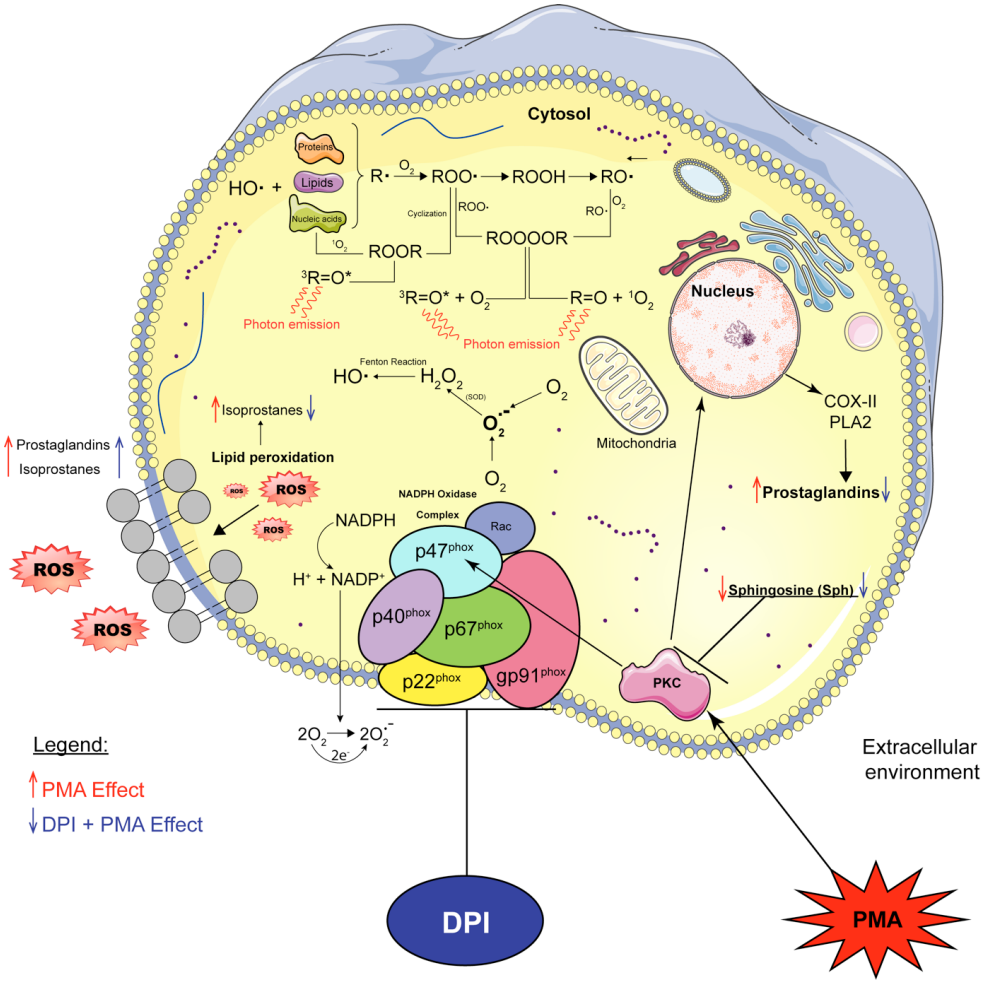

Figure 4. Schematic overview of the biological events involved in NADPH oxidase during PMA-induced respiratory burst in differentiated HL-60 cells. PMA activates protein kinase C (PKC), which signals to the nucleus, activating cyclooxygenase (COX) and phospholipase A_2 (PLA2) pathways, leading to the production of prostaglandins. $O_2^{\bullet-}$ is first produced by NADPH oxidase as a primary ROS and is subsequently dismutated to H_2O_2 by superoxide dismutase (SOD). Thus, H_2O_2 serves as a substrate for generating hydroxyl radicals ($OH^{\bullet}$) via the Fenton reaction. Hydroxyl radicals ($OH^{\bullet}$) are potent oxidants that can produce the initial radical ($R^{\bullet}$) form of a wide range of biomolecules, including lipids, proteins, and nucleic acids. Via this mechanism, molecular oxygen is added to produce a peroxyl radical ($ROO^{\bullet}$), followed by cyclisation to produce dioxetane (ROOR) and decomposition to produce triplet excited carbonyl[23]. Alternatively, two $ROO^{\bullet}$ moieties can recombine to form tetroxide (ROOOOR), which can decompose to form triplet excited carbonyl or singlet oxygen via the Russel reaction[23]. These electron-excited species emit photons, giving rise to UPE[23]. Eventually, intracellular ROS can react with biomolecules in the cell membrane (i.e. lipid peroxidation), giving rise to isoprostanes. Treating differentiated HL-60 cells with DPI, which binds to the NADPH oxidase complex, partially inhibits ROS production, decreases UPE emission, and decreases the levels of prostaglandins and isoprostanes. This figure was drawn by the

CONCLUSIONS

In summary, we report a strong correlation between ultra-weak photon emission intensity, NADPH oxidase activity and intracellular metabolism. The intracellular levels of the isoprostanes 8-iso-PGE_1 and 8-iso-PGE_2 and the prostaglandin PGE_1 significantly increased during PMA-induced respiratory burst, and DPI inhibited 50-60% of the PMA-induced UPE signal. These results indicate that UPE can be used as a dynamic readout tool in combination with metabolomics to monitor oxidative metabolism in ROS-related physiological processes. Follow-up studies should focus on identifying the specific radical species using spin-trapping electron paramagnetic resonance, which may also help identify the molecules that undergo oxidative damage. Optical spectral analysis of the UPE signal may also help identify the specific photon-emitting molecules.

ACKNOWLEDGEMENTS

This work was supported by CNPq, the National Council for Scientific and Technological Development – Brazil. R.C.R.B. is the recipient of a scholarship from Science without Borders (scholarship number 230827/2012-8). The authors thank Dr Slavik Koval for help with statistical analyses.

REFERENCES

1 Babior, B. M. The respiratory burst oxidase. In: *Molecular Aspects of Inflammation* (Sies, H., Flohe, L., Zimmer, G. Eds) Springer-Verlag Berlin Heidelberg. 41-47 (1991).
2 Dahlgren, C. & Karlsson, A. Respiratory burst in human neutrophils. *J Immunol Methods* **232**, 3-14 (1999).
3 Glass, G. A. *et al.* The respiratory burst oxidase of human neutrophils. Further studies of the purified enzyme. *J Biol Chem* **261**, 13247-13251 (1986).
4 Bylund, J., Björnsdottir, H., Sundqvist, M., Karlsson, A. & Dahlgren, C. Measurement of respiratory burst products, released or retained, during activation of professional phagocytes. *Neutrophil methods and protocols*, 321-338 (2014).
5 Bylund, J., Brown, K. L., Movitz, C., Dahlgren, C. & Karlsson, A. Intracellular generation of superoxide by the phagocyte NADPH oxidase: how, where, and what for? *Free Radic Biol and Med* **49**, 1834-1845 (2010).
6 Panday, A., Sahoo, M. K., Osorio, D. & Batra, S. NADPH oxidases: an overview from structure to innate immunity-associated pathologies. *Cell Mol Immunol* **12**, 5-23 (2015).
7 Babior, B. M. NADPH oxidase: an update. *Blood* **93**, 1464-1476 (1999).
8 Bedard, K. & Krause, K. H. The NOX family of ROS-generating NADPH oxidases: physiology and pathophysiology. *Physiol Rev* **87**, 245-313, (2007).
9 Ray, P. D., Huang, B. W. & Tsuji, Y. Reactive oxygen species (ROS) homeostasis and redox regulation in cellular signaling. *Cell Signal* **24**, 981-990, (2012).

10 Bartsch, H. & Nair, J. Chronic inflammation and oxidative stress in the genesis and perpetuation of cancer: role of lipid peroxidation, DNA damage, and repair. *Langenbecks Arch Surg* **391**, 499-510, (2006).

11 Kumar, B., Koul, S., Khandrika, L., Meacham, R. B. & Koul, H. K. Oxidative stress is inherent in prostate cancer cells and is required for aggressive phenotype. *Cancer Res* **68**, 1777-1785, (2008).

12 Perry, G., Castellani, R. J., Hirai, K. & Smith, M. A. Reactive Oxygen Species Mediate Cellular Damage in Alzheimer Disease. *J Alzheimers Dis* **1**, 45-55 (1998).

13 Sugamura, K. & Keaney, J. F., Jr. Reactive oxygen species in cardiovascular disease. *Free Radic Biol Med* **51**, 978-992, (2011).

14 Altenhofer, S., Radermacher, K. A., Kleikers, P. W., Wingler, K. & Schmidt, H. H. Evolution of NADPH Oxidase Inhibitors: Selectivity and Mechanisms for Target Engagement. *Antioxid Redox Signal* **23**, 406-427, (2015).

15 Drummond, G. R., Selemidis, S., Griendling, K. K. & Sobey, C. G. Combating oxidative stress in vascular disease: NADPH oxidases as therapeutic targets. *Nat Rev Drug Discov* **10**, 453-471, (2011).

16 Schieber, M. & Chandel, N. S. ROS function in redox signaling and oxidative stress. *Curr Biol* **24**, R453-462, (2014).

17 Bylund, J., Bjornsdottir, H., Sundqvist, M., Karlsson, A. & Dahlgren, C. Measurement of respiratory burst products, released or retained, during activation of professional phagocytes. *Methods Mol Biol* **1124**, 321-338, (2014).

18 Prasad, A. & Pospisil, P. Linoleic acid-induced ultra-weak photon emission from Chlamydomonas reinhardtii as a tool for monitoring of lipid peroxidation in the cell membranes. *PLoS One* **6**, e22345, (2011).

19 Rastogi, A. & Pospisil, P. Ultra-weak photon emission as a non-invasive tool for the measurement of oxidative stress induced by UVA radiation in Arabidopsis thaliana. *J Photochem Photobiol B* **123**, 59-64 (2013).

20 Ives, J. A. *et al.* Ultraweak photon emission as a non-invasive health assessment: a systematic review. *PLoS One* **9**, e87401 (2014).

21 Cifra, M. & Pospisil, P. Ultra-weak photon emission from biological samples: definition, mechanisms, properties, detection and applications. *J Photochem Photobiol B* **139**, 2-10 (2014).

22 Devaraj, B., Usa, M. & Inaba, H. Biophotons: Ultraweak light emission from living systems. *Curr Opin Solid St M* **2**, 188-193 (1997).

23 Pospisil, P., Prasad, A. & Rac, M. Role of reactive oxygen species in ultra-weak photon emission in biological systems. *J Photochem Photobiol B* **139**, 11-23 (2014).

24 Van Wijk, R., Van Wijk, E. P., Wiegant, F. A. & Ives, J. Free radicals and low-level photon emission in human pathogenesis: state of the art. *Indian J Exp Biol* **46**, 273-309 (2008).

25 Rastogi, A. & Pospisil, P. Spontaneous ultraweak photon emission imaging of oxidative metabolic processes in human skin: effect of molecular oxygen and antioxidant defense system. *J Biomed Opt* **16**, 096005 (2011).

26 Burgos, R. C., van Wijk, E. P., van Wijk, R., He, M. & van der Greef, J. Crossing the Boundaries of Our Current Healthcare System by Integrating Ultra-Weak Photon Emissions with Metabolomics. *Front Physiol* **7**, 611 (2016).

27 Burgos, R. C. *et al.* Tracking biochemical changes correlated with ultra-weak photon emission using metabolomics. *J Photochem Photobiol B* **163**, 237-245 (2016).

28 Galantsev, V. P., Kovalenko, S. G., Moltchanov, A. A. & Prutskov, V. I. Lipid peroxidation, low-level chemiluminescence and regulation of secretion in the mammary gland. *Experientia* **49**, 870-875 (1993).

29 McCarthy, M. K. & Weinberg, J. B. Eicosanoids and respiratory viral infection: coordinators of inflammation and potential therapeutic targets. *Mediators Inflamm* **2012**, 236345 (2012).

30 Montuschi, P., Barnes, P. J. & Roberts, L. J., 2nd. Isoprostanes: markers and mediators of oxidative stress. *FASEB J* **18**, 1791-1800 (2004).

31 Cadenas, E., Boveris, A. & Chance, B. in *Free Radicals in Biology* 211-242 (Academic Press, 1984).

32 Cadenas, E. & Sies, H. Formation of electronically excited states during the oxidation of arachidonic acid by prostaglandin endoperoxide synthase. *Methods Enzymol* **319**, 67-77 (2000).

33 Cadenas, E., Sies, H., Nastainczyk, W. & Ullrich, V. Singlet oxygen formation detected by low-level chemiluminescence during enzymatic reduction of prostaglandin G2 to H2. *Hoppe Seylers Z Physiol Chem* **364**, 519-528 (1983).

34 Nakano, M. Low-level chemiluminescence during lipid peroxidations and enzymatic reactions. *J Biolumin Chemilumin* **4**, 231-240 (1989).

35 Breitman, T. R., Selonick, S. E. & Collins, S. J. Induction of differentiation of the human promyelocytic leukemia cell line (HL-60) by retinoic acid. *Proc Natl Acad Sci U S A* **77**, 2936-2940 (1980).

36 Levy, R., Rotrosen, D., Nagauker, O., Leto, T. L. & Malech, H. L. Induction of the respiratory burst in HL-60 cells. Correlation of function and protein expression. *J Immunol* **145**, 2595-2601 (1990).

37 Xia, J., Mandal, R., Sinelnikov, I. V., Broadhurst, D. & Wishart, D. S. MetaboAnalyst 2.0--a comprehensive server for metabolomic data analysis. *Nucleic Acids Res* **40**, W127-133 (2012).

38 Xia, J., Sinelnikov, I. V., Han, B. & Wishart, D. S. MetaboAnalyst 3.0--making metabolomics more meaningful. *Nucleic Acids Res* **43**, W251-257 (2015).

39 Fu, J. *et al.* Metabolomics profiling of the free and total oxidised lipids in urine by LC-MS/MS: application in patients with rheumatoid arthritis. *Anal Bioanal Chem* **408**, 6307-6319 (2016).

40 Collins, S. J. The HL-60 promyelocytic leukemia cell line: proliferation, differentiation, and cellular oncogene expression. *Blood* **70**, 1233-1244 (1987).

41 Gallagher, R. *et al.* Characterization of the continuous, differentiating myeloid cell line (HL-60) from a patient with acute promyelocytic leukemia. *Blood* **54**, 713-733 (1979).

42 Dang, P. M., Fontayne, A., Hakim, J., El Benna, J. & Perianin, A. Protein kinase C zeta phosphorylates a subset of selective sites of the NADPH oxidase component p47phox and participates in formyl peptide-mediated neutrophil respiratory burst. *J Immunol* **166**, 1206-1213 (2001).

43 el Benna, J., Faust, L. P. & Babior, B. M. The phosphorylation of the respiratory burst oxidase component p47phox during neutrophil activation. Phosphorylation of sites recognized by protein kinase C and by proline-directed kinases. *J Biol Chem* **269**, 23431-23436 (1994).

44 Tardif, M., Rabiet, M. J., Christophe, T., Milcent, M. D. & Boulay, F. Isolation and characterization of a variant HL60 cell line defective in the activation of the NADPH oxidase by phorbol myristate acetate. *J Immunol* **161**, 6885-6895 (1998).

45 Cross, A. R. & Jones, O. T. The effect of the inhibitor diphenylene iodonium on the superoxide-generating system of neutrophils. Specific labelling of a component polypeptide of the oxidase. *Biochem J* **237**, 111-116 (1986).

46 Hancock, J. T. & Jones, O. T. G. The Inhibition by Diphenyleneiodonium and Its Analogs of Superoxide Generation by Macrophages. *Biochemical Journal* **242**, 103-107 (1987).

47 Liu, Y., Fiskum, G. & Schubert, D. Generation of reactive oxygen species by the mitochondrial electron transport chain. *J Neurochem* **80**, 780-787 (2002).

48 Li, Y. & Trush, M. A. Diphenyleneiodonium, an NAD(P)H oxidase inhibitor, also potently inhibits mitochondrial reactive oxygen species production. *Biochem Bioph Res Co* **253**, 295-299 (1998).

49 Buczynski, M. W., Dumlao, D. S. & Dennis, E. A. Thematic Review Series: Proteomics. An integrated omics analysis of eicosanoid biology. *J Lipid Res* **50**, 1015-1038 (2009).

50 Fullerton, J. N., O'Brien, A. J. & Gilroy, D. W. Lipid mediators in immune dysfunction after severe inflammation. *Trends Immunol* **35**, 12-21 (2014).

51 Parchmann, S. & Mueller, M. J. Evidence for the Formation of Dinor Isoprostanes E1from α-Linolenic Acid in Plants. *J Biol Chem* **273**, 32650-32655 (1998).

52 Morrow, J. D. *et al.* Free radical-induced generation of isoprostanes in vivo. Evidence for the formation of D-ring and E-ring isoprostanes. *J Biol Chem* **269**, 4317-4326 (1994).

53 Longmire, A. W., Roberts, L. J. & Morrow, J. D. Actions of the E2-isoprostane, 8-ISO-PGE2, on the platelet thromboxane/endoperoxide receptor in humans and rats: additional evidence for the existence of a unique isoprostane receptor. *Prostaglandins* **48**, 247-256 (1994).

54 Wilson, J. R. & Kapoor, S. C. Contribution of prostaglandins to exercise-induced vasodilation in humans. *Am J Physiol* **265**, H171-175 (1993).

55 Smith, J. B. Prostaglandins and platelet aggregation. *Acta Med Scand Suppl* **651**, 91-99 (1981).

56 Rieser, C., Bock, G., Klocker, H., Bartsch, G. & Thurnher, M. Prostaglandin E2 and tumor necrosis factor alpha cooperate to activate human dendritic cells: synergistic activation of interleukin 12 production. *J Exp Med* **186**, 1603-1608 (1997).

57 Van Brocklyn, J. R. & Williams, J. B. The control of the balance between ceramide and sphingosine-1-phosphate by sphingosine kinase: oxidative stress and the seesaw of cell survival and death. *Comp Biochem Physiol B Biochem Mol Biol* **163**, 26-36 (2012).

58 Lambeth, J., Burnham, D. & Tyagi, S. Sphinganine effects on chemoattractant-induced diacylglycerol generation, calcium fluxes, superoxide production, and on cell viability in the human neutrophil. Delivery of sphinganine with bovine serum albumin minimizes cytotoxicity without affecting inhibition of the respiratory burst. *J Biol Chem* **263**, 3818-3822 (1988).

59 Hannun, Y. A., Loomis, C. R., Merrill, A. H., Jr. & Bell, R. M. Sphingosine inhibition of protein kinase C activity and of phorbol dibutyrate binding in vitro and in human platelets. *J Biol Chem* **261**, 12604-12609 (1986).

60 Satoshi, K. *et al.* Effect of sphingosine and its N-methyl derivatives on oxidative burst, phagokinetic activity, and trans-endothelial migration of human neutrophils. *Biochem Pharmacol* **44**, 1585-1595 (1992).

61 Shishikura, K. *et al.* Prostaglandin E2 inhibits neutrophil extracellular trap formation through production of cyclic AMP. *Br J Pharmacol* **173**, 319-331 (2016).

62 Mitsuyama, T., Takeshige, K. & Minakami, S. Cyclic-Amp Inhibits the Respiratory Burst of Electropermeabilized Human Neutrophils at a Downstream Site of Protein-Kinase-C. *Biochim Biophys Acta* **1177**, 167-173 (1993).

63 Heinemann, A., Schuligoi, R., Sabroe, I., Hartnell, A. & Peskar, B. A. Delta 12-prostaglandin J2, a plasma metabolite of prostaglandin D2, causes eosinophil mobilization from the bone marrow and primes eosinophils for chemotaxis. *J Immunol* **170**, 4752-4758 (2003).

64 Saito, S., Tsuda, H. & Michimata, T. Prostaglandin D2 and reproduction. *Am J Reprod Immunol* **47**, 295-302 (2002).

SUPPLEMENTARY INFORMATION

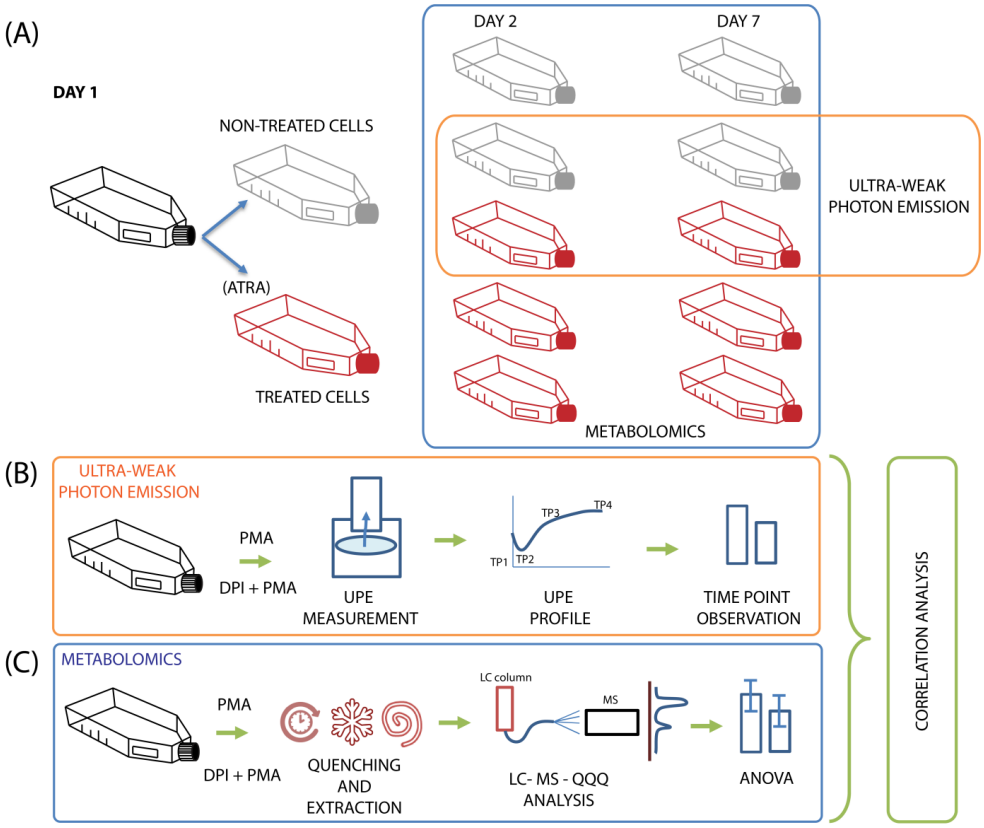

Supplementary Figure S1. Experimental design. (A) Cultured HL-60 cells were split into 10 flasks; six flasks were treated with ATRA (red), and four flasks received only vehicle (grey). (B) Ultra-weak photon emission (UPE) was measured on days 2 and 7. PMA or DPI+PMA was applied to each flask to induce respiratory burst, and UPE was recorded for 9000 seconds. (C) Samples were collected for metabolomics analyses at the specified time points (TP1, TP2, TP3, and TP4) indicated in (B). TP1 samples were collected prior to the addition of PMA/ DPI. After sample collection, liquid-liquid extraction was used to obtain cell extracts and medium extracts. The metabolic profile was recorded using LC-MS-QQQ. The metabolic data were analysed using an ANOVA, and Spearman's correlation coefficient was calculated in order to analyse the relationship between the UPE data and metabolic profiles.

Supplementary Table S1. List of metabolites detected in the intracellular (cell lysates) and extracellular (culture medium) samples.

METABOLITE	INTRACELLULAR ANALYSIS	EXTRACELLULAR ANALYSIS
8-iso-PGE_2	Detected	Not detected
8-iso-PGE_1	Detected	Not detected
PGE_2	Detected	Detected
PGE_1	Detected	Detected
PGD_2	Not detected	Detected
PGF_{2a}	Detected	Detected
(±)5-iPF2a-IV	Not detected	Detected
8-iso-PGA_1	Detected	Detected
PGA_2	Detected	Detected
8-12-iPF2a-IV	Detected	Detected
Sph C18_1	Detected	Not detected
Spha C18_0	Detected	Detected
NO_2-LA	Not detected	Detected

PGE, prostaglandin E; PGD, prostaglandin D; PGF, prostaglandin F; iPF, isoprostane F; PGA, prostaglandin A; Sph, sphingosine C18:1; Spha, sphinganine C18:0; NO2-LA, nitro-linoleic acid.

Supplementary Table S2. Intracellular metabolites with significant changes during PMA and DPI+PMA treatment (n=3/ TP) collected on Day 7.

		ANOVA			SPEARMAN'S CORRELATION	
Sample Treatment	***Compound***	***p-value***	***FDR*** [a]	***Fisher's LSD*** [b]	***Corr. Coefficient***	**p-*value***
PMA	**Sphinganine C18:0**	$3.93E^{-05}$	0.00017	TP3 vs TP1; TP4 vs TP1; TP3 vs TP2; TP4 vs TP2; TP4 vs TP3	0.60	0.40
	8-iso-PGE1	$4.23E^{-05}$	0.00017	TP3 vs TP1; TP4 vs TP1; TP3 vs TP2; TP4 vs TP2	0.80	0.20
	8-iso-PGE2	$4.51E^{-05}$	0.00017	TP2 vs TP1; TP3 vs TP1; TP4 vs TP1; TP3 vs TP2; TP4 vs TP2	1.0	0.01
	PGE1	0.00097	0.00232	TP3 vs TP1; TP4 vs TP1; TP3 vs TP2; TP4 vs TP2	1.0	0.01
	Sphingosine C18:1	0.024	0.04847	TP1 vs TP3; TP2 vs TP3	-1.0	0.01
DPI + PMA	**8-iso-PGE1**	0.00017	0.00180	TP3 vs TP1; TP4 vs TP1; TP3 vs TP2; TP4 vs TP2	1.0	0.01
	8-iso-PGE2	0.0003	0.00180	TP3 vs TP1; TP4 vs TP1; TP3 vs TP2; TP4 vs TP2	1.0	0.01
	PGE1	0.018	0.07216	TP3 vs TP1; TP4 vs TP1; TP3 vs TP2; TP4 vs TP2	0.60	0.40

[a] FDR: false discovery rate.

[b] Fisher's LSD: significance between the Time Points (TP) indicated (*p-value*<0.05).

Supplementary Table S3. Extracellular metabolites with significant changes during PMA and DPI+PMA treatment (n=3 samples/group) collected on Day 7.

		ANOVA			SPEARMAN'S CORRELATION	
Sample Treatment	***Compound***	***p-value***	***FDR*** [a]	***Fisher's LSD*** [b]	***Corr. Coefficient***	**p-*value***
PMA	**(±)5-iPF2α-IV**	9.25E^{-09}	1.02E-07	TP3 vs TP1; TP4 vs TP1; TP3 vs TP2; TP4 vs TP2; TP4 vs TP3	0.74	0.26
	PGD2	5.28E^{-06}	2.90E-05	TP3 vs TP1; TP4 vs TP1; TP3 vs TP2; TP4 vs TP2; TP4 vs TP3	0.80	0.20
	8-12-iPF2α-IV	0.000158	0.00058	TP3 vs TP1; TP4 vs TP1; TP3 vs TP2; TP4 vs TP2; TP4 vs TP3	0.80	0.20
	PGE2	0.018996	0.05223	TP4 vs TP1; TP4 vs TP2	0.80	0.20
DPI + PMA	**PGD2**	2.04E^{-07}	2.24E-06	TP3 vs TP1; TP4 vs TP1; TP3 vs TP2; TP4 vs TP2; TP4 vs TP3	0.60	0.40
	PGE2	3.69E^{-06}	2.03E-05	TP3 vs TP1; TP4 vs TP1; TP3 vs TP2; TP4 vs TP2; TP4 vs TP3	0.80	0.20
	(±)5-iPF2α-IV	3.11E^{-05}	0.00011	TP1 vs TP2; TP3 vs TP1; TP4 vs TP1; TP3 vs TP2; TP4 vs TP2; TP4 vs TP3	0.60	0.40
	8-12-iPF2α-IV	0.00027	0.00074	TP1 vs TP3; TP2 vs TP3; TP4 vs TP3	0.60	0.40

[a] FDR: false discovery rate.

[b] Fisher LSD: significance between the Time Points (TP) indicated (*p-value*<0.05).

Chapter 5

Cellular glutathione levels in HL-60 cells during respiratory burst are not correlated with ultra-weak photon emission

Based on

Rosilene Cristina Rossetto Burgos, Wei Zhang, Eduard P.A. van Wijk, Thomas Hankemeier, Rawi Ramautar and Jan van der Greef

Cellular glutathione levels in HL-60 cells during respiratory burst are not correlated with ultra-weak photon emission

Journal of Photochemistry and Photobiology B: Biology **175**, 291-296, (2017)

doi:10.1016/j.jphotobiol.2017.09.002

ABSTRACT

Recently, ultra-weak photon emission (UPE) was developed as a novel tool for measuring oxidative metabolic processes, as its generation is related to reactive oxygen species (ROS). Both an imbalance in ROS or the uncontrolled production of ROS can lead to oxidative stress, which is commonly associated with many diseases. In addition to playing several biological functions, the thiol amino acid glutathione has an important antioxidant function in the body's defense against ROS. Specifically, glutathione is an important endogenous antioxidant that helps maintain oxidant levels. At the cellular level, glutathione is present in its reduced form (GSH) at relatively high concentrations (in the millimolar range) and in its oxidized form (GSSG) at low concentrations (in the micromolar range). Thus, the GSH/GSSG ratio is often used as an indicator of cellular redox state. Here, we used the HL-60 cell line as a model system in order to determine whether UPE is correlated with intracellular GSH and GSSG levels. HL-60 cells were differentiated into neutrophil-like cells and then stimulated to undergo respiratory burst. We then recorded UPE in real time for 9000 seconds and used capillary electrophoresis coupled to mass spectrometry to measure GSH and GSSG levels in cell extracts. We found that although respiratory burst significantly decreased the GSH/GSSG ratio, this change was not correlated with the UPE profile.

INTRODUCTION

Ultra-weak photon emission (UPE) is endogenous light emitted by virtually all living systems during oxidative metabolism and under stress conditions[1,2]. During biochemical oxidative reactions, reactive oxygen species (ROS) are generated, leading to the spontaneous emission of weak photons as a result of the electrons' transition from an excited state to the ground state[1,2]. When ROS are produced at high levels, they can react with biomolecules, leading to several forms of damage at the cellular to macromolecular levels; this condition — known as oxidative stress — has been associated with many pathological mechanisms[3-6]. In recent years, UPE has often been associated with oxidative stress based on the notion that UPE is directly linked to ROS production; therefore, UPE has been used as a label-free, non-invasive tool to dynamically monitor oxidative stress during metabolic processes[7]. For example, reactions between radicals and biomolecules such as proteins and lipids (e.g., lipid peroxidation) have been reported to increase UPE intensity[7-9].

Glutathione (L-γ-glutamyl-L-cysteinylglycine, or GSH) is the most abundant thiol amino acid and is present in virtually every cell in the body[10,11]. The biosynthesis of GSH (see **Fig. 1**) begins with cysteine, glutamate, and glycine and requires two ATP molecules and two enzymatic steps involving γ-glutamylcysteine synthetase and glutathione synthetase[12]. GSH has many biological functions, including the synthesis of proteins and DNA, molecular transport, and redox signaling. However, its function as an antioxidant is the most biologically significant; specifically, GSH functions as a major scavenger of free radicals and ROS[10-12]. Under oxidative conditions, GSH is oxidized via the glutathione peroxidase system to produce glutathione disulfide (GSSG), which can be converted back to GSH via the glutathione reductase system (**Fig. 1**); this process maintains physiological levels of ROS[10-12]. In this context, glutathione plays a role in the cellular redox system, and the GSH/GSSG ratio has been considered an important indicator of cellular redox state[13]. Because glutathione plays a role in the cellular antioxidant system, UPE may be correlated with the cell's glutathione antioxidant capacity.

As a follow-up to our previous studies[7,14], we examined whether UPE is associated with GSH/GSSG ratio in HL-60 cells during respiratory burst. Given that the GSH/GSSG ratio is often reported as a marker of oxidative stress, our aim was to determine whether UPE indeed reflects this process and whether UPE can be used as a non-invasive tool for monitoring cellular levels of oxidative stress.

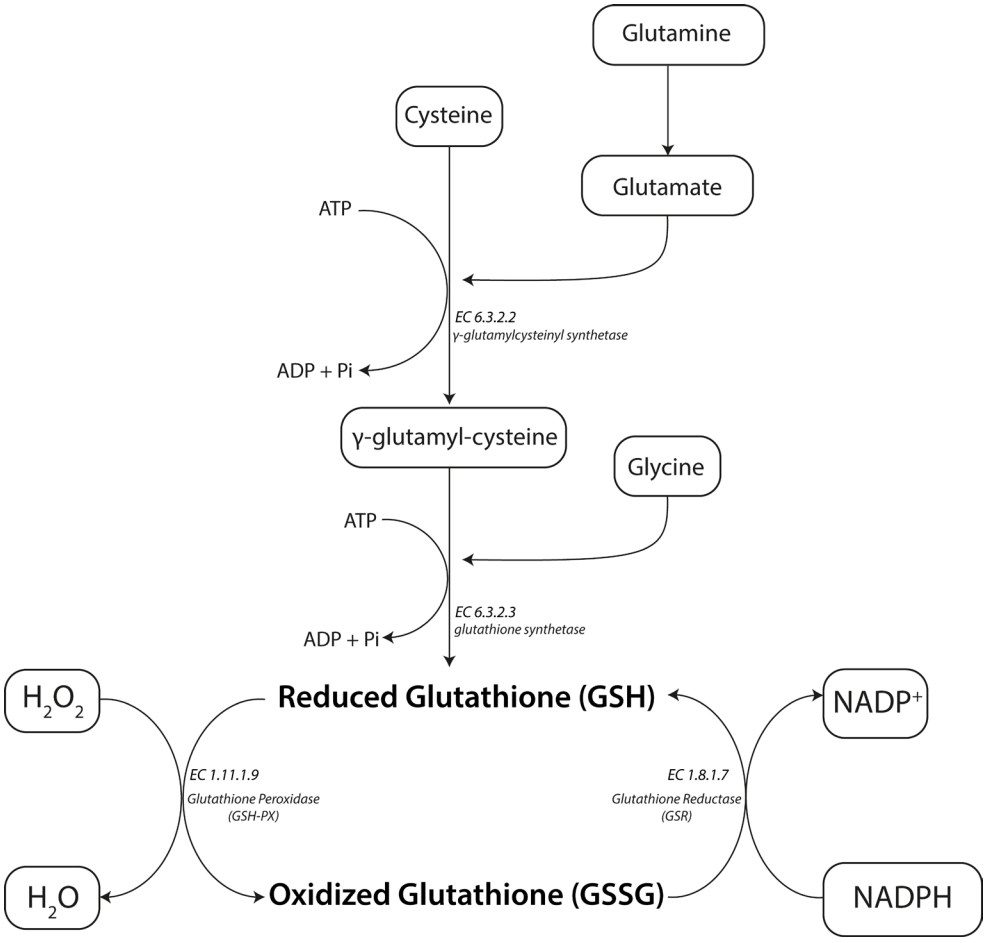

Figure 1. The biosynthetic pathway for the production, consumption, and regeneration of GSH in biological systems. In the presence of energy (ATP) and γ-glutamylcysteine synthetase (EC 1.8.1.7), cysteine and glutamate are used to produce γ-glutamyl-cysteine. GSH is then formed using a second molecule of ATP and glutathione synthetase (EC 6.3.2.3). In presence of radicals, GSH is oxidized to GSSG via glutathione peroxidase (EC 1.11.1.9). GSSG can then be reduced back to GSH by glutathione reductase (EC 1.8.1.7) using NADPH.

Several methods have been used by various groups to measure GSH and GSSG. Classic approaches such as spectrophotometric-based methods are well described in the literature; the most common of these methods are the glutathione S-transferase 1-chloro-2,4-dinitrobenzene (CDNB) endpoint method and the GSH–5,5′-dithio-bis (2-nitrobenzoic acid) "enzymatic recycling assay"[15-17]. Despite its popularity, however, the CDNB endpoint method measures only GSH and lacks sensitivity[15]; moreover, in both methods GSH can be readily oxidized during sample preparation, leading to an error when calculating GSH and GSSG levels[18,19]. Thus, these methods provide unsatisfactory levels of specificity and selectivity.

Chromatographic methods such as HPLC-UV, HPLC-FL, LC-MS, and GC-MS are commonly used to measure glutathione[20,21]. Capillary electrophoresis coupled to mass spectrometry (CE-MS) is particularly well suited due to its high separation efficiency, high selectivity, and low solvent and sample consumption[22,23].

With respect to the auto-oxidation of GSH, several derivatization compounds have been used recently to prevent the oxidation of GSH during sample collection, preparation, and analysis[24,25]. *N*-ethylmaleimide (NEM) is a preferred alkylating agent for the derivatization of GSH for several reasons. First, NEM is a specific alkylating agent for sulfhydryl groups. Second, NEM forms a stable thioether bond by reacting with sulfhydryl groups, leading to the formation of the GSH adducts *N*-ethyl succinimide-*S*-glutathione (GS-NEM)[26-31]. Third, NEM inhibits glutathione reductase, blocking the reduction of GSSG to GSH[18]. Finally, NEM requires only a short incubation time. Despite these advantages, however, NEM is not suitable for use in spectrophotometric methods due to enzyme inhibition[16,17].

Here, we studied the relationship between UPE and intracellular GSH/GSSG ratio as an indicator of oxidative stress marker in differentiated HL-60 cells. The respiratory burst was induced in HL-60 cells using phorbol 12-myristate 13-acetate (PMA), and UPE intensity was measured for 9000 seconds[7,14]. The intracellular levels of glutathione (GS-NEM and GSSG) were measured in cell pellets collected during this time interval and analyzed using CE-MS. Finally, the GS-NEM/GSSG ratio was calculated, and the relationship between the dynamic UPE profile and glutathione levels was determined.

METHODS

Culture, differentiation, and induction of respiratory burst in HL-60 cells

HL-60 cells (CCL-240; American Type Culture Collection, ATCC, Manassas, VA) were cultured in Iscove's Modified Dulbecco's Medium (IMDM) without phenol red (Gibco-Life Technologies, Grand Island, NY) supplemented with 10% (v/v) fetal calf serum and 1% (v/v) penicillin/streptomycin (Sigma-Aldrich, St. Louis, MO). Cells were seeded at 0.2 x 10^6 cells/ml and maintained in the exponential growth phase in a CO_2 incubator at 37°C in accordance with the instructions provided by ATCC. The trypan-blue exclusion method was used to count the cells and determine their viability (>85%) with an automated cell counter (Bio-Rad, Hercules, CA).

During a new cell passage, the cells were split into two flasks. The cells in one flask were differentiated by the addition of freshly prepared 1 µM all-*trans*-retinoic acid (ATRA; Sigma-Aldrich) in DMSO (differentiated cells); the cells in the other flask received no treatment

(undifferentiated control cells). The cells were then incubated for up to 7 days. PMA (54 nM, Sigma-Aldrich) was then applied in order to induce respiratory burst, and UPE was measured. All experiments were performed on cells at passage number P10 or P11.

Experimental design

In this study, we used an optimized experimental design (see **Supplementary Fig. S1**) based on our previous studies[7,14]. On day 7, PMA was applied to the differentiated and control cells in order to induce respiratory burst. At four times points (TP1, TP2, TP3, and TP4), cell samples were collected and used to measure GSH and GSSG. Aliquots of 10^7 cells per time point were used for the colorimetric assay and CE-MS analysis. UPE was measured for 9000 seconds (2.5 hours) after PMA induction. TP1 corresponds to the samples which were collected and analyzed before PMA induction; TP2 samples after 60 seconds, TP3 after 4500 seconds and TP4 after 9000 seconds respectively.

Ultra-weak photon emission

A series 9558B photomultiplier tube equipped with an S20 photocathode (ET Enterprises, Sweetwater, TX) was used to record the UPE profile. The detector was cooled to -25°C in order to reduce noise. Photon emission intensity (in counts/second) was recorded for 9000 seconds in a dark chamber that was maintained at 37°C using a Peltier element. To measure UPE, a 6-ml aliquot of suspended cells was transferred to the dark chamber immediately after induction with PMA (54 nM).

Sample collection and quenching of the cell pellets

For GS-NEM and GSSG analysis, 10^7 cells were collected at specific time points (see **Supplementary Fig. S1**), centrifuged for 4 minutes at 1000 rpm, and the supernatant (culture medium) was discarded. The cell pellets were resuspended in 1 ml cold (0-2°C) saline solution containing 0.9% NaCl and 1.5 mg/ml ethylenediaminetetraacetic acid (EDTA; Merck, Darmstadt, Germany). To analyze GSH and GSSG using our CE-MS approach, 50 mM NEM (Sigma-Aldrich) was added to the saline solution. The cells were centrifuged for 4 minutes at 1000 rpm, the supernatant was discarded, and the cell pellets were stored at -80°C until analysis.

CE-MS

Sample preparation

To extract the adduct GS-NEM and GSSG, the cell pellets were resuspended in 250 µl ice cold (-20°C) MeOH (80%; Biosolve BV, Valkenswaard, the Netherlands) containing 5 mM NEM.

The samples were processed in a bullet blender for 2 minutes on setting 8. The lysed cell suspension was then transferred to a 0.5-ml Eppendorf tube and dried in a speed-vac. The dried samples were resuspended in 20 µl of 250 mM ammonium acetate (Sigma-Aldrich), vortexed for 5 minutes at speed 8, centrifuged for 5 minutes at 13.2 rpm, and transferred to vials for CE-MS analysis.

CE-MS methodology

CE-MS was performed using an Agilent CE 7100 system (Agilent Technologies, Palo Alto, CA) coupled to an Agilent 6230 time-of-flight mass spectrometer. CE was coupled to MS via a sheath-liquid interface using an Agilent 1100 isocratic HPLC pump. The sheath-liquid was a mixture of water, methanol, and formic acid (50/50/0.1, v/v/v) that was delivered at a flow rate of 10 µl/min. An Agilent G1603A adapter kit and an Agilent G1607A CE-ESI-MS sprayer kit (Agilent Technologies, Waldbronn, Germany) were used for the linking, and an Agilent Mass Hunter Workstation was used to control the system and to acquire the data.

For the separation, a 90-cm long, bare fused-silica capillary (ID: 50 µm; Polymicro Technologies, Palo Alto, CA) was used, with 1 M formic acid (pH 1.8; Acros Organics, Geel, Belgium) as the background electrolyte (BGE). Milli-Q water (EMD Millipore, Billerica, MA) and 1 M NaOH (Merck) were used for capillary pre-conditioning. Prior to each run, the capillary was preconditioned by rinsing sequentially with water, sodium hydroxide, water, and BGE for 2 min at the pressure of 935 mbar.

Samples were injected hydrodynamically by applying a pressure of 50 millibars for 120 seconds, corresponding to circa 120 nl; this relatively high volume of sample injection was possible due to the application of dynamic pH junction[32]. After sample injection, a plug of BGE was added at a pressure of 50 millibars for 10 seconds. Voltage (30 kV) was then applied for 30 minutes at 25°C. Electrospray ionization-mass spectrometry (ESI-MS) was performed in the positive-ion mode. The capillary, fragmentor, and skimmer voltages were set to 4000, 100, and 50 V, respectively. The nebulizer pressure was 5 psi, and the drying gas was delivered at 7 l/min at 300°C. Data were recorded at a rate of 1.5 cycles per second (range: 50-1000 m/z). GS-NEM and GSSG were identified according to accurate mass and migration time using standard compounds as a reference. Standard solutions of GS-NEM (prepared in-house using a mixture of glutathione obtained from Cayman Chemicals and NEM) and GSSG (Sigma-Aldrich) were prepared fresh in Milli-Q water. The peak areas obtained for GS-NEM and GSSG were corrected using an internal standard (response ratio) and were then used to calculate the GSH/GSSG ratio.

Spectrophotometric assay

Total GSH (GSH + GSSG) and oxidized glutathione (GSSG) were measured using a spectrophotometric assay (enzymatic recycling method; Sigma-Aldrich). The samples were prepared and measured at room temperature in accordance with the protocol provided the manufacturer. In brief, pellets containing 10^7 cells per time point were lysed, the proteins were precipitated, and the samples were centrifuged. The supernatant was then split into two aliquots. One aliquot (10 µl) was diluted 50x and used to measure total GSH; the other aliquot (120 µl) was used undiluted to measure GSSG. GSH concentration was calculated using the following equation: GSH = total glutathione (GSH + GSSG) – GSSG x 2.

Statistical analysis

GraphPad Prism version 7.0 was used to create the smoothed UPE curve. We smoothed the curve using the function xy analysis (smooth - 2nd order of smoothing with 100 neighbors data points). Next, the smoothed data were normalized by the highest UPE intensity. The results obtained for levels of GS-NEM, GSSG and GS-NEM/GSSG ratio were uploaded to the web-based tool MetaboAnalyst for statistical analysis[33-35]. Data were log-transformed and auto-scaled in order to obtain a normal distribution[36]. Changes in GS-NEM and GSSG were analyzed over the four-time points using an ANOVA. The correlation between the UPE data and GSH levels was analyzed using Spearman's correlation coefficient (SPSS version 23; IBM Corp., Armonk, NY).

RESULTS

Ultra-weak photon emission

First, we differentiated HL-60 cells into neutrophil-like cells by incubating the cells in ATRA for 7 days. We then stimulated both differentiated and undifferentiated (control-treated) cells with PMA in order to induce respiratory burst. The UPE profile was then measured for 9000 seconds after PMA stimulation, as shown in **Fig. 2**.

Differentiated cells had a stronger PMA-induced UPE response compared to undifferentiated cells, consistent with the production of higher amounts of ROS[7,14]. Therefore, we hypothesized that intracellular glutathione (GSH) levels decrease during respiratory burst due to increased levels of ROS, thereby leading to oxidative stress conditions.

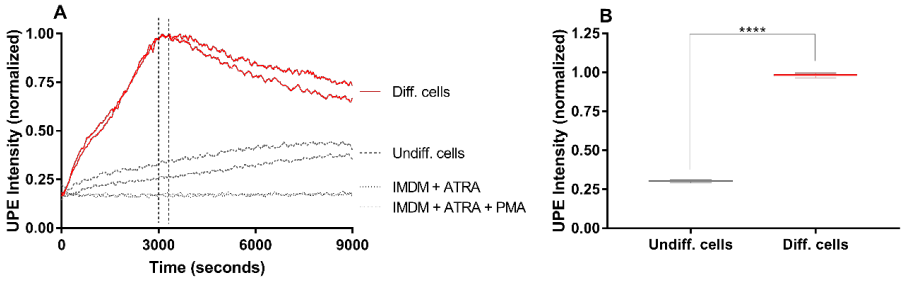

Figure 2. UPE profiles measured in differentiated and undifferentiated HL-60 cells during respiratory burst. **(A)** Cell suspensions (10^6 cells/ml) were recorded in the dark at 37°C for 9000 seconds following PMA stimulation. The lines (duplicate measurements) represent the normalized smoothed curve of 100 points. Control experiments were performed with medium IMDM + ATRA and medium IMDM + ATRA + PMA **(B)** Interval Analysis (analysis between 3000-3600 seconds as indicated in A). Student's paired t-test performed with ****$p < 0.0001$.

Intracellular GS-NEM and GSSG levels measured using CE-MS

Next, we examined the relationship between glutathione levels (GSH and GSSG) and the UPE profile using CE-MS to measure the levels of GSH and GSSG. We used the alkylating agent NEM when collecting the cell samples, allowing us to measure the adduct GS-NEM. We measured the intracellular levels of GS-NEM and GSSG in PMA-stimulated differentiated and undifferentiated HL-60 cells and compared the results with the dynamic UPE profile. Cells were collected and analyzed at four time points relative to PMA stimulation (see **Supplementary Fig. S1**).

Fig. 3 shows GS-NEM and GSSG levels measured using CE-MS. The levels of GS-NEM were similar between undifferentiated and differentiated cells, peaking at the second time point (TP2); in contrast, GSSG levels differed significantly, with a steep increase in the differentiated cells at TP3 and TP4. Thus, the GS-NEM/GSSG ratio — which is commonly used as a marker for cellular redox state — was significantly lower in the differentiated cells at TP3 and TP4. Intragroup ANOVA analysis revealed significant changes in the concentrations of GS-NEM, GSSG, and the GS-NEM/GSSG ratio in the differentiated cells over the four time points (see **Fig. 3** and **Supplementary Table S1**).

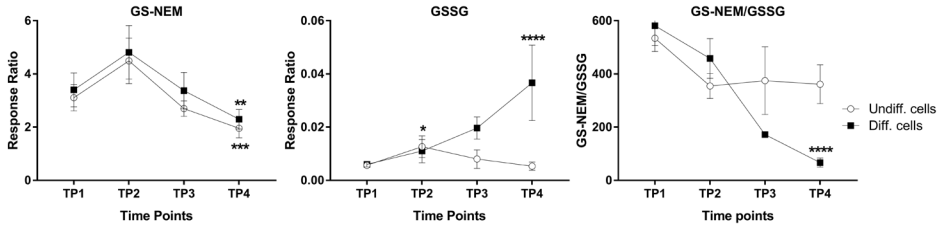

Figure 3. Intracellular levels of GS-NEM, GSSG, and GS-NEM/GSSG ratio measured in differentiated and undifferentiated HL-60 cells during PMA induced respiratory burst. GS-NEM and GSSG levels were measured using CE-MS. Intragroup ANOVA was performed over the four time points to analyze the differences in glutathione levels. Data are plotted as the mean (n=3) ± SD. **p*<0.05, ***p*<0.01, ****p*<0.001, and *****p*<0.0001. TP1, TP2, TP3, and TP4 correspond to 0, 60, 4500, and 9000 seconds, respectively, relative to PMA stimulation.

Correlation between UPE and Glutathione levels

Table 1 shows the Spearman's rank results obtained for the correlation between UPE data and the GS-NEM, GSSG and GS-NEM/GSSG ratio. Interestingly, there is an absence of significant correlations (*p*-values>0.05) although it shows correlation coefficients (r_s) ≥ 0.6.

Table 1. Spearman's rank correlation between the UPE and glutathione levels.

Compound	Cell Type	Correlation Coeficient (r_s)	*p*-value
GS-NEM	Diff. cells	-0.6	0.4
	Undiff. Cells	-0.6	0.4
GSSG	Diff. cells	0.8	0.2
	Undiff. Cells	0.0	1.0
GS-NEM/GSSG	Diff. cells	-0.8	0.2
	Undiff. Cells	-0.8	0.2

DISCUSSION

Treating HL-60 cells with ATRA causes the cells to differentiate into neutrophil-like cells[37]. During the respiratory burst, neutrophils are responsible for the first line of defense by generating high amounts of reactive oxygen species (ROS) in order to kill invading pathogens[38]. Because UPE is correlated with ROS production, it is considered a viable tool for monitoring dynamic oxidative processes in biological systems[7]. Glutathione is an endogenous cellular antioxidant that modulates physiological levels of ROS and is involved in the cell's response to oxidative stress[11]. Our goal was to study the role of glutathione in differentiated HL-60 cells during respiratory burst[7,14] and compare the UPE profile with glutathione (GS-NEM and GSSG) measured using our optimized CE-MS approach.

Several groups reviewed the challenges and pitfalls associated with analyzing glutathione in biological samples[18,19,25]. Sample preparation is a critical step in the process, as GSH can

undergo enzymatic and non-enzymatic autoxidation catalyzed by γ-glutamyltranspeptidase. GSH can also interact with and bind to proteins via S-H bonds, leading to the removal of GSH during sample preparation. Therefore, it is important to protect the thiol group during sample preparation in order to avoid possible miscalculations. Compared with spectrophotometric methods for measuring GSH, chromatographic methods have many advantages, including high specificity and the ability to detect concentrations in the picomolar range[39]. CE is in particular suited for the highly efficient analysis of polar and charged metabolites as compounds are separated according to their charge-to-size ratio. CE in combination with TOF-MS has proven to be a very efficient and selective tool for the separation of charged metabolites in biological samples[40,41]. Additional advantages of CE-MS include the capability to deal with biomass-limited samples and low solvent consumption[40,41].

Our optimized CE-MS method clearly demonstrates that GSH is readily oxidized during sample preparation, as samples collected and analyzed in the absence of the alkylating agent NEM contain GSSG, reflecting the auto-oxidation of GSH during sample manipulation (see **Supplementary Fig. S2** and **S3**). Therefore, it is important to use an alkylating agent such as NEM in order to prevent the auto-oxidation of GSH, thereby increasing the accuracy of the GSH/GSSG ratio.

Our GS-NEM and GSSG measurements using CE-MS show that glutathione levels (GS-NEM and GSSG) change in differentiated cells during respiratory burst, leading to cellular oxidative damage (i.e., a decrease in the GS-NEM/GSSG ratio). To support our results obtained using CE-MS, we also measured glutathione levels (total GSH and GSSG) using the conventional enzymatic recycling assay (see **Supplementary Fig. S4**), and we measured total GSH using our validated LC-MS platform[42] (see **Supplementary Fig. S5**). The results obtained using these additional analyses are consistent with our CE-MS results. Although it is not possible to compare the absolute concentrations obtained in the spectrophotometric assay with the results obtained using CE-MS or LC-MS, we found a similar trend with respect to total GSH, GSSG, and the calculated cellular redox ratio (GSH/GSSG). However, the absolute concentrations of total GSH in our study were in the micromolar range, and the GSH/GSSG ratio was considerably lower than the ratio obtained using our CE-MS approach, as well as previously reported values[19,43].

Here, we attempted to determine the association between UPE and the GSH/GSSG ratio in HL-60 cells during respiratory burst. In differentiated cells, glutathione (GS-NEM and total GSH) levels were significantly decreased, whereas the levels of GSSG increased significantly, causing a decrease in the GS-NEM/GSSG ratio and leading to cellular oxidation conditions. However, we found no statistically significant correlation between the UPE profile and

glutathione levels. In neutrophils, intracellular GSH levels decrease during respiratory burst, whereas glutathione synthesis and glutathione recycling pathways are upregulated in order to maintain homeostasis[44,45]. Because glutathione is an endogenous antioxidant, its response is relatively rapid; in contrast, the UPE profile likely reflects the sum of all oxidative processes. Thus, additional pathways are probably involved, operating at several organizational levels on a variety of time scales, possibly explaining the apparent lack of significant correlation between the GSH/GSSG ratio and the UPE profile. In addition to that, the respiratory burst is a physiological mechanism of defense capable to restore homeostasis.

Severe oxidative stress is the uncontrolled ROS formation overpowering the inherent homeostasis-restoring ability and consequently, it affects the process of GSSG being reduced to GSH, causing the accumulation of GSSG in cells[46]. Another hypothesis to be considered is that under such prolonged oxidative conditions GSSG can be eventually exported out of the cells to prevent a cellular shift in the redox equilibrium[47]. Therefore, prolonged exposed time of cellular oxidative conditions is required for the observation of glutathione depletion. In conclusion, there are many other biochemical processes which might be taken into consideration and that probably explain the absence of direct and significant correlation.

CONCLUSIONS AND FUTURE PERSPECTIVES

In summary, we have used our optimized CE-MS approach as a tool for measuring the GSH/GSSG ratio in cellular extracts. Intracellular GSH/GSSG ratio was measured during the oxidative burst, and the results were compared with dynamic UPE data recorded over the same time period. Although the GSH/GSSG ratio decreased in differentiated cells during respiratory burst, we found no statistically significant correlation between GSH/GSSG ratio and the UPE profile.

This experimental design can be expanded in future studies in order to increase the time exposure of cellular oxidative conditions, including more time points. In addition, computational models may provide mechanistic insight into the chemical kinetics processes that underlie UPE, thereby providing predictive value and the ability to better interpret UPE data.

ACKNOWLEDGMENTS

This work was supported by CNPq (the National Council for Scientific and Technological Development, Brazil). RCRB is the recipient of a scholarship from Science without Borders (scholarship number 230827/2012-8). The authors thank Johannes Cornelius Schoeman for valuable and constructive suggestions regarding the biochemistry experiments and Prof. Ruud Berger for the discussions and revision of the biochemical content described in this research.

REFERENCES

1 Cifra, M. & Pospisil, P. Ultra-weak photon emission from biological samples: definition, mechanisms, properties, detection and applications. *J Photochem Photobiol B* **139**, 2-10, (2014).
2 Pospisil, P., Prasad, A. & Rac, M. Role of reactive oxygen species in ultra-weak photon emission in biological systems. *J Photochem Photobiol B* **139**, 11-23, (2014).
3 Finkel, T. & Holbrook, N. J. Oxidants, oxidative stress and the biology of ageing. *Nature* **408**, 239-247, (2000).
4 Heitzer, T., Schlinzig, T., Krohn, K., Meinertz, T. & Munzel, T. Endothelial dysfunction, oxidative stress, and risk of cardiovascular events in patients with coronary artery disease. *Circulation* **104**, 2673-2678 (2001).
5 Lin, M. T. & Beal, M. F. Mitochondrial dysfunction and oxidative stress in neurodegenerative diseases. *Nature* **443**, 787-795, (2006).
6 Markesbery, W. R. Oxidative stress hypothesis in Alzheimer's disease. *Free Radic Biol Med* **23**, 134-147 (1997).
7 Burgos, R. C. R. *et al.* Ultra-weak photon emission as a dynamic tool for monitoring oxidative stress metabolism. *Sci Rep* **7**, 1229, (2017).
8 Birtic, S. *et al.* Using spontaneous photon emission to image lipid oxidation patterns in plant tissues. *Plant J* **67**, 1103-1115, (2011).
9 Prasad, A. & Pospisil, P. Linoleic acid-induced ultra-weak photon emission from Chlamydomonas reinhardtii as a tool for monitoring of lipid peroxidation in the cell membranes. *PLoS One* **6**, e22345, (2011).
10 Meister, A. & Anderson, M. E. Glutathione. *Annu Rev Biochem* **52**, 711-760 (1983).
11 Wu, G., Fang, Y. Z., Yang, S., Lupton, J. R. & Turner, N. D. Glutathione metabolism and its implications for health. *J Nutr* **134**, 489-492 (2004).
12 Lu, S. C. Glutathione synthesis. *Biochim Biophys Acta* **1830**, 3143-3153, (2013).
13 Asensi, M. *et al.* in *Methods in Enzymology* **299**, 267-276 (Academic Press, 1999).
14 Burgos, R. C. R. *et al.* Tracking biochemical changes correlated with ultra-weak photon emission using metabolomics. *J Photochem Photobiol B* **163**, 237-245, (2016).
15 Brigelius, R., Muckel, C., Akerboom, T. P. & Sies, H. Identification and quantitation of glutathione in hepatic protein mixed disulfides and its relationship to glutathione disulfide. *Biochem Pharmacol* **32**, 2529-2534, (1983).
16 Rahman, I., Kode, A. & Biswas, S. K. Assay for quantitative determination of glutathione and glutathione disulfide levels using enzymatic recycling method. *Nat Protoc* **1**, 3159-3165, (2006).
17 Tietze, F. Enzymic method for quantitative determination of nanogram amounts of total and oxidized glutathione: applications to mammalian blood and other tissues. *Anal Biochem* **27**, 502-522 (1969).
18 Blonska-Sikora, E., Oszczudlowski, J., Witkiewicz, Z. & Widel, D. Glutathione: method of sample preparation for chromatography and capillary electrophoresis. *Chem Aust* **66**, 929-942 (2012).
19 Giustarini, D. *et al.* Pitfalls in the analysis of the physiological antioxidant glutathione (GSH) and its disulfide (GSSG) in biological samples: An elephant in the room. *J Chromatogr B Anal Technol Biomed Life Sci* **1019**, 21-28, (2016).
20 Iwasaki, Y. *et al.* Chromatographic and mass spectrometric analysis of glutathione in biological samples. *J Chromatogr B Anal Technol Biomed Life Sci* **877**, 3309-3317, (2009).
21 Camera, E. & Picardo, M. Analytical methods to investigate glutathione and related compounds in biological and pathological processes. *J Chromatogr B Anal Technol Biomed Life Sci* **781**, 181-206 (2002).
22 D'Agostino, L. A., Lam, K. P., Lee, R. & Britz-McKibbin, P. Comprehensive plasma thiol redox status determination for metabolomics. *J Proteome Res* **10**, 592-603, (2011).
23 Lee, R. & Britz-McKibbin, P. Differential rates of glutathione oxidation for assessment of cellular redox status and antioxidant capacity by capillary electrophoresis-mass

spectrometry: an elusive biomarker of oxidative stress. *Anal Chem* **81**, 7047-7056, (2009).
24 Griffith, O. W. Determination of Glutathione and Glutathione Disulfide Using Glutathione-Reductase and 2-Vinylpyridine. *Anal Biochem* **106**, 207-212, (1980).
25 Monostori, P., Wittmann, G., Karg, E. & Turi, S. Determination of glutathione and glutathione disulfide in biological samples: an in-depth review. *J Chromatogr B Anal Technol Biomed Life Sci* **877**, 3331-3346, (2009).
26 McLaggan, D., Rufino, H., Jaspars, M. & Booth, I. Glutathione-Dependent Conversion ofN-Ethylmaleimide to the Maleamic Acid by Escherichia coli: an Intracellular Detoxification Process. *Appl Environ Microbiol* **66**, 1393-1399 (2000).
27 Mojica, E. R., Kim, S. & Aga, D. S. Formation of N-ethylmaleimide (NEM)-glutathione conjugate and N-ethylmaleamic acid revealed by mass spectral characterization of intracellular and extracellular microbial metabolites of NEM. *Appl Environ Microbiol* **74**, 323-326, (2008).
28 Smyth, D. G., Blumenfeld, O. O. & Konigsberg, W. Reactions of N-ethylmaleimide with peptides and amino acids. *Biochem J* **91**, 589-595 (1964).
29 Gorin, G., Martic, P. & Doughty, G. Kinetics of the reaction of N-ethylmaleimide with cysteine and some congeners. *Arch Biochem Biophys* **115**, 593-597 (1966).
30 Haugaard, N., Cutler, J. & Ruggieri, M. R. Use of N-Ethylmaleimide to Prevent Interference by Sulfhydryl-Reagents with the Glucose-Oxidase Assay for Glucose. *Anal Biochem* **116**, 341-343, (1981).
31 Heitz, J. R., Anderson, C. D. & Anderson, B. M. Inactivation of yeast alcohol dehydrogenase by N-alkylmaleimides. *Arch Biochem Biophys* **127**, 627-636 (1968).
32 Tak, Y. H., Somsen, G. W. & de Jong, G. J. Optimization of dynamic pH junction for the sensitive determination of amino acids in urine by capillary electrophoresis. *Anal Bioanal Chem* **401**, 3275-3281, (2011).
33 Xia, J., Mandal, R., Sinelnikov, I. V., Broadhurst, D. & Wishart, D. S. MetaboAnalyst 2.0--a comprehensive server for metabolomic data analysis. *Nucleic Acids Res* **40**, W127-133, (2012).
34 Xia, J., Psychogios, N., Young, N. & Wishart, D. S. MetaboAnalyst: a web server for metabolomic data analysis and interpretation. *Nucleic Acids Res* **37**, W652-660, (2009).
35 Xia, J., Sinelnikov, I. V., Han, B. & Wishart, D. S. MetaboAnalyst 3.0--making metabolomics more meaningful. *Nucleic Acids Res* **43**, W251-257, (2015).
36 van den Berg, R. A., Hoefsloot, H. C., Westerhuis, J. A., Smilde, A. K. & van der Werf, M. J. Centering, scaling, and transformations: improving the biological information content of metabolomics data. *BMC Genomics* **7**, 142, (2006).
37 Breitman, T. R., Selonick, S. E. & Collins, S. J. Induction of differentiation of the human promyelocytic leukemia cell line (HL-60) by retinoic acid. *Proc Natl Acad Sci USA* **77**, 2936-2940 (1980).
38 Dahlgren, C. & Karlsson, A. Respiratory burst in human neutrophils. *J Immunol Methods* **232**, 3-14 (1999).
39 Dettmer, K., Aronov, P. A. & Hammock, B. D. Mass spectrometry-based metabolomics. *Mass Spectrom Rev* **26**, 51-78, (2007).
40 Britz-McKibbin, P. in *Metabolic Profiling: Methods and Protocols* (ed Thomas O. Metz) 229-246 (Humana Press, 2011).
41 Hirayama, A. & Soga, T. in *Capillary Electrophoresis–Mass Spectrometry (CE-MS)* 293-314 (Wiley-VCH Verlag GmbH & Co. KGaA, 2016).
42 Noga, M. J. *et al.* Metabolomics of cerebrospinal fluid reveals changes in the central nervous system metabolism in a rat model of multiple sclerosis. *Metabolomics* **8**, 253-263, (2012).
43 Zitka, O. *et al.* Redox status expressed as GSH:GSSG ratio as a marker for oxidative stress in paediatric tumour patients. *Oncol Lett* **4**, 1247-1253, (2012).

44 Bilzer, M. & Lauterburg, B. H. Glutathione metabolism in activated human neutrophils: stimulation of glutathione synthesis and consumption of glutathione by reactive oxygen species. *Eur J Clin Invest* **21**, 316-322 (1991).
45 Voetman, A. A., Loos, J. A. & Roos, D. Changes in the levels of glutathione in phagocytosing human neutrophils. *Blood* **55**, 741-747 (1980).
46 Lu, S. C. Regulation of glutathione synthesis. *Mol Asp Med* **30**, 42-59, (2009).
47 Lu, S. C. Regulation of hepatic glutathione synthesis: current concepts and controversies. *FASEB J* **13**, 1169-1183 (1999).

SUPPLEMENTARY INFORMATION

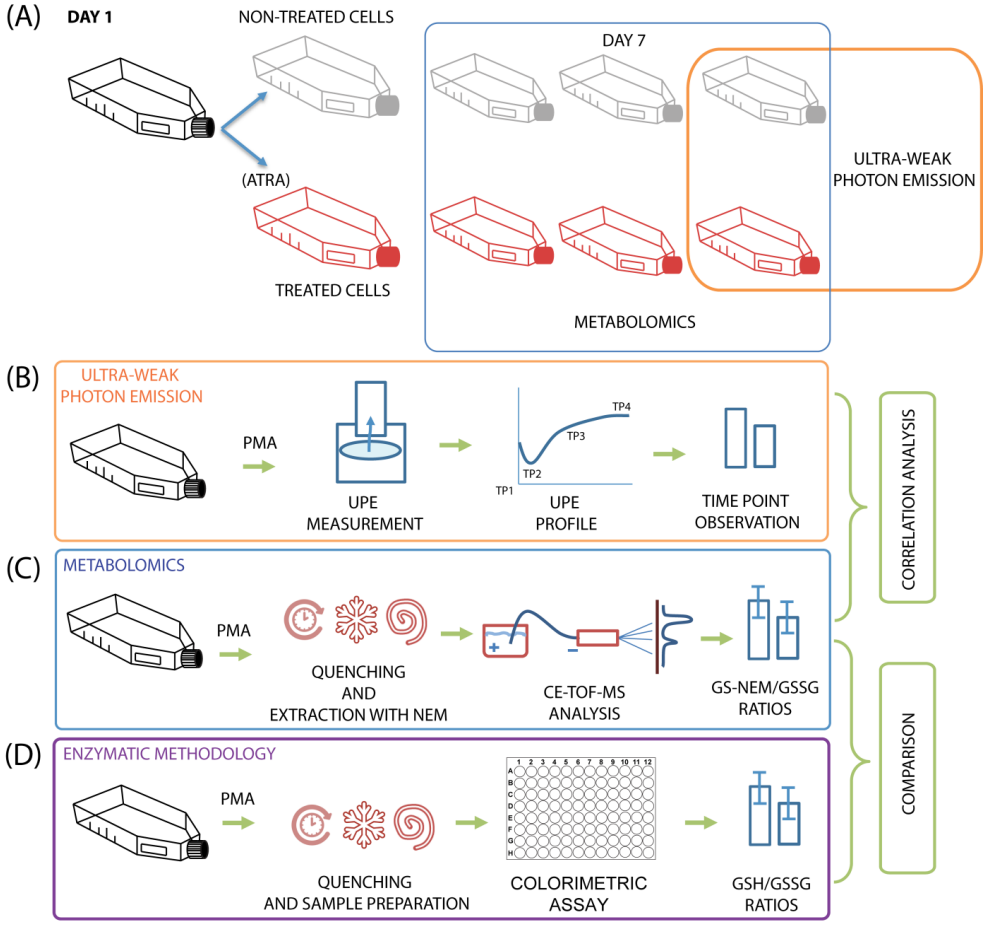

Supplementary Figure S1. Experimental design. **(A)** Cultured HL-60 cells were split into two flasks; one flask was treated with ATRA to produce differentiated cells, and the other flask was not treated with ATRA) and undifferentiated cells (control). **(B)** On day 7, PMA was applied to each flask to induce respiratory burst, and UPE was recorded for 9000 seconds. Samples were collected for glutathione measurements the indicated time points (TP1, TP2, TP3, and TP4, corresponding to 0, 60, 4500, and 9000 seconds, respectively, relative to with PMA stimulation). **(C)** After samples were collected in the presence of NEM, cells were extracted with 80% methanol in the presence of NEM, and GS-NEM and GSSG levels were measured using CE-TOF-MS. **(D)** The enzymatic recycling assay was used to obtain the GSH/GSSG ratio. Finally, the results obtained in **C** and **D** were compared.

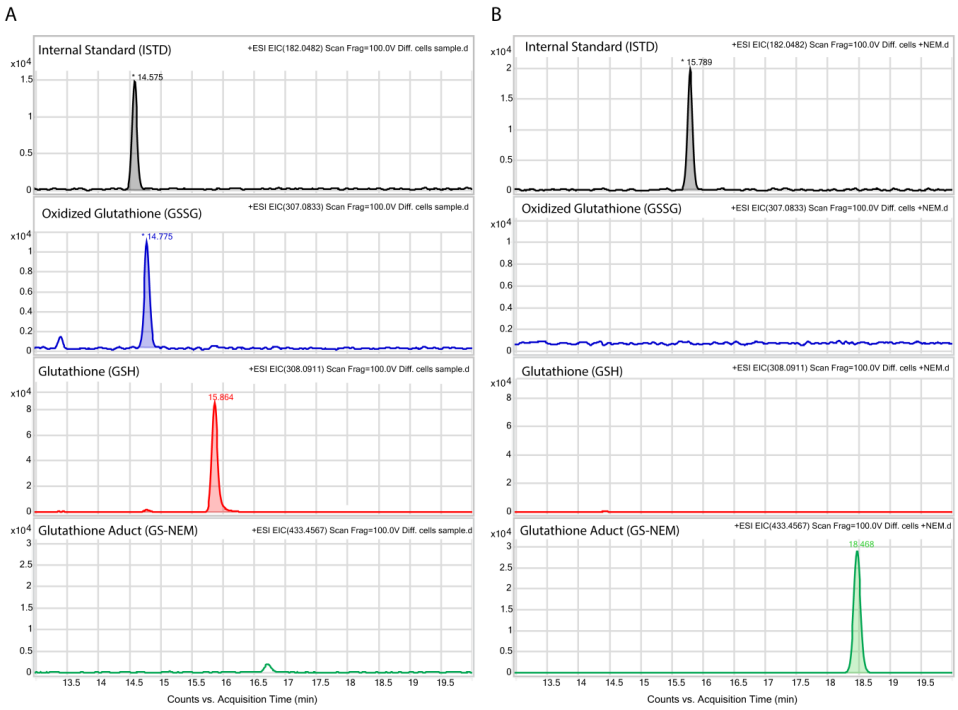

Supplementary Figure S2. CE-MS electropherograms obtained for GS-NEM and GSSG in HL-60 cell extracts. Peak area intensity is plotted on the *y*-axis, and migration time is plotted on the *x*-axis. We used 2.5 nl of NH_4OH (12.5% v/v) as the stacking volume, and we injected approximately 25 nl of cell extract. **(A)** Electropherograms from cell samples prepared in the absence of *N*-ethylmaleimide (NEM). Note that GSSG is present due to auto-oxidation of GSH during sample preparation. **(B)** Electropherograms from cell samples prepared in the presence of NEM.

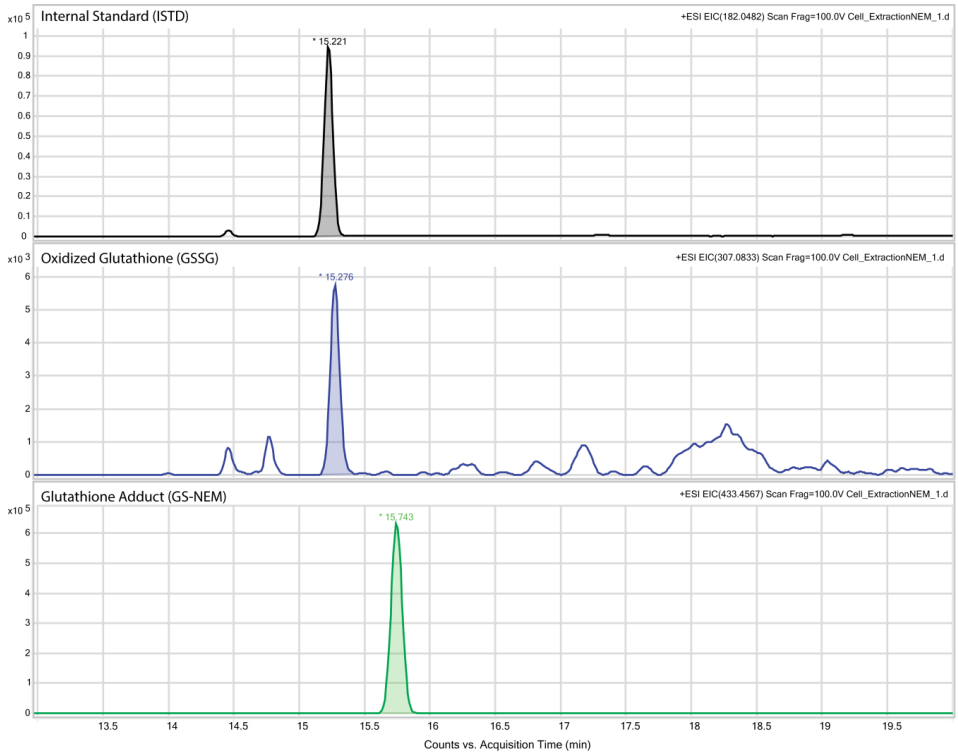

Supplementary Figure S3. CE-MS electropherograms obtained for GS-NEM and GSSG in HL-60 cell extracts. Peak area intensity is plotted on the *y*-axis, and migration time is plotted on the *x*-axis. We used 10 nl of NH_4OH (12.5% v/v) as the stacking volume and injected approximately 120 nl of cell extract.

Supplementary Table S1. ANOVA results for the indicated intracellular compounds with significant changes during PMA treatment over the four time points.

ANOVA ANALYSIS						
Methodology	***Compound***	***Cell Type***	**p-*value***	***F value***	***FDR*[a]**	***Fisher's LSD*[b]**
CE-MS	**GS-NEM**	**Diff. cells**	0.0112	7.278	0.0112	TP1 vs TP4; TP2 vs TP4; TP3 vs TP4
	GSSG	**Diff. cells**	0.00052	19.126	0.0008	TP3 vs TP1; TP4 vs TP1; TP3 vs TP2; TP4 vs TP2; TP4 vs TP3
	GS-NEM/GSSG	**Diff. cells**	0.00000075	110.61	0.0000022462	TP1 vs TP3; TP1 vs TP4; TP2 vs TP3; TP2 vs TP4; TP3 vs TP4
	GS-NEM	**Undiff. cells**	0.0021793	12.501	0.0065379	TP2 vs TP1; TP1 vs TP4; TP2 vs TP3; TP2 vs TP4; TP3 vs TP4
	GSSG	**Undiff. cells**	0.02887	5.116	0.043306	TP2 vs TP1; TP2 vs TP4
Enzymatic	**Total GSH**	**Diff. cells**	0.0034	10.853	0.0064	TP1 vs TP4; TP2 vs TP3; TP2 vs TP4; TP3 vs TP4
	GSH/GSSG	**Diff. cells**	0.0042	10.113	0.0064	TP1 vs TP4; TP2 vs TP4; TP3 vs TP4
LC-MS	**Total GSH**	**Diff. cells**	0.00000104	101.75	0.0000020721	TP1 vs TP3; TP1 vs TP4; TP2 vs TP3; TP2 vs TP4
	Total GSH	**Undiff. cells**	0.0003119	22.185	0.0003119	TP1 vs TP3; TP1 vs TP4; TP2 vs TP3; TP2 vs TP4

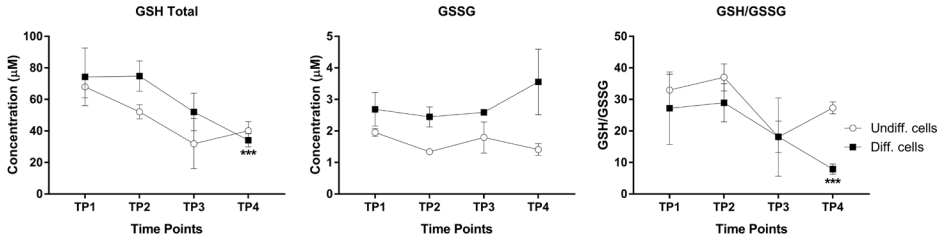

Supplementary Figure S4. Total GSH and GSSG levels were measured using a spectrophotometric (enzymatic recycling) assay in differentiated and undifferentiated HL-60 cells during PMA-induced respiratory burst. GSH concentration was calculated using the following equation: GSH = total glutathione (GSH + GSSG) – GSSG x 2. Intragroup ANOVA was performed over the four time points in order to identify significant changes in the glutathione levels. Data are plotted as the mean (n=3) ± SD. ***p<0.001. For details, see **Supplementary Table S1.**

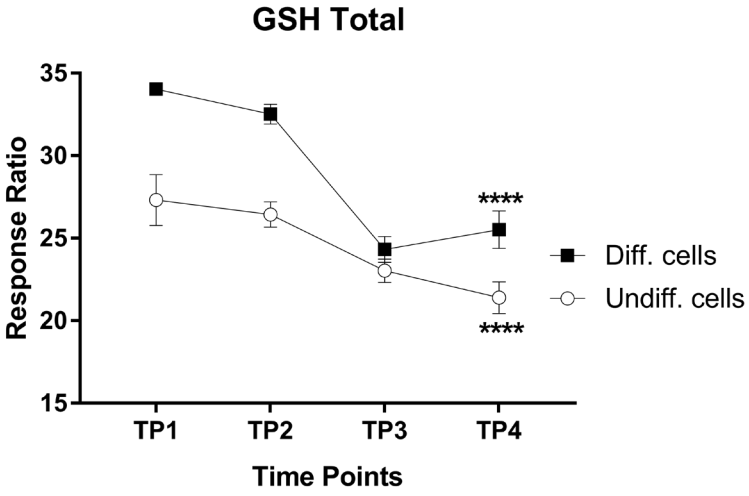

Supplementary Figure S5. Total GSH was measured using a validated LC-MS method. Intragroup ANOVA was performed over the four time points in order to identify significant changes in total GSH levels. Data are plotted as the mean (n=3) ± SD. ****p<0.0001. For details, see **Supplementary Table S1**.

Chapter 6

Pharmacological targeting of a cellular ROS reaction network monitored by ultra-weak photon emission

Based on

Rosilene Cristina Rossetto Burgos, Rawi Ramautar, Eduard P.A. van Wijk, Thomas Hankemeier, Jan van der Greef and Alireza Mashaghi.

Pharmacological targeting of a cellular ROS reaction network monitored by ultra-weak photon emission

Manuscript submitted for publication

ABSTRACT

Acute myeloid leukemia (AML) is a blood cancer that is caused by a disorder of the process that normally generates neutrophils. Function and dysfunction of neutrophils are key to physiologic defense against pathogens as well as pathologies including autoimmunity and cancer. A major mechanism through which neutrophils contribute to health and disease is oxidative burst, which involves rapid release of reactive oxygen species (ROS) generated by a chemical reaction network catalyzed by enzymes including NADPH oxidase and myeloperoxidase (MPO). Due to the involvement of reactive oxygen species in many diseases progression, monitoring this process and modulating it by pharmacological interventions is of great interest. In this work, we have evaluated the potential of a label-free method using ultra-weak photon emission (UPE) to monitor ROS production in acute myeloid leukemia cells. Suppression of ROS was achieved by several drug candidates that target different parts of the reaction pathway. Our results show that UPE can report on ROS production as well as suppression by pharmacological inhibitors. We find that UPE is primarily generated by MPO catalyzed reaction and thus will be affected when an upstream reaction is pharmacologically modulated.

INTRODUCTION

Innate immune cells are key to health and many diseases. Neutrophil granulocytes (also called neutrophils), the most abundant innate immune cells, are at the forefront to fight against infections, regulate the adaptive immune system, and contribute to tissue damage when activated in excess[1-4]. During phagocytosis, neutrophils react to microbes, virus, and bacteria releasing several types of oxidants to kill the invading pathogens. The respiratory burst is the first mechanism of defense during phagocytosis and requires oxygen (O_2) consumption to produce and release reactive oxygen species (ROS)[5]. The rapid release of superoxide anion radicals ($O_2^{\cdot-}$) and hydrogen peroxide (H_2O_2), which are the primary source of the oxidants, is followed by rapid conversion into other oxidant species ($OH^{\cdot}$, HOCl, etc)[5]. These processes are catalyzed mainly by two enzymes, NADPH oxidase and myeloperoxidase (MPO), the latter being a signature protein of neutrophils. Physiologically, ROS production is beneficial at right doses; however, the overproduction of ROS (usually called as oxidative stress) has been related to several disorders such as Alzheimer's disease[6], Parkinson's disease[7], cancer[8,9], cardiovascular diseases[10] and chronic diseases such as diabetes[11], and rheumatoid arthritis[12].

Acute myeloid leukemia (AML) is a blood cancer that is caused by a disorder of the process that normally generates neutrophils [13]. AML is most commonly seen in adults and is associated with high morbidity and mortality[14]. Mutations in receptor tyrosine kinases (RTKs) and its downstream effectors are believed to underlie this cancerous process[15]. MPO is a lineage marker for acute myeloid leukemia and can serve as a prognostic factor. On the other hand, NADPH oxidase-derived reactive oxygen species serves as an immune evasion strategy by which AML cells kill the healthy immune cells. In brief, NADPH oxidase and MPO-mediated reactions are important in progression and treatment of AML.

Given the involvement of ROS in many diseases, drug therapies which target specific sites of ROS production are getting attention[16-18]. Various antioxidants and specific inhibitors of NADPH oxidase have been developed in recent years as a promising target for treating several types of cardiovascular diseases such as atherosclerosis[18,19]. MPO inhibitors have also been considered as new potential drugs[20,21]. MPO is the downstream pathway of NADPH oxidase, acting only at inflammation sites[22]. The overproduction of oxidants species by MPO has been reported to cause tissue damage and others complications in several diseases[23]. Modulation of ROS response could also be beneficial in AML therapy as well as in tissue destruction caused by excessive recruitment and activation of neutrophils.

In this work, we propose a label-free method using ultra-weak photon emission (UPE) to monitor pharmacological inhibition of ROS machinery in AML (HL-60) cells. UPE is

endogenous light emitted by human tissues and is believed to be related to ROS generation[24,25]. This weak light is emitted in the ultraviolet/visible range (100 – 800nm) possibly reaching the near-IR spectrum (801 – 1300nm) and originates from radiative (non-thermal) electronic transitions of excited electron states during reactions with biomolecules[24,25]. Due to the close relation of UPE and ROS generation, UPE can be used as a dynamic monitoring tool for oxidative metabolism[26]. In this work, we used three classes of drugs, namely anti-oxidants, specific NADPH oxidase inhibitors and an MPO inhibitor and monitored their response by UPE analysis. This analysis demonstrates whether or not UPE can report on the activity of these drugs and reveals reactions that primarily generate the emitted light.

METHODS

Cell culture, differentiation, and induction of the respiratory burst in HL-60 cells

Acute promyelocytic leukemia cell line – HL-60 (catalogue number CCL-240; lot number 62690063; ATCC, Manassas, VA) was cultured in Iscove's Modified Dulbecco's Medium – IMDM without phenol red (Gibco-Life Technologies, Grand Island, NY), supplemented with 10% (v/v) of fetal calf serum (FCS) and 1% (v/v) penicillin/streptomycin (Sigma-Aldrich, St. Louis, MO). Cell seed and maintenance were kept between the exponential growths ($2x10^5$ - $1.0x10^6$ cells per ml) in a CO_2 incubator at 37 °C. The cell count and viability (>85%) was determined using the trypan blue exclusion method with an automated cell counter (Bio-Rad Laboratories, Hercules, CA). For the differentiation into *neutrophils-like* cells, we have used the standard protocol as described previously[26,27]. In brief, when the cells were split and adjusted for cell density, 1 µM all-trans retinoic acid (ATRA; 98% grade, catalog number R250, Sigma-Aldrich) was added to the cells in order to induce differentiation via the granulocytic pathway. The cells were incubated for up to 7 days, and UPE experiments were performed on day 7. Cells were stimulated with 54 nM of phorbol 12-myristate 13-acetate – PMA (98% grade, Sigma-Aldrich, St. Louis, MO) in the presence or absence of inhibitors: 4-Aminobenzoic acid hydrazide – 4-ABAH (Cayman Chemicals, Ann Arbor, MI); 4-(2-Aminoethyl)benzene sulfonyl fluoride hydrochloride – AEBSF; 1,3-Benzoxazol-2-yl-3-benzyl-3H-[1,2,3]triazolo[4,5-d]pyrimidin-7-yl sulfide – VAS2870; 5-hydroxy-2-methyl-1,4-naphthoquinone – Plumbagin; 4-Hydroxy-3-methoxyacetophenone – Apocynin (Sigma-Aldrich, St. Louis, MO). Measurements were performed between cell passage numbers P07 - P28. As a standard protocol in immunology, ROS generation in neutrophil or neutrophil-like cells is typically assessed following stimulation by PMA and comparing it to ROS response by the cells in their resting state[28].

Ultra-weak photon emission (UPE) measurement

A 2-inch photomultiplier tube – PMT (series 9558B with S20 photocathode) purchased from ET Enterprises (Sweetwater, TX) was used for the UPE measurements. The detector was cooled to -25°C in order to reduce the noise. The photon emission intensity was recorded over the time (counts/sec). A Peltier element was used inside the dark chamber to maintain the sample at 37°C and the PMT was set in a vertical position at the top of the dark chamber (see **Supplementary Fig. S1**). UPE was measured in HL-60 cells after PMA (54nM) induction. For each UPE measurement, a small aliquot of the cell suspension (6 ml at a cell density of $1x10^6$ cells/ml) was used to record the UPE profile. First, the background was measured for 1000 seconds before PMA induction and subsequently, cells were stimulated with PMA in the presence or absence of inhibitors for 9000 seconds.

Myeloperoxidase and NADPH oxidase inhibitors

We have used HL-60 cells differentiated into *neutrophil-like* cells and induced a respiratory burst by applying phorbol 12-myristate 13-acetate (PMA). The respiratory burst was recorded for 9000 seconds and the potential of several NADPH inhibitors (VAS2870, Plumbagin, AEBSF, and Apocynin) and the irreversible myeloperoxidase inhibitor (4-ABAH) were evaluated. Apocynin, AEBSF, VAS2870, Plumbagin, and 4-ABAH were added at the indicated concentrations prior PMA induction. Only AEBSF was added 15 minutes before PMA stimulation.

Data analysis

UPE data were processed and plotted using the software GraphPad Prism 7.0. The UPE data were smoothed using the function xy analysis (smooth - 2^{nd} order of smoothing with 100 neighbors data points). Thus, the smoothed data were normalized by the highest UPE intensity. The smoothed curve is presented as dynamic data. Next, we have analyzed specific regions of the dynamic data (3000-3600 seconds and 6000-6600 seconds) to generate statistics averaging the smoothed data. Normalization was done by the average value of the UPE intensity induced only by PMA. Two-way ANOVA followed by Tukey multiple comparison tests with GraphPad Prism 7 was used to identify significant differences. Differences with a *p*-value<0.05 were considered significant.

RESULTS

Monitoring ROS by UPE measurement

We first demonstrate that AML cells generate UPE upon triggering ROS response[26]. We find that AML cells generate a weak UPE signal in resting state and this signal is amplified when

the cells are treated with PMA. **Fig.1** shows a representative time trace of UPE during PMA stimulation of AML cells. PMA is known to induce respiratory bursts in AML and neutrophils, thus we attribute the recorded UPE signal to ROS response[26].

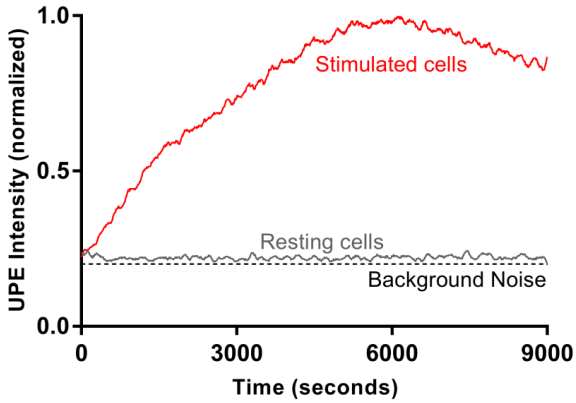

Figure 1. A representative UPE profile of HL-60 cells in resting state and upon triggering ROS response stimulated by PMA. UPE profile was recorded for 9000 seconds at 37°C in the dark. The lines represent the smoothed UPE intensity followed by normalization by the highest UPE intensity

To better demonstrate the link between the recorded signal and the ROS process, we quenched ROS response by two scavengers namely plumbagin and apocynin. We observed that UPE signal gets suppressed significantly by administration of these drugs (**Fig. 2**). These lines of evidence clearly show that UPE analysis can detect ROS response and antioxidant activities in AML cells. Our experiments above show that UPE can inform about oxidative metabolism, but it does not provide any molecular or pathway information. Plumbagin and apocynin scavenge ROS and also non-specifically inhibit the enzymatic reaction pathway that leads to ROS generation[29-36]. To provide mechanistic insights, in the following we target the reaction network using specific inhibitors of the key elements involved in ROS generation.

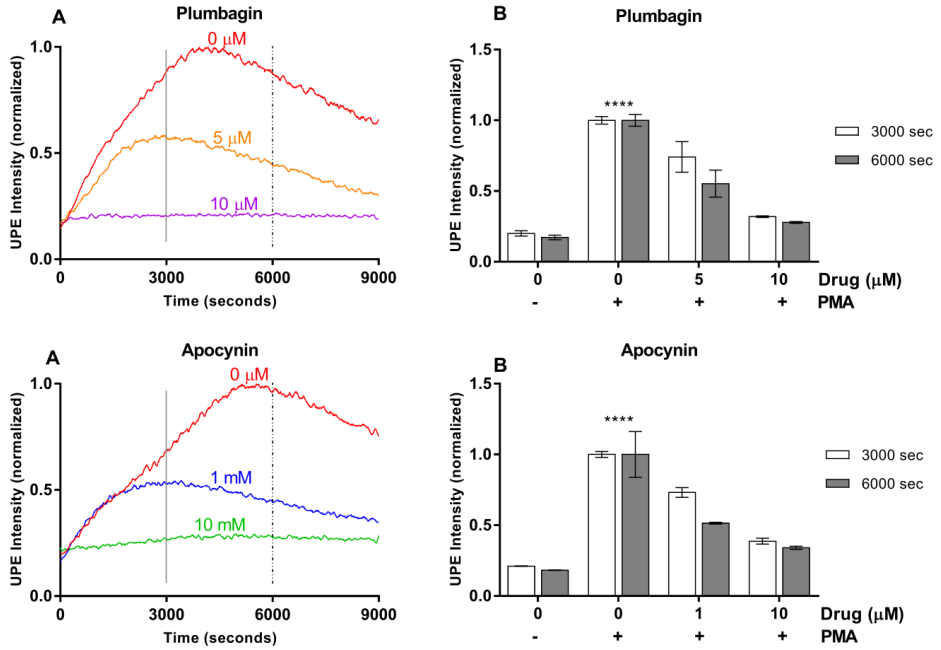

Figure 2. Plumbagin and Apocynin effects on UPE profile in HL-60 cells. **(A)** Dynamic UPE profile showing the suppression of UPE intensity with the administration of scavengers Plumbagin and Apocynin in two different concentrations (n=1). **(B)** Analysis of the interval (3000 – 3600 seconds and 6000 – 6600 seconds) as indicated in (A) by the vertical lines. Statistical significance was determined by two-way ANOVA with errors bars represented as standard deviation (SD) and n≥3. ****p<0.0001.

Targeting NADPH oxidase

To gain better mechanistic and molecular insights, we investigated if UPE reports on ROS pathway downstream or upstream (or both) to NADPH oxidase. To address this question, we inhibited NADPH oxidase specifically (**Fig. 3**) and checked whether the UPE signal is affected or not. Two specific drugs were tested and the results indicate that downstream processes to NADPH oxidase contribute to the recorded UPE signal. By increasing the concentration of the drugs we could fully block the UPE signal, indicating that nearly all of the UPE signal is due to NADPH oxidase-mediated reaction and/or downstream processes with no detectable contributions from upstream or parallel reactions.

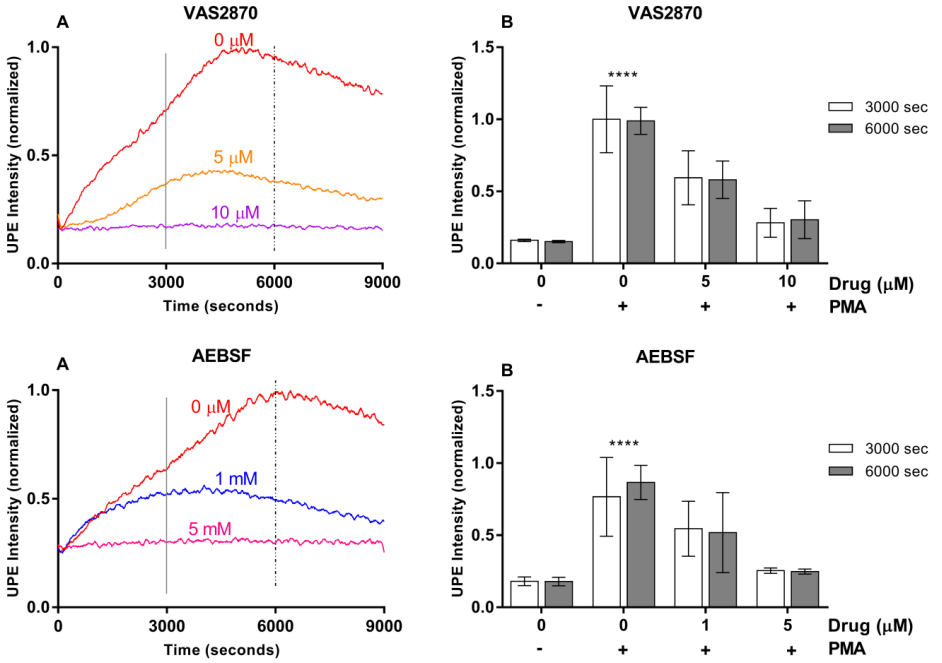

Figure 3. VAS2870 and AEBSF effects on UPE profile in HL-60 cells. **(A)** Dynamic UPE profile showing the suppression of UPE intensity with the administration of NADPH oxidase inhibitor VAS2870 and AEBSF in two different concentrations (n=1). **(B)** Analysis of the interval as indicated in (A) by the vertical lines. Statistical significance was determined by two-way ANOVA with errors bars represented as standard deviation (SD) and n≥3

Targeting Myeloperoxidase

Next, we aimed to resolve the contribution of MPO-mediated reactions to the UPE signal and to see if the signal is directly due to NADPH oxidase activity or whether it is caused by an MPO-mediated process which is downstream to the NADPH oxidase-mediated process. For this aim, we tested a specific MPO inhibitor and measured the UPE signal. If the signal is caused by a process that depends on NADPH oxidase but not on MPO, we expect no effect by MPO inhibition. **Fig.4** presents the results obtained for the MPO inhibitor 4-ABAH tested. Intriguingly, MPO inhibition clearly suppressed UPE signal. By increasing the concentration of MPO inhibitor we could nearly reach a full suppression. The results clearly indicate that UPE reports on ROS processes that are downstream to MPO catalysis and as such UPE can specifically report on MPO activity.

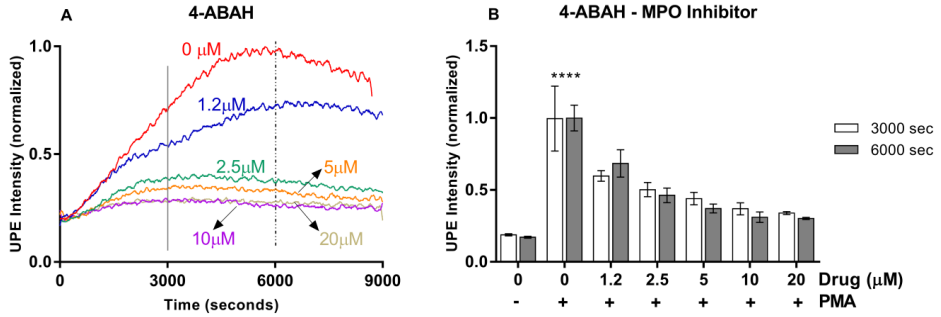

Figure 4. MPO inhibitor tested in the HL-60 cell model system measured by UPE. **(A)** Dynamic UPE profile showing the suppression of UPE intensity with the administration of 4-ABAH in five different concentrations (n=1). **(B)** Analysis of the interval as indicated in (A) by the vertical lines. Statistical significance was determined by two-way ANOVA with errors bars represented as standard deviation (SD) and n≥3. ****p<0.0001

DISCUSSION

UPE has been considered a potential tool to monitor dynamic oxidative metabolism, but its utilization for medical diagnostics and pharmacology still requires more insights into the mechanism and the biochemical pathways that drive its generation. For this aim, we modulated ROS pathways pharmacologically and monitored UPE in time. We focused our study on neutrophil-like cell HL-60[37-40] because ROS generation by neutrophils is critically important in disease processes including cancer, infection, and tissue destruction in excessive immune responses. We tested several NADPH oxidase inhibitors with a wide range of specificity (antioxidants, NOX, etc.) and also the downstream pathway specific for neutrophils (see **Supplementary Fig. S2**) using an irreversible MPO inhibitor.

Our results show that UPE was able to monitor ROS production and suppression in all potential drug candidates tested independently of the specificity of the inhibitor. In addition, UPE response was dose-dependent for all drugs tested and in agreement with the IC_{50} found in the literature. Importantly, we have also checked cell viability during the drug treatment period of 9000 seconds recorded by UPE being the cells with a great viability during the time recorded (see **Supplementary Fig. S3**). Our analysis indicates that the UPE signal can be fully suppressed when one of the few parallel pathways that form the ROS reaction network is blocked. ROS reaction network involves not only NADPH oxidase-MPO pathway but also the xanthine oxidase and mitochondrial pathways[41-43]. The fact that blocking NADPH oxidase-MPO pathway leads to full suppression of the UPE signal (see **Figs. 2**, **3**, **4**) suggesting that contributions from other reactions are negligible. Thus, specific reporters need to be designed and used to monitor other pathways in ROS reaction network.

Our pharmacological manipulation of ROS reaction pathway in AML cells and monitoring the outcome by UPE revealed that UPE can report on ROS generation and suppression. Our data indicate that MPO-mediated reaction is mainly responsible for the UPE signal. This is a unique capability for UPE because it provides a very simple, low-cost, label-free method for providing dynamic information on MPO-mediated ROS response. The application of this technology will not be limited to AML, where MPO-mediated ROS response can be used as a prognostic measure, but also in other cancers where tumor-associated neutrophils suppress T cell immunity via generation of ROS response[44,45].

REFERENCES

1 Murphy, K. & Weaver, C. *Janeway's immunobiology*. (Garland Science, 2016).
2 Gupta, S. & Kaplan, M. J. The role of neutrophils and NETosis in autoimmune and renal diseases. *Nat Rev Nephrol* **12**, 402-413, (2016).
3 de Oliveira, S., Rosowski, E. E. & Huttenlocher, A. Neutrophil migration in infection and wound repair: going forward in reverse. *Nat Rev Immunol* **16**, 378-391, (2016).
4 Coffelt, S. B., Wellenstein, M. D. & de Visser, K. E. Neutrophils in cancer: neutral no more. *Nat Rev Cancer* **16**, 431-446, (2016).
5 Dahlgren, C. & Karlsson, A. Respiratory burst in human neutrophils. *J Immunol Methods* **232**, 3-14 (1999).
6 Chauhan, V. & Chauhan, A. Oxidative stress in Alzheimer's disease. *Pathophysiology* **13**, 195-208, (2006).
7 Barnham, K. J., Masters, C. L. & Bush, A. I. Neurodegenerative diseases and oxidative stress. *Nat Rev Drug Discov* **3**, 205-214, (2004).
8 Visconti, R. & Grieco, D. New insights on oxidative stress in cancer. *Curr Opin Drug Discov Devel* **12**, 240-245 (2009).
9 Reuter, S., Gupta, S. C., Chaturvedi, M. M. & Aggarwal, B. B. Oxidative stress, inflammation, and cancer: how are they linked? *Free Radic Biol Med* **49**, 1603-1616, (2010).
10 Sugamura, K. & Keaney, J. F., Jr. Reactive oxygen species in cardiovascular disease. *Free Radic Biol Med* **51**, 978-992, (2011).
11 Giacco, F. & Brownlee, M. Oxidative stress and diabetic complications. *Circ Res* **107**, 1058-1070, (2010).
12 Szabó-Taylor, K. É., Nagy, G., Eggleton, P. & Winyard, P. G. in *Studies on Arthritis and Joint Disorders* (eds Maria Jose Alcaraz, Oreste Gualillo, & Olga Sánchez-Pernaute) 145-167 (Springer New York, 2013).
13 Kasper, D. et al. Harrison's principles of internal medicine, 19e. (Mcgraw-hill, 2015).
14 Goldman, L. & Schafer, A. I. Goldman's Cecil medicine. (Elsevier Health Sciences, 2011).
15 Sangwan, V. & Park, M. Receptor tyrosine kinases: role in cancer progression. *Curr Oncol* **13**, 191-193 (2006).
16 Schramm, A., Matusik, P., Osmenda, G. & Guzik, T. J. Targeting NADPH oxidases in vascular pharmacology. *Vascul Pharmacol* **56**, 216-231, (2012).
17 Rabêlo, L. A., Souza, V. N. d., Fonseca, L. J. S. d. & Sampaio, W. O. Desbalanço redox: NADPH oxidase como um alvo terapêutico no manejo cardiovascular. *Arq Bras Cardiol* **94**, 684-693, (2010).
18 Altenhofer, S., Radermacher, K. A., Kleikers, P. W., Wingler, K. & Schmidt, H. H. Evolution of NADPH Oxidase Inhibitors: Selectivity and Mechanisms for Target Engagement. *Antioxid Redox Signal* **23**, 406-427, (2015).
19 Guzik, T. J. & Harrison, D. G. Vascular NADPH oxidases as drug targets for novel antioxidant strategies. *Drug Discov Today* **11**, 524-533, (2006).

20 Lazarevic-Pasti, T., Leskovac, A. & Vasic, V. Myeloperoxidase Inhibitors as Potential Drugs. *Current Drug Metabolism* **16**, 168-190, (2015).
21 Malle, E., Furtmuller, P. G., Sattler, W. & Obinger, C. Myeloperoxidase: a target for new drug development? *Br J Pharmacol* **152**, 838-854, (2007).
22 Kettle, A. J. & Winterbourn, C. C. Myeloperoxidase: a key regulator of neutrophil oxidant production. *Redox Rep* **3**, 3-15, (1997).
23 Lau, D. & Baldus, S. Myeloperoxidase and its contributory role in inflammatory vascular disease. *Pharmacol Ther* **111**, 16-26, (2006).
24 Cifra, M. & Pospisil, P. Ultra-weak photon emission from biological samples: definition, mechanisms, properties, detection and applications. *J Photochem Photobiol B* **139**, 2-10, (2014).
25 Pospisil, P., Prasad, A. & Rac, M. Role of reactive oxygen species in ultra-weak photon emission in biological systems. *J Photochem Photobiol B* **139**, 11-23, (2014).
26 Burgos, R. C. R. et al. Ultra-weak photon emission as a dynamic tool for monitoring oxidative stress metabolism. *Sci Rep* **7**, 1229, (2017).
27 Burgos, R. C. R. et al. Tracking biochemical changes correlated with ultra-weak photon emission using metabolomics. *J Photochem Photobiol B* **163**, 237-245, (2016).
28 Honda, F. et al. The kinase Btk negatively regulates the production of reactive oxygen species and stimulation-induced apoptosis in human neutrophils. *Nat Immunol* **13**, 369-378, (2012).
29 Gangabhagirathi, R. & Joshi, R. Antioxidant role of plumbagin in modification of radiation-induced oxidative damage. *Oxid Antioxid Med Sci* **4**, 85-90 (2015).
30 Tilak, J. C., Adhikari, S. & Devasagayam, T. P. Antioxidant properties of Plumbago zeylanica, an Indian medicinal plant and its active ingredient, plumbagin. *Redox Rep* **9**, 219-227, (2004).
31 Ding, Y. et al. Inhibition of Nox-4 activity by plumbagin, a plant-derived bioactive naphthoquinone. *J Pharm Pharmacol* **57**, 111-116, (2005).
32 Ben-Shaul, V. et al. The effect of natural antioxidants, NAO and apocynin, on oxidative stress in the rat heart following LPS challenge. *Toxicol Lett* **123**, 1-10 (2001).
33 Gaascht, F. et al. Plumbagin modulates leukemia cell redox status. *Molecules* **19**, 10011-10032, (2014).
34 Heumüller, S. et al. Apocynin is not an inhibitor of vascular NADPH oxidases but an antioxidant. *Hypertension* **51**, 211-217 (2008).
35 Stolk, J., Hiltermann, T. J., Dijkman, J. H. & Verhoeven, A. J. Characteristics of the inhibition of NADPH oxidase activation in neutrophils by apocynin, a methoxy-substituted catechol. *Am J Respir Cell Mol Biol* **11**, 95-102, (1994).
36 Xu, K. H. & Lu, D. P. Plumbagin induces ROS-mediated apoptosis in human promyelocytic leukemia cells in vivo. *Leuk Res* **34**, 658-665, (2010).
37 Dwivedi, P. et al. Role of Bcr1-Activated Genes Hwp1 and Hyr1 in Candida Albicans Oral Mucosal Biofilms and Neutrophil Evasion. *PLOS ONE* **6**, e16218, (2011).
38 Millius, A. & Weiner, O. D. in *Live Cell Imaging: Methods and Protocols* (ed Dmitri B. Papkovsky) 147-158 (Humana Press, 2010).
39 Mousa, A. A., Strauss, J. F. & Walsh, S. W. Reduced Methylation of the Thromboxane Synthase Gene Is Correlated With Its Increased Vascular Expression in Preeclampsia. *Hypertension*, (2012).
40 Park, D. W. et al. Activation of AMPK Enhances Neutrophil Chemotaxis and Bacterial Killing. *Mol Med* **19**, 387-398, (2013).
41 Hancock, J. T., Desikan, R. & Neill, S. J. Role of reactive oxygen species in cell signalling pathways. *Biochem Soc Trans* **29**, 345-350 (2001).
42 Sauer, H., Wartenberg, M. & Hescheler, J. Reactive oxygen species as intracellular messengers during cell growth and differentiation. *Cell Physiol Biochem* ***11*****,** 173-186, (2001).
43 Droge, W. Free radicals in the physiological control of cell function. *Physiol Rev* **82**, 47-95, (2002).

44 Coffelt, S. B., Wellenstein, M. D. & de Visser, K. E. Neutrophils in cancer: neutral no more. *Nat Rev Cancer* **16**, 431-446, (2016).
45 Uribe-Querol, E. & Rosales, C. Neutrophils in Cancer: Two Sides of the Same Coin. *J Immunol Res* 2015, (2015).
46 Hideg, E. & Inaba, H. Biophoton emission (ultraweak photoemission) from dark adapted spinach chloroplasts. *Photochem Photobiol* **53**, 137-142 (1991).
47 Slawińska, D. & Slawiński, J. Ultraweak photon emission in model reactions of the in vitro formation of eumelanins and pheomelanins. *Pigment Cell Melanoma Res* **1**, 171-175 (1987).

SUPPLEMENTARY INFORMATION

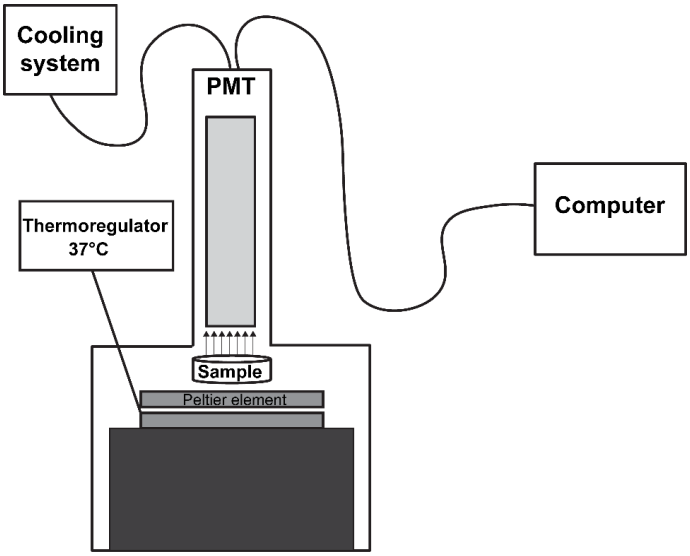

Supplementary Figure S1. Instrument set up for UPE measurements. A PMT was used for the UPE measurements was set in a vertical position at the top of the dark chamber. The detector was cooled to -25°C in order to reduce the noise. A Peltier element was used inside the dark chamber to maintain the sample at 37°C.

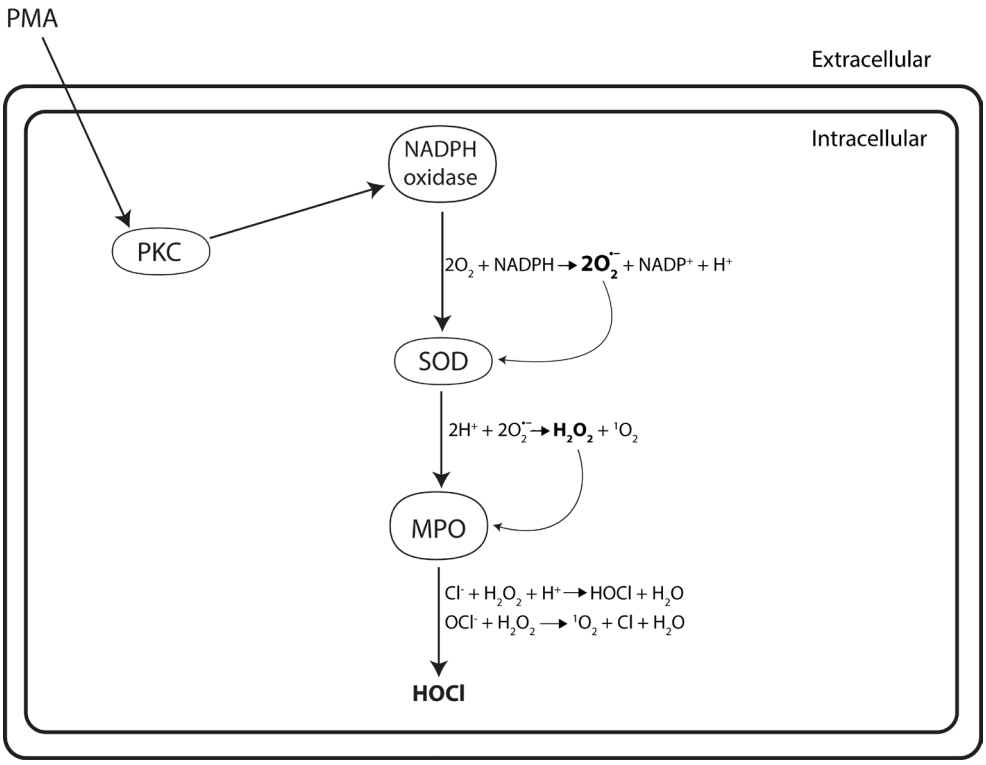

Supplementary Figure S2. Downstream ROS pathway NADPH – MPO enzymatic system. In our HL-60 cells model, PMA activates protein kinase C (PKC) and NADPH oxidase. Activated NADPH oxidase transfers electrons from NADPH coupling to molecular oxygen in order to produce superoxide anion as a primary ROS source which is quickly dismutated to H_2O_2 by superoxide dismutase (SOD). Peroxide is the substrate for myeloperoxidase (MPO) which catalyzes the oxidant production (e.g. HOCl) to kill pathogens at the inflammation sites. In this study, we targeted PKC with PMA, NADPH oxidase with a few specific and non-specific inhibitors, and MPO with a specific inhibitor. Our findings and conclusions are in agreement with previous studied where SOD is targeted[46,47].

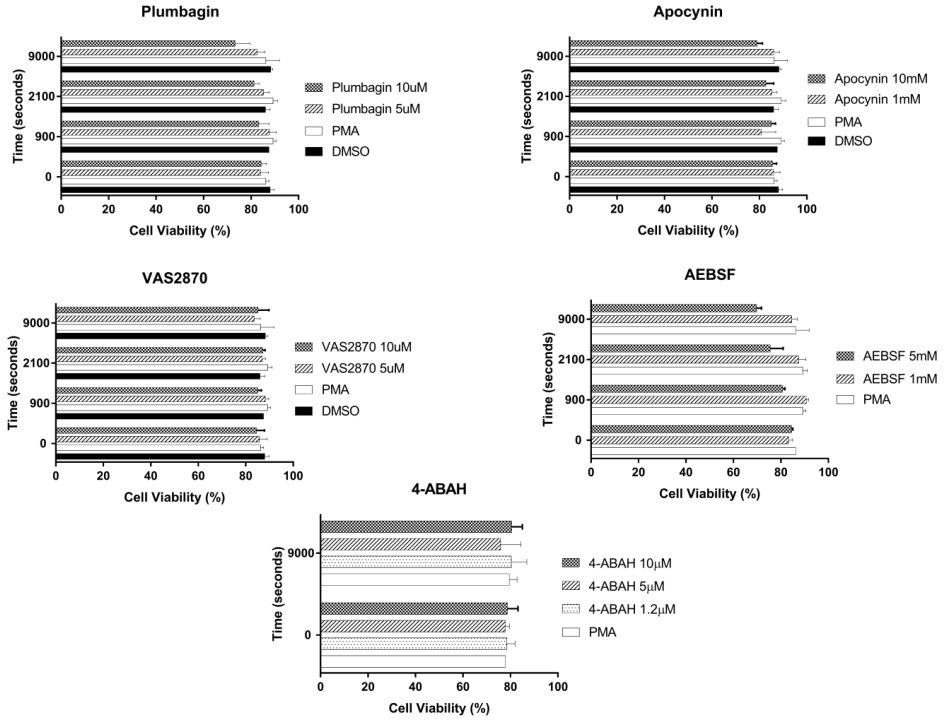

Supplementary Figure S3. Cell Viability during drug administration in HL-60 cells. The viability was checked during 900, 2100 and 9000 seconds for antioxidants and NADPH oxidase inhibitors (Plumbagin, Apocynin, VAS2870 and AEBSF) and at 9000 seconds for MPO inhibitor (4-ABAH). In some drug administration, we also tested the vehicle (DMSO) when necessary.

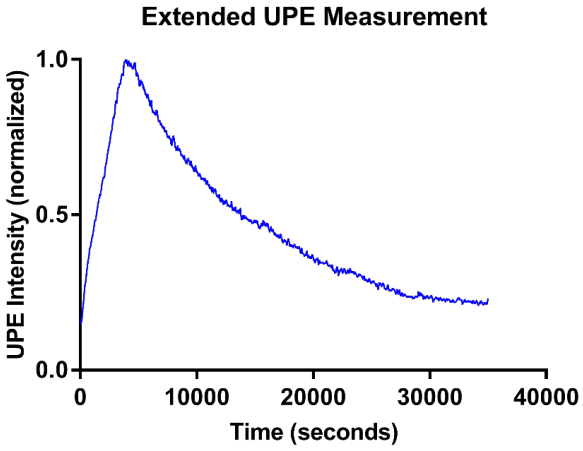

Supplementary Figure S4. Long-term UPE measurement. UPE profile of HL-60 cells upon triggering ROS response stimulated by PMA. UPE profile was recorded for 35000 seconds (about 9.7 hours) at 37°C in the dark. The lines represent the smoothed UPE intensity followed by normalization by the highest UPE intensity.

Chapter 7

Conclusions and perspectives

CONCLUSIONS

In recent decades, the use of a systems-based view of life has provided key insight into fundamental processes with respect to biology. In life sciences, important paradigm shifts are the way in which we approach health and disease. Although modern medicine has traditionally emphasized pathology and acute conditions, our current understanding is that different interventions are needed for treating and preventing chronic disease. To design better interventions, new diagnostic tools are urgently needed in order to create new opportunities for achieving personalized health and medicine. The focus in diagnosis is therefore shifting from measuring single biomarkers such as glucose and cholesterol to creating complex maps of the dynamic patterns underlying regulatory processes. Moreover, the notion of "health" is viewed in a holistic context using biochemistry as a basis and then expanding this basis to include the psycho-social environment, including the individual's world view. In the field of diagnostics, a highly promising new tool has recently emerged based on ultra-weak photon emission (UPE) from biological systems, including all living cells. Thus, the aim of this thesis was to explore the applications of UPE and to correlate UPE with biochemistry in order to obtain a deeper understanding of the processes that occur in living systems.

In **Chapter 2**, we provided the general context for this thesis. In addition, we discussed the role of a systems-based view of health and disease, as well as the role of biophotonics in this context. Specifically, we present the potential of integrating UPE with metabolomics as a novel approach to bridging multi-dimensional information regarding regulatory processes in biological systems. We believe that this approach will improve our understanding of dynamic biological systems at higher organizational levels and can reveal regulatory connections over various time scales.

In **Chapters 3**, **4**, **5**, and **6**, we introduced an *in vitro* model to research and understand UPE as a dynamic monitoring tool from a biochemistry point of view. *In vitro* models provide a relatively simplified view of the human body's complexity and are a suitable starting point for testing new hypotheses and the feasibility of new diagnostic applications. To correlate UPE with biochemical processes, we used metabolomics in **Chapters 3** and **4**, and we performed a follow-up study in **Chapter 5**. In metabolomics-based studies, selecting a suitable biological sample is essential in order to obtain a clear representation of the biochemical processes that participate in a given system[1]. Samples such as blood, urine, cells, and tissues are commonly used for metabolomics studies, with a preference for blood, which can reflect the metabolism within the entire body[1,2]. In this context, we used HL-60 cells, a human promyelocytic cell line, for the experiments described in this thesis. Importantly, this cell line

also meets the sample requirements for metabolomics studies. With respect to measuring UPE, leukocytes were used to represent the host defense system[3] and disease progression. Finally, chemiluminescence has been described during respiratory burst[4], and a previous study showed that UPE can be measured in isolated neutrophils without the need to use a signal enhancer[5]; therefore, the relationship between UPE and other physiological processes has been studied previously.

This thesis in general — and **Chapter 3** in particular — describes one of the first studies in which UPE was correlated with biochemistry. Our study focused on the analysis of amino acids and related compounds, as these molecules play an essential role in central carbon metabolism and — by extension — metabolism-related energy production. Our first experimental data yielded information regarding the biochemical changes that are related to an increase in UPE during oxidative burst. These experiments were designed to detect the potential metabolites that play a role in oxidative burst, as well as changes in the UPE profile; this experimental design was also used in the follow-up studies presented in **Chapters 4** and **5**. Our results revealed a link between UPE and biochemical processes during respiratory burst and showed that some biochemical pathways may play a role in photon emission. In addition, our results provide new directions for studying regulatory effects and their relationship with biophoton emission. As a follow-up study designed to gain further insight into regulatory metabolism, we measured cellular glutathione levels as well as UPE during respiratory burst; these data were reported in **Chapter 5**.

We also examined metabolomics in further detail by studying specific pathways that may be related to UPE; these results were described in **Chapter 4**. Specifically, we studied metabolites that are often correlated with inflammation, lipid peroxidation, and oxidative stress conditions, processes that are commonly associated with an increase in spontaneous photon emissions[6-8]. Our goal was to include the best-characterized signaling metabolites related to oxidative stress and inflammation, and to analyze the correlation between the concentrations of these metabolites and the dynamic UPE profile. Using a general, non-specific NADPH oxidase inhibitor revealed a direct correlation between reactive oxygen species (ROS) production, UPE, and metabolites. Interestingly, the metabolites that had the strongest correlation are closely related with the peroxidation of fatty acids by free radicals and with ROS. We therefore conclude that UPE can be used as a robust tool for monitoring ROS-related oxidative metabolism.

Finally, in **Chapter 6** we evaluated the feasibility of using UPE as a label-free tool for monitoring pharmacological targeting of ROS signaling. ROS signaling was inhibited in our *in vitro* model using various types of pharmacological drugs with different inhibitory

mechanisms. For example, we targeted specific ROS pathways by modulating NADPH oxidase and the myeloperoxidase (MPO) enzymatic system. Our results show that UPE can detect the pharmacological effect of candidate drugs on ROS signaling. Furthermore, we found that the MPO enzymatic system catalyzes reactions that may contribute to the production of UPE, possibly explaining why UPE is affected when an upstream reaction is pharmacologically modulated. Importantly, this is the first study of its kind to investigate the pharmacological potential of measuring UPE.

This thesis provides experimental data that can improve our understanding of UPE from a biochemical perspective. Furthermore, we show that UPE can be used to dynamically monitor regulatory processes in simplified biological model systems, thereby helping to diagnose both health and disease. From a systems biology point of view, UPE may provide a dynamic “fingerprint” of the overarching regulatory processes, whereas metabolomics can provide specific phenotypic information regarding the underlying biochemical mechanisms. In this respect, biophotons may be the key to understanding and linking different regulatory processes coupled over a wide range of time scales.

FUTURE PERSPECTIVES

In this thesis, we used metabolomics to bridge biochemistry with ultra-weak photon emission. Although we covered a relatively large number of biologically relevant endogenous metabolites in our studies, UPE can provide even more information regarding mechanistic and/or biochemical pathways if studied in association with an even wider range of metabolites. For example, the tricarboxylic acid (TCA) cycle may be an important pathway for future investigation, as this pathway is related to energy metabolism and is intimately connected with other metabolic pathways that were studied in this thesis, including amino acids and lipids.

With respect to pharmacology, UPE may open new avenues for exploration, particularly given the results obtained in this thesis in terms of the biochemical pathways that underlie UPE. Other enzymatic pathways related to ROS production should be investigated in future studies. The use of metabolomics as a tool for exploring the role of biophotons during drug modulation (the so-called “pharmaco-metabolomics” approach) can be a useful new approach in pharmacology studies. Given the ability to measure dynamic UPE profiles, spatiotemporal UPE data may be a powerful tool for use in detailed studies regarding personalized medicine.

In terms of models for studying UPE, other simplified models may be highly valuable. For example, zebrafish may be a good candidate model for measuring UPE due to the relatively

simplified organizational view of biological systems. In addition, the zebrafish model has several advantages over other animal models and human subject with respects to genetics, pharmacology, and drug development. Finally, zebrafish research is highly advanced, enabling the researcher to use non-invasive imaging techniques such as UPE, providing a clear advantage with respect to spatiotemporal UPE profiling.

The addition of UPE to observational clinical studies regarding certain diseases may also provide a valuable contribution to improving our understanding of biophoton-related processes. Given that increased UPE levels have been reported in some diseases[9-11], and given the close correlation between UPE and ROS, it would be highly interesting to measure the UPE profile in various patient groups, including patients with cancer, mitochondrial dysfunction, chronic granulomatous disease, and/or atherosclerosis. In the context of diagnostics, UPE may serve as a useful tool for screening many ROS-related diseases.

In this thesis, we focused on measuring the correlation between the UPE profile and the metabolites that change significantly at four time points measured over the span of 2.5 hours. Nevertheless, several questions remain, and other strategies, including the development of computational models, may reveal the power of using UPE to predict specific mechanisms. Another approach that may increase the value of the biochemical perspective is to combine metabolomics information with other omics data (e.g., proteomics and genomics) in the computational models. UPE is therefore likely to provide holistic information regarding the biochemical processes, as well as specific information regarding the underlying pathways.

Thanks to recent studies, the role of UPE is now well understood, and a growing body of evidence suggests that UPE plays an essential role in biological processes[12]. This valuable feature of UPE is gaining more attention, and the emerging view of light as a signaling messenger may provide a robust tool for detecting new phenomena, ultimately opening new avenues for studying personalized health from a holistic perspective. Photons of life might develop into a journey of discovery tackling fundamental unanswered questions in science.

REFERENCES

1 Alvarez-Sanchez, B., Priego-Capote, F. & de Castro, M. D. L. Metabolomics analysis I. Selection of biological samples and practical aspects preceding sample preparation. *Trac-Trend Anal Chem* **29**, 111-119 (2010).

2 Zhang, A., Sun, H., Xu, H., Qiu, S. & Wang, X. Cell metabolomics. *OMICS* **17**, 495-501 (2013).

3 Birkness, K. A. *et al.* An in vitro model of the leukocyte interactions associated with granuloma formation in Mycobacterium tuberculosis infection. *Immunol Cell Biol* **85**, 160-168 (2007).

4 Cheson, B. D., Christensen, R. L., Sperling, R., Kohler, B. E. & Babior, B. M. The origin of the chemiluminescence of phagocytosing granulocytes. *J Clin Invest* **58**, 789-796 (1976).
5 van Wijk, E., van der Greef, J. & van Wijk, R. Photon count statistics in leukocyte cell dynamics. *Journal of Physics: Conference Series* **329**, 12-21 (IOP Publishing, 2011).
6 Birtic, S. *et al.* Using spontaneous photon emission to image lipid oxidation patterns in plant tissues. *Plant J* **67**, 1103-1115 (2011).
7 Prasad, A. & Pospisil, P. Linoleic Acid-Induced Ultra-Weak Photon Emission from Chlamydomonas reinhardtii as a Tool for Monitoring of Lipid Peroxidation in the Cell Membranes. *Plos One* **6**, e22345 (2011).
8 Rastogi, A. & Pospisil, P. Ultra-weak photon emission as a non-invasive tool for the measurement of oxidative stress induced by UVA radiation in Arabidopsis thaliana. *J Photochem Photobiol B* **123**, 59-64 (2013).
9 Kim, H. W. *et al.* Spontaneous photon emission and delayed luminescence of two types of human lung cancer tissues: adenocarcinoma and squamous cell carcinoma. *Cancer Lett* **229**, 283-289 (2005).
10 Kim, J. *et al.* Measurements of spontaneous ultraweak photon emission and delayed luminescence from human cancer tissues. *J Altern Complement Med* **11**, 879-884 (2005).
11 Kobayashi, M. *et al.* In vivo imaging of spontaneous ultraweak photon emission from a rat's brain correlated with cerebral energy metabolism and oxidative stress. *Neurosci Res* **34**, 103-113 (1999).
12 The light fantastic. *Nat Chem Biol* **10**, 483 (2014).

Apendix

SAMENVATTING

Biologische systemen bestaan uit vele componenten, zoals DNA, eiwitten en metabolieten. Een systeembiologische benadering beoogt de dynamische interacties tussen al deze componenten in kaart te brengen, resulterend in een enorme hoeveelheid informatie die nieuwe inzichten kunnen opleveren op biologisch en biomedisch gebied. Om een beter begrip te krijgen van de moleculaire processen die ten grondslag liggen aan (met name complexe en chronische) ziektebeelden, worden binnen de levenswetenschapen nieuwe concepten geëvalueerd. Een belangrijke doel daarbij is om uiteindelijk een meer op maat (medische) behandeling te ontwikkelen die beter aansluit bij de actuele fysiologische gesteldheid en leefwijze van ieder individu/patiënt, ook wel personalized medicine genoemd. In deze context kan Ultra-weak Photon Emission, afgekort UPE, als een relatief nieuwe technologie beschouwd worden met een enorm potentieel voor het bepalen van de fysiologische toestand van een biologisch systeem op een non-invasieve wijze. UPE meet het zwakke licht (biofotonen) dat intrinsiek door een biologisch systeem wordt uitgezonden, d.w.z. iedere cel zendt licht uit. Recente studies wijzen op een mogelijk verband tussen het gemeten UPE signaal en reactieve zuurstofverbindigen. Echter, op dit moment is er nog weinig bekend over het onderliggende moleculaire mechanisme van UPE.

Dit proefschrift beschrijft het onderzoek dat uitgevoerd is om een beter begrip te krijgen van dynamische UPE-metingen op moleculair niveau. Daartoe wordt een metabolomics benadering gebruikt voor het bepalen van de concentraties van endogene metabolieten, d.w.z. producten van de stofwisseling, aanwezig in het biologisch systeem. Vervolgens wordt dan bekeken of er een correlatie/associatie is tussen de gemeten UPE-profielen en de metabolomics data verkregen voor hetzelfde biologische systeem. Dergelijke informatiewinning is cruciaal voor het karakteriseren van UPE als een mogelijke non-invasieve diagnostische techniek op biomedisch gebied. UPE zou wellicht een nieuwe tool kunnen worden voor het detecteren van algemene veranderingen in de stofwisseling (homeostase) met metabolomics als een follow-up benadering voor het verkrijgen van gedetailleerd inzicht op zowel moleculair als systemisch niveau.

In **Hoofdstuk 1** worden de uitgangspunten en het doel van het uitgevoerde onderzoek beschreven in de context van het huidige (bio)medisch onderzoek. De mogelijke diagnostische rol die UPE zou kunnen spelen in combinatie met een metabolomics benadering wordt uiteengezet in **Hoofdstuk 2.** Op basis van de beschreven studies wordt de aanname gemaakt dat UPE geschikt is als een techniek voor de beschrijving van algemene systemische/fysiologische veranderingen binnen een bepaald biologisch systeem. Een

metabolomics benadering kan dan gebruikt worden voor het verder in kaart brengen van de actuele biochemische veranderingen.

In **Hoofdstuk 3** wordt onderzocht of UPE metingen gecorreleerd kunnen worden aan metabolomics data, waarbij gebruik wordt gemaakt van de HL-60 (Human promyelocytic leukemia cells) cellijn als een *in vitro* modelsysteem. De UPE techniek is gebruikt voor het volgen van het respiratory burst proces, d.w.z. het vrijkomen van reactieve zuurstofverbindingen, in dit modelsysteem. Vervolgens is met een gerichte metabolomics-benadering gekeken naar de veranderingen in de concentraties van aminozuren en gerelateerde verbindingen in dit systeem, gebruikmakend van capillaire elektroforese gekoppeld aan massaspectrometrie. De verkregen resultaten tonen aan dat de gemeten UPE-emissie gecorreleerd kan worden met het gedrag van een aantal aminozuren, waarbij de metabole route van methionine sterk naar voren komt. Verder onderzoek is nodig om effectief de rol van de methionine pathway vast te stellen, bijv. via onderdrukking van enzymen gerelateerd aan de totstandkoming van de gemeten UPE-emissie.

Recente studies wijzen op een mogelijk verband tussen het gemeten UPE-signaal en reactieve zuurstofverbindigen. In **Hoofdstuk 4** is daarom gekeken of er een associatie is tussen de gemeten UPE-emissie en metabolieten, die processen als oxidatieve stress en inflammatie selectief kunnen duiden, gebruikmakend van hetzelfde modelsysteem. Een reversed-phase vloeistofchromatografie methode gekoppeld aan massaspectrometrie is gebruikt voor het profileren van zowel intracellulaire als extracellulaire metabolieten. De bevindingen van deze studie geven een correlatie tussen de gemeten UPE-emissie en het gedrag van een aantal intracellulaire metabolieten aan. Het experiment is herhaald met onderdrukking van het enzym NAPHD-oxidase. Ook deze studie laat duidelijk een verband zien tussen de gemeten UPE-emissie en de aanmaak van reactieve zuurstofverbindingen en de intracellulaire metabolieten. Op grond van deze bevindingen wordt geconcludeerd dat de UPE techniek ingezet kan worden voor het uitlezen van oxidatieve metabolisme gerelateerd aan reactieve zuurstofverbindingen.

Om te achterhalen of UPE-metingen ook informatie kunnen verschaffen op het niveau van biochemische regelsystemen, die gezamenlijk verantwoordelijk zijn voor de homeostase, is in **Hoofdstuk 5** specifiek gekeken naar de verhouding glutathione (GSH) en glutathione disulfide (GSSG) in het HL-60 cellijn systeem gedurende het respiratory burst proces. De GSH/GSSG verhouding wordt vaak als een marker voor oxidatieve stress gebruikt. Dit onderzoek laat geen correlatie tussen de gemeten UPE-emissie en de GSH/GSSG verhouding zien. Op basis hiervan wordt aangenomen dat UPE-emissies veranderingen in de biochemie op systemisch niveau weergeven.

De bruikbaarheid van de UPE techniek voor farmacologisch onderzoek is beschreven in **Hoofdstuk 6**. Hiertoe is gekeken naar een aantal biochemische processen dat specifiek betrokken is bij de aanmaak van reactieve zuurstofverbindingen. Onderzocht is of UPE ingezet kan worden als een directe methode voor het registreren van veranderingen in deze biochemische processen door ze selectief te moduleren met potentiële geneesmiddelen. Voor onderdrukking van de biochemische processen in de HL-60 cellijn zijn verschillende geneesmiddelen gebruikt elk met een ander werkingsmechanisme. Op grond van de verkregen data wordt geconcludeerd dat UPE in staat is om de farmacologische respons, geïnduceerd door de geneesmiddelen, van reactieve zuurstof gerelateerde biochemische processen, kan detecteren. De veelbelovende resultaten geven duidelijk aan dat de mogelijkheden van UPE voor systeemfarmacologisch onderzoek verder uitgezocht dient te worden.

Tenslotte wordt in **Hoofdstuk 7** ingegaan op de voornaamste bevindingen van het onderzoek beschreven in dit proefschrift en worden er aanbevelingen gedaan voor vervolgstudies.

Samenvattend kan gesteld worden dat het beschreven werk tot meer inzicht heeft geleid in de moleculaire mechanismen achter UPE-metingen, maar vooral dat UPE in combinatie met metabolomics een veelbelovende benadering kan zijn voor systeemfarmacologisch onderzoek. De wetenschappelijke brug tussen fotonemissie en moleculaire processen biedt niet alleen de basis voor niet-invasieve wijze systeemdynamische diagnose, maar geeft in combinatie met recente publicaties rond licht-communicatie tussen cellen en organismen tevens nieuwe inzichten in de rol van licht in de biologie.

ACKNOWLEDGMENTS

My special thanks are to Prof. Dr. Jan van der Greef and Prof. Thomas Hankemeier for their enthusiasm, when we first discussed my wish to study at the Leiden University. It encouraged me to continue improving my knowledge, so I could enter the PhD program in the very nice environment at the Division of Analytical Biosciences (ABS) of the LACDR.

I am grateful for all support and inspiration from my co-promotors Dr. Rawi Ramautar for his supervision and Dr. Eduard van Wijk for helping me with all UPE-related challenges including instrumental issues during my thesis project.

I am extremely thankful to Prof. Ruud Berger for his excellent suggestions and comments for my research project. I also would like to thank Prof. Thomas Hankemeier for his insightful comments and encouragement, which motivated me to widen my research to various other perspectives and also for all his support in the department.

My sincere thanks also go to Dr. Michal Cifra who provided me the opportunity to join and work in his laboratory for a short period and for the great collaboration. Also, I thank all the colleagues which I met there and in particular I thank Dr. Ondřej Kučera for all his help and discussions about my research project.

I also would like to thank the master students Tom van der Laan and Lennart van den Winden and the Bachelor students Seyma Taspinar and Saide Cetinayak, who contributed to this research and also for giving me the opportunity to develop my teaching skills by learning together with them.

I would like to thank all the ABS colleagues which I have met during these 4 years, in special Loes for all her support, since I started my journey to come to the Netherlands. I thank my lab mates Amar, Vasu, Wei, Cornelius, Mengmeng, and Min, for the stimulating discussions about projects, analytical chemistry and Science club moments. I also thank Junzeng and Nelus for all the fun we have had in the last four years. I thank Amanda and Marta for the sincere friendship and all the good moments shared in Leiden.

Finally, I must express my very profound gratitude to my parents and in special to my mom Ana and my sister Regina for providing me with unfailing support and continuous encouragement keeping me harmonious and helping me putting pieces together during these 4 years abroad. This accomplishment would not have been possible without them. I will be grateful forever for your love.

Thank you all.

CURRICULUM VITAE

Rosilene Cristina Rossetto Burgos was born on February 8th, 1983 in Mineiros do Tietê, São Paulo, Brazil. After obtaining her high school diploma in 2000, Rosilene studied chemistry at the São Paulo State University (UNESP) and received her bachelor degree in 2007. During that time, she started as an intern in the research group of Núcleo de Bioensaios Biossíntese e Ecofisiologia de Produtos Naturais (NuBBE) being granted with a national research scholarship to undergraduate students. Subsequently, she continued her education with master studies at the same university focusing on *in silico* strategies for detection and identification of bioactive compounds making the use of hyphenated analytic techniques under the supervision of Prof. Dr. Ian Castro-Gamboa. After finishing her master studies in 2010, she continued to work with chromatographic techniques as analytical research technician in several companies (environmental, biotechnological and pharmaceutical) in Brazil. After a successful grant application in 2013 for a PhD. study abroad scholarship (230827/2012-8) from the Brazilian National Council for Research and Development (CNPq) she started the investigations described in this thesis under the supervision of Prof. Dr. Jan van der Greef, Dr. Rawi Ramautar and Dr. Eduard van Wijk in the division of Analytical Biosciences at Leiden Academic Centre for Drug Research (LACDR), Leiden University, Leiden, The Netherlands.

LIST OF PUBLICATIONS

Burgos, R. C. R.*, Ramautar R., van Wijk, E. P., Hankemeier T., van der Greef, J. & Mashaghi A. Targeting of ROS reaction network in HL-60 myeloid leukemia cells monitored by ultra-weak photon emission. *Manuscript submitted*.

Burgos, R. C. R.*, Zhang W., van Wijk, E. P., Hankemeier T., Ramautar R. & van der Greef, J. Cellular glutathione levels in HL-60 cells during respiratory burst are not correlated with ultra-weak photon emission. *J Photochem Photobiol B* **175**, 291-296, doi.org/10.1016/j.jphotobiol.2017.09.002 (2017).

Burgos, R. C. R.*, Schoeman J.C, Winden L.J.V., Červinková K., Ramautar R., Van Wijk E.P., Cifra M., Berger R., Hankemeier T., van der Greef J. Ultra-weak photon emission as a dynamic tool for monitoring oxidative stress metabolism. *Sci Rep* **7**, 1229, doi:10.1038/s41598-017-01229-x (2017).

Burgos, R. C. R*, van Wijk, E. P., van Wijk, R., He, M. & van der Greef, J. Crossing the Boundaries of Our Current Healthcare System by Integrating Ultra-Weak Photon Emissions with Metabolomics. *Front Physiol* **7**, 611, doi:10.3389/fphys.2016.00611 (2016).

Burgos, R. C. R.*, Červinková K., van der Laan T., Ramautar R., Van Wijk E.P., Cifra M., Koval S., Berger R., Hankemeier T., van der Greef J. Tracking biochemical changes correlated with ultra-weak photon emission using metabolomics. *J Photochem Photobiol B* **163**, 237-245, doi:10.1016/j.jphotobiol.2016.08.030 (2016).

Gallep, C. M., Barlow, P. W., **Burgos, R. C. R.** & van Wijk, E. P. Simultaneous and intercontinental tests show synchronism between the local gravimetric tide and the ultra-weak photon emission in seedlings of different plant species. *Protoplasma* **254**, 315-325, doi:10.1007/s00709-016-0947-1 (2017).

Batista, A. N. L., Colombo, R., de Pascoli, I. C., Teles, H. L., Silva, G. H., Bomfim, G. C. C., **Burgos, R. C. R.**, Cavalheiro, A. J., Bolzani, V. S., Silva, D. H. S., & Reimberg, M. C. H. Development and validation of a HPLC method for standardization of herbal and commercial extracts of *Myrcia uniflora*. *Rev Bras Farmacogn* **21**, 402-406, doi:10.1590/S0102-695x2011005000066 (2011).

Colombo, R., Batista, A. N. L., Bomfim, G. C. C., **Burgos, R. C. R.**, Cavalheiro, A. J., Bolzani, V. S., Silva, D. H. S., & Reimberg, M. C. H. Validated high-performance liquid chromatographic method for the standardisation of *Ptychopetalum olacoides* Benth., Olacaceae, commercial extracts. *Rev Bras Farmacogn* **20**, 781-788, doi:10.1590/S0102-695x2010005000027 (2010).

Colombo, R., Batista, A. N., Teles, H. L., Silva, G. H., Bomfim, G. C. C., **Burgos, R. C. R.**, Cavalheiro, A. J., Bolzani, V. S., Silva, D. H. S., Pelícia, C. R., Guimarães, F. M. and Heimberg, M. C. H. Validated HPLC method for the standardization of Phyllanthus niruri (herb and commercial extracts) using corilagin as a phytochemical marker. *Biomed Chromatogr* **23**, 573-580, doi:10.1002/bmc.1155 (2009).

* First Author